A STUDY OF AN ELECTROSTATIC PROBE IN A CONTINUUM PLASMA CONTAINING NEGATIVE IONS

A THESIS

Presented to

The Faculty of the Division of

Graduate Studies

By

Basil Pearson Cooper, Jr.

In Partial Fulfillment

of the Requirements for the Degree

Doctor of Philosophy

in the School of Aerospace Engineering

Georgia Institute of Technology

June, 1975

A STUDY OF AN ELECTROSTATIC PROBE IN A CONTINUUM PLASMA CONTAINING NEGATIVE IONS

Approved:

James C. Wu, Chairman

Howard M. McMahon

James E. Hubbartt

Date approved by Chairman: 5/23/75

ACKNOWLEDGMENTS

I would like to express my deepest appreciation to Dr. James C. Wu for his suggestion of this problem and for his guidance throughout the course of this investigation.

I also wish to thank Dr. Howard M. McMahon and Professor James E. Hubbartt for their guidance in the preparation of this manuscript.

To those who helped construct the test facility, I am grateful. I wish to thank Mr. George T. Bird and, especially, Mr. John C. Handley for their advice and help in the fabrication of this facility.

My continuing education was made financially possible by an NSF Traineeship, an NDEA Traineeship, and the Georgia Institute of Technology. I wish to thank these organizations for their financial support.

I also wish to thank my parents for their inspiration and assistance throughout my life. Their years of sacrifice are deeply appreciated.

Finally, I wish to thank my wife, Virginia, whose confidence in me has never wavered and without whose constant support and assistance this thesis would not be possible.

TABLE OF CONTENTS

LIST OF TABLES

LIST OF ILLUSTRATIONS

Figure Page

LIST OF SYMBOLS

a	positive ion mean free path
A_i	plasma sheath area
A_w	area of collecting electrode
c	charged particle concentration
$\bar{c}$	average particle thermal speed, $\sqrt{8kT/\pi m}$
$\bar{c}_p$	frozen specific heat
d	sheath thickness
D	diffusion coefficient
D_a	ambipolar diffusion coefficient
D_o	diameter of electrostatic probe
e	electronic charge
E	electric field
f	nondimensional stream function equal to the Blasius function
$\bar{f}$	particle distribution function
$\bar{g}(\eta)$	$\bar{h}_t(\eta)/\bar{h}_{t2}$
h	static enthalpy
h_r	enthalpy of recombination
$\bar{h}_t(\eta)$	stagnation enthalpy at η
$\bar{h}_{t2}$	free stream stagnation enthalpy
j	charged particle current
J	Γ/Γ_o
k	Boltzmann constant
K	electron capture reaction rate constant

K_o permittivity of a vacuum

ℓ Chapman-Rubesin factor, $\rho\mu/\rho_2\mu_2$

m particle mass

m_p neutral partial mass

$\bar{m}$ reduced mass

n number density

n_o positive ion number density at the plasma sheath edge

n_p neutral partial number density

N_e $n_e/(1-\alpha)n_0$

N_i n_i/n_o

N_n $n_n/\alpha n_o$

p pressure

p_o free stream stagnation pressure

p_s free stream static pressure

$\bar{Q}$ average collision cross section

$\dot{Q}$ rate of heat loss due to radiation

s dimensionless coordinate, $\int_o^x \rho_2 u_2 \mu_2 x^2 dx$

S schmidt number, $\mu/\rho D_a$

t time

T temperature

T_{η_d} temperature at the dimensionless sheath thickness

u velocity in x-direction

v velocity in y-direction

$\bar{V}$ velocity, $\sqrt{u^2+v^2+w^2}$

w velocity in z-direction

x	distance
y	distance normal to x, or a nondimensional electrostatic potential
z	c/c_2, or distance normal to x and y-direction
Z	number of net electronic charges per ionized particle
α	n_n/n_i
$\overline{\alpha}$	average value for the recombination coefficient
α_n	charge exchange coefficient between the negative and positive ions
α_r	recombination rate constant
β	ratio of initial electrophilic additive and negative ion number density to positive ion number density, $(n_{ao} + n_{no})/n_i$
$\overline{\beta}$	boundary layer pressure gradient
γ	ratio of specific heats
Γ	rate of particle flux
δ	microwave wavelength
ε	T_e/T_i
ζ	x/a
ζ_s	nondimensional sheath thickness
η	dimensionless coordinate, $u_2/(2s)^{\frac{1}{2}} \int_o^y x\rho dy$
η_d	transformed sheath thickness
λ	positive ion mean free path
λ_d	Debye length, $(K_o k T_i/n_i e^2)^{\frac{1}{2}}$
λ_T	coefficient of thermal conductivity
μ	coefficient of viscosity
$\overline{\mu}$	charged particle mobility coefficient
ρ	density

ρ_o free stream stagnation density

σ electron capture cross section

$\bar{\sigma}$ Prandtl number, $\mu\bar{c}_p/\lambda_T$

σ_{Ar} collision diameter of argon

σ_{SF_6} collision diameter of sulphur hexafluoride

σ_{UF_6} collision diameter of uranium hexafluoride

ϕ electrostatic potential

ϕ_f floating potential

ϕ_o probe potential at which no electric current flows

ϕ_p potential at the surface of the electrostatic probe

ψ dimensional stream function

Superscript

' denotes differentiation with respect to η

Subscripts

a denotes property of electrophilic additive

Ar denotes property of argon atom

e denotes property of electrons

FS denotes free stream static conditions

g denotes property of a particle group

i denotes property of positive ions

n denotes property of negative ions

o denotes initial condition

p denotes a plasma property

s denotes saturation value

SF_6 denotes property of sulphur hexafluoride molecule

UF_6 denotes property of uranium hexafluoride molecule

η	denotes property at transformed distance η from electrostatic probe surface
2	denotes property at boundary layer edge

SUMMARY

An analysis of a stagnation point electrostatic probe theory and a study of two electrophilic compounds is presented. The analysis of Lees, for stagnation point flow, was coupled with an electrostatic probe equation and a sheath thickness equation, derived herein, to produce an electrostatic probe theory which is applicable to a plasma containing negative ions. This theory was experimentally evaluated to determine its ability to predict the free stream properties of a flowing argon plasma. This electrostatic probe theory was also used to evaluate the electrophilic properties of sulphur hexafluoride and of uranium hexafluoride.

The electrostatic probe theory was evaluated for a plasma enthalpy range of 4×10^4 k-cal./kg.-mole to 9×10^4 k-cal./kg.-mole and a pressure range of 15 mm. Hg. to 45 mm. Hg. For all of the enthalpies and pressures studied, the electrostatic probe theory was able to predict the free stream stagnation temperature to within an accuracy of 20 percent. The ability of the theory to predict the free stream ionization levels could not be evaluated because of ion recombination in the boundary layer of the electrostatic probe. However, it was possible to determine the positive ion recombination coefficient of argon for a temperature range of 6,600°K to 8,500°K.

Sulphur hexafluoride was found to be an effective electrophilic compound and the electron capture cross section of sulphur hexafluoride was determined for a temperature range of 6,500°K to 9,000°K. Sulphur

hexafluoride was also found to be effective in increasing the rate of positive ion recombination in an argon plasma.

The addition of sulphur hexafluoride to the plasma made it possible to extend the usefulness of the electrostatic probe theory. Under many test conditions, the electron currents to the electrostatic probe are too large to permit an accurate analysis of the plasma properties. By adding a measured amount of sulphur hexafluoride, or any other electrophilic material whose properties are known, the electron currents can be reduced by a known amount. If a sufficient reduction of electron current can be achieved, the plasma can then be analyzed.

Uranium hexafluoride was evaluated at a lower temperature than was sulphur hexafluoride and its electron capture cross section could not be determined. The data indicated, however, that uranium hexafluoride is at least as effective as sulphur hexafluoride as an electrophilic compound and also in increasing the rate of positive ion recombination in an argon plasma.

CHAPTER I

INTRODUCTION

In recent years, there has been a great deal of interest in plasma diagnostics. One of the simplest diagnostic tools that has been used is the electrostatic probe. An electrostatic probe is merely an electrode which is placed within the plasma and which can be biased to any desired electrical potential with respect to the plasma. The current collected by the electrode is a function of the potential and can be used to determine the electron and ion temperatures and number densities. Most of the analytical work concerning electrostatic probes has been with cylindrical or spherical probes whose diameter has been *less than the mean free path of the charged particles contained within* the plasma. Consequently the electrostatic probe has been useful mainly with low density plasmas and its application to high density plasmas has been difficult.

In addition, all but a very few workers have assumed that only two species of charged particles existed within the plasma, i.e., only positive ions and electrons. Little serious attention has been paid to the cases in which negatively charged ions form a significant part of the flow.

In the past decade, however, interest has developed in studying plasmas of moderate density in which negative ions are a significant component of the negative particles. Those negative ions either occur naturally or are formed in the flow when a substance is deliberately

injected to absorb some or all of the electrons.

Plasmas containing negative ions are especially important in studies of reentry conditions. The heat shields of many reentry vehicles are composed of certain ablating substances, such as Teflon, which introduce negative ions into the boundary layer and thus change the current-voltage characteristics of an electrostatic probe placed within the boundary layer. Any study of this type of reentry plasma using electrostatic probes placed within the boundary layer must take these negative ions into account.

Also, during part of the reentry, the vehicle is sheathed in a plasma which normally contains large numbers of free electrons. Within the plasma, these electrons are sufficiently mobile to absorb radio signals and thus prevent communication with the vehicle during part of the reentry phase of the flight. If an electrophilic compound is injected into the plasma, many of these electrons will be absorbed and thus the number of free electrons will be reduced. If enough electrons can be absorbed, then communication with the reentering vehicle is possible. Any study of the effectiveness or electron absorption rate of these electrophilic compounds will require an analysis of a plasma containing negative ions.

One further use of plasmas containing negative ions arises from one of the difficulties with the use of the electrostatic probe. In a plasma with a high free electron concentration, the electrical current at the probe can be so high as to damage the probe and, by depleting the electron concentration near the probe, cause distortion in the probe's current-voltage characteristic. The probe then yields

inaccurate information about the plasma. If an electrophilic compound is added to the plasma, then these high electron current levels can be reduced, thus reducing or eliminating the distortion of the current-voltage characteristic. If, further, this addition of electrophilic material does not alter the plasma properties, such as temperature and density, then these properties can be determined to a greater degree of accuracy. One major advantage to the reduction of the electron current is that, if the current can be reduced enough, the ion temperature can be determined directly from the current-voltage characteristic rather than being deduced from the floating potential. The floating potential is defined as the potential, relative to the potential of the plasma, at which no net current flows to the probe. It is a function of the ion and electron temperatures as well as the ion and electron concentrations and energy distribution functions. Because of the greater complexity in determining its value, the error in determining the ion temperature is normally greater than is the error in determining the electron temperature. In addition, the value of the plasma potential is normally difficult to determine because of the distortions to the current-voltage characteristic caused by the high electron currents. This introduces additional errors into the determination of the ion temperature. An electrostatic probe theory which can be used when the plasma contains negative ions could thus improve the accuracy to which the plasma conditions can be determined.

A theory which will allow an analysis of this type of plasma was developed and evaluated experimentally in this research.

Background and Review of Recent Literature

The various types of electrostatic probes have been treated analytically by many authors. In the early twenties, Langmuir and his coworkers[1] developed the original electrostatic probe theories and undertook much of the early research. Langmuir confined himself to the case in which the plasma was at low pressure, where collisions between plasma particles could be neglected, and in which there was no large scale motion of the plasma. He was able to develop a relatively simple and self-consistent theory which still forms the basis of all considerations in regard to probes.

During the last forty years, the experimental techniques and the theory of probes have been refined by many workers. A number of theoretical investigations dealt with the disturbance of a plasma by a probe, and in particular with the transition region between the space charge sheath surrounding a probe and the undisturbed plasma.[2-7] Of special importance have been the attempts to extend the Langmuir probe theory to high pressures.[3,4,8-10] The probe analysis for these high pressure plasmas has been extraordinarily complicated and often the results cannot be applied directly to the experimentally determined characteristics. While Langmuir's theory can be derived from mechanical conservation laws (i.e., angular momentum and energy) and Poisson's equation, the theories for higher pressures require additional knowledge of parameters such as mobilities, diffusion constants, and ionization frequencies. Furthermore, these parameters depend in a rather complicated way on quantities such as the electrical field strength and the velocity distributions of plasma particles which vary abruptly in the

vicinity of the probe.

Efforts were also made to adapt the Langmuir probe theory to the case of a flowing plasma.[11] The mass motion of the plasma relative to the probe again complicated the probe theory. At very high plasma velocities relative to the probe, it was possible to ignore the thermal motion of the ions and assume that only the electrons had a velocity distribution. However, at lower velocities, the ion motion had to be taken into account and this complicated the probe theory.

In an effort to eliminate some of these difficulties, Talbot[12] developed a theory for the use of a Langmuir probe placed at the stagnation point of a blunt body immersed in the flow. Talbot's theory was based upon the work of Lees[13] who formulated the equations for stagnation point flow at high temperatures. Talbot assumed that the stagnation point flow field was adequately described by Lees' equations, and that the Langmuir theory for the electrostatic probe was sufficiently accurate to enable him to determine the plasma conditions at some point within the stagnation point boundary layer. Then, by use of the flow equations, the plasma conditions within the undisturbed flow could be determined. Talbot did not assume that there were any negative ions present within the plasma.

Grey and Jacobs[14] performed experiments with a water-cooled electrostatic probe to evaluate the ability of Talbot's theory to measure local electron temperature, electron density, floating potential, and saturation current ratio in dense plasmas. The measurements of electron temperature were compared with temperatures obtained from simultaneous local measurements of total plasma enthalpy under conditions of known

equilibrium by use of a calorimetric probe technique and were found to be in agreement within normal experimental error (3% standard deviation from the mean). Using this electron temperature, the measurements of floating potential and saturation current ratio were found to agree with a first-order theoretical approximation to within the accuracy of the approximation. No experiments were run in which negative ions were present in the plasma and Grey and Jacobs were unable to determine the free stream plasma temperature through the use of the electrostatic probe.

Purpose of the Research

While the electrostatic probe has been in use for many years, its use has generally been restricted to low density plasmas whose velocities relative to the probe have been either very low or else very high. No readily usable theory for medium to high density plasmas with moderate flow velocities and which contain negative ions has previously been developed and experimentally evaluated. An important purpose of this research was to extend existing theories regarding the effects of negative ions, and thus to extend their range of applicability, and to experimentally evaluate the results. An additional purpose of the research was to evaluate the electrophilic properties of sulphur hexafluoride and uranium hexafluoride. Sulphur hexafluoride is known to be an electrophilic compound and has been proposed as an additive to reduce the electron number density in plasmas. Uranium hexafluoride has been suggested as the uranium carrying compound in gas core nuclear reactors. These reactors are expected to use magnetrohydrodynamic generators as part of the generating process. Since these generators require high

electron densities in order to be efficient, the electrophilic properties of uranium hexafluoride are of interest.

The research program included an analytical extension of Talbot's theory to include the presence of negative ions and an experimental evaluation of the extended theory. The effects of the plasma pressure and enthalpy with the associated changes in ionization percentage, plasma density, and plasma temperature were investigated.

The ability of the extended theory to measure plasma temperatures and ionization percentages was evaluated by comparing the values for these parameters determined by reducing electrostatic probe measurements with the new theory to the values for these parameters indicated by a thermodynamic analysis of the flow. The analysis was performed for cases in which no negative ions were present and also for cases in which the negatively charged particles consisted almost entirely of negative ions.

The plasma conditions predicted by the theory agreed with those of the thermodynamic analysis to within the limits of the experimental error. This agreement was considered to be sufficiently good to permit the use of the theory to examine the electrophilic properties of sulphur hexafluoride and uranium hexafluoride. The degree of free electron reduction with increasing additive concentration was examined for both compounds and both were found to be highly effective electrophilic additives.

CHAPTER II

STAGNATION POINT FLOW THEORY

An electrostatic probe will only determine the plasma conditions at the edge of the probe sheath, while the desired properties are those of the free stream. For probes whose size is comparable to the mean free path in the plasma, this is not a problem since probes of this size do not produce significant perturbations in the plasma. However, for significantly larger probes the effects of the thermal and viscous boundary layers on the probe are important and the results produced by the electrostatic probe must be corrected for these effects. This chapter presents the stagnation point flow theory used in this research.

As shown in Figure 1, the subsonic flowfield around the probe is divided into three regions. These are the inviscid flow, boundary layer, and sheath regions. The equations for the boundary layer region are presented in this chapter. The formulation of the boundary layer equations is based upon the works of Talbot[12] and of Lees.[13]

Assumptions

The problem of stagnation point flow in a plasma is complicated but it can be simplified if the assumptions are made that (a) completely frozen flow exists throughout the boundary layer and (b) ambipolar diffusion exists outside of the sheath.

Frozen Flow Assumption

To justify the frozen flow assumption it is necessary to compare

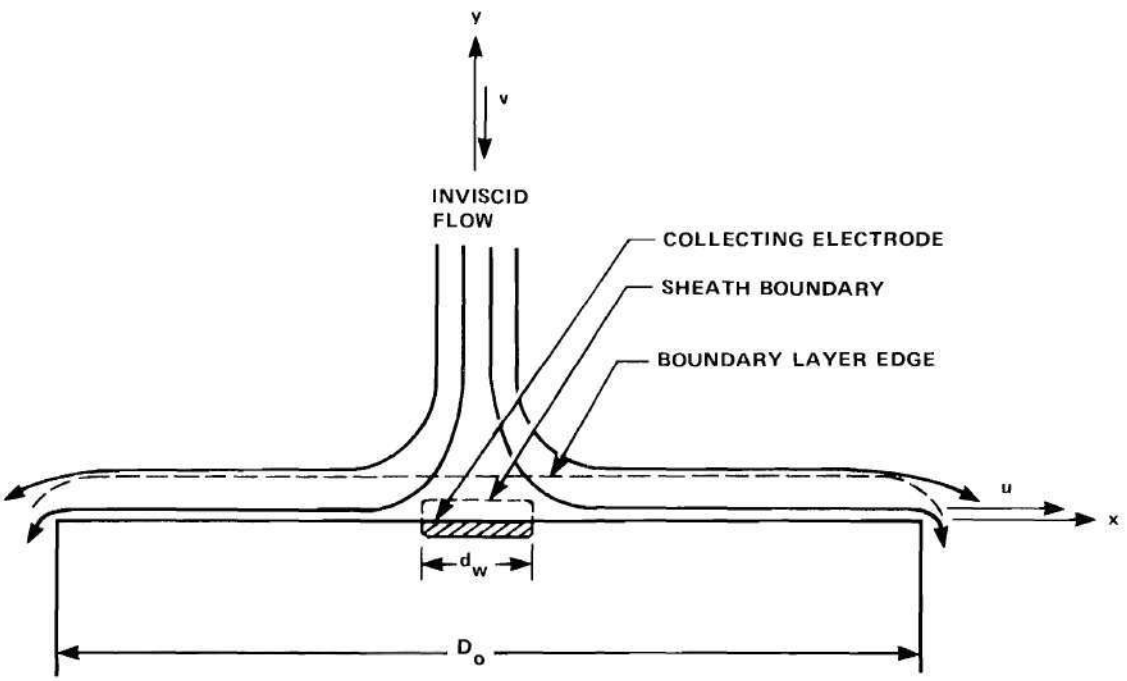

Figure 1. Probe Tip

the time required for an ion or electron to pass through the boundary layer to the time required for particle reactions. These reactions are electron-positive ion recombination, negative ion formation, and negative ion deionization. The electron-positive ion recombination reaction has been checked by Grey and Jacobs[14,15] for the case of an argon plasma at 1 atmosphere pressure. All possible recombination mechanisms were considered and it was concluded that the characteristic recombination times were considerably greater than the electron or ion transit times within the boundary layer for all temperatures below 11,000°K. The recombination time is a function of pressure and temperature and varies inversely with the temperature and the square or cube of the pressure depending upon whether the recombination process is a two- or three-body collision process. Consequently, for pressures that are less than 1 atmosphere, the temperature limit of 11,000°K can be raised somewhat.

In addition to the work done by Grey and Jacobs, Talbot has shown that the time, t, required for an electron or ion to travel through the stagnation point boundary layer is given by

$$t = \frac{1.05}{\overline{\beta}} \tag{2-1}$$

where $\overline{\beta}$ is the dimensional boundary layer pressure gradient parameter given in Appendix A as

$$\overline{\beta} = \frac{2}{D_o}\sqrt{2\left(\frac{p_o - p_s}{\rho_o}\right)} \tag{2-2}$$

for subsonic flow. In Equation (2),* D_o is the probe diameter, p_o and ρ_o are the stagnation point pressure and density respectively, and p_s is the free stream static pressure. Talbot has also shown that the equation for ion recombination within the boundary layer is

$$\frac{n_i}{n_{i2}} = \frac{1}{1 + \alpha_r n_{i2} t} \tag{2-3}$$

where n_i is the ion number density after time t, n_{i2} is the ion number density at the boundary layer edge, and α_r is the recombination rate constant.

The correct value of α_r for argon is subject to considerable uncertainty. Table 6.4 of Loeb[16] gives values ranging from 1.1×10^{-6} cm^3/sec to 2.5×10^{-13} cm^3/sec. Recently, Maxwell and Wessling[17] developed an analytical approximation to the recombination coefficient of hydrogen which was valid for an optically thin plasma when the electron concentration varied between 10^{10} cm^{-3} and 10^{16} cm^{-3} and when the electron temperature varied between 2×10^3°K and 16×10^3°K. Maxwell and Wessling noted that at the higher electron concentrations their results would be approximately valid for argon. For the present test conditions, the results of Maxwell and Wessling give values for α_r ranging between 10^{-10} cm^3/sec and 10^{-11} cm^3/sec, the ion and electron concentrations were of the order of 10^{14} cm^{-3} and $\bar{\beta}$ was of the order of 10^5 sec^{-1}. Using the conservative value for α_r of

---

*Unless especially noted, all references to equations in this dissertation are to equations within the same chapter as the reference.

$$\alpha_r = 10^{-10} \text{ cm}^3/\text{sec} \tag{2-4}$$

the ratio of n_i to n_{i2} becomes

$$\frac{n_i}{n_{i2}} = 0.91 \tag{2-5}$$

indicating that the electron-positive ion recombination process is very nearly frozen.

When electrophilic additives are present in the plasma, the times of negative ion formation and deionization must also be large compared to the time of ion diffusion through the boundary layer in order to justify the frozen flow assumption. The rate of formation of negative ions is given by

$$\frac{dn_n}{dt} = Kn_e n_a \tag{2-6}$$

where n_n, n_e, and n_a are the negative ion, electron, and unionized additive number densities respectively, and K is the reaction rate constant. As negative ions are formed, the additive number density decreases such that

$$n_a = n_{ao} - (n_{eo} - n_e) \tag{2-7}$$

where n_{ao} and n_{eo} are the initial additive and electron number densities respectively. Substituting Equation (7) into Equation (6) and noting that

$$n_n = n_{eo} - n_e + n_{no} \tag{2-8}$$

yields

$$\frac{n_n - n_{no}}{n_{eo}} = \frac{1 - e^{-K\left(\frac{n_{ao} - n_{eo}}{n_{i2}}\right)n_{i2}t}}{1 - \frac{n_{eo}}{n_{ao}} e^{-K\left(\frac{n_{ao} - n_{eo}}{n_{i2}}\right)n_{i2}t}} \tag{2-9}$$

where n_{no} is the initial negative ion number density. In the boundary layer, t is given by Equation (1). For the experiments performed in the present investigation in which negative ions were present in the plasma, typical sheath edge conditions were

$$n_{i2} = 10^{13} \text{ cm}^{-3} , \tag{2-10}$$

$$\overline{\beta} = 10^{5} \text{ sec}^{-1} , \tag{2-11}$$

$$n_{no} = n_{eo} = 5 \times 10^{12} \text{ cm}^{-3} , \tag{2-12}$$

and

$$n_{ao} = 2 \times 10^{13} \text{ cm}^{-3} . \tag{2-13}$$

The parameter K is given by

$$K = \overline{c}_e \sigma_a \tag{2-14}$$

where σ_a is the electron attachment cross section and $\overline{c}_e$ is the average electron thermal speed which is given by

$$\overline{c}_e = \sqrt{\frac{8kT_e}{\pi m_e}} \tag{2-15}$$

where T_e is the electron temperature, k is the Boltzmann constant given by

$$k = 1.38 \times 10^{-16} \text{ erg/°K} \tag{2-16}$$

and m_e is the mass of an electron given by

$$m_e = 9.1 \times 10^{-28} \text{ gm} . \tag{2-17}$$

For the present experiments, a typical value for the electron temperature is 12,000°K which, from Equation (15), gives an average electron thermal speed of

$$\bar{c}_e = 6 \times 10^{7} \text{ cm/sec} . \tag{2-18}$$

The value for σ_a for sulphur hexafluoride is highly dependent upon the attaching electron energy and is subject to some uncertainty. Asundi and Craggs[18] give values for σ_a varying between 10^{-15} cm^2 and 10^{-19} cm^2 for electron energies varying between 0 and 2 electron-volts. For an electron energy of 1 e.v. (corresponding to an electron temperature of 12,000°K), Asundi and Craggs give a value of 10^{-17} cm^2 for σ_a. Using this value, the parameter K becomes

$$K = 6 \times 10^{-10} \text{ cm}^3/\text{sec} \tag{2-19}$$

and Equation (9) yields

$$\frac{n_n - n_{no}}{n_{eo}} = 0.17 . \tag{2-20}$$

This indicates that only 17 percent of the free electrons at the sheath

edge are absorbed by the electrophilic additive and hence the negative ion formation process is very nearly frozen.

In order for the negative ions to be in equilibrium in the plasma, the rate of negative ion deionization must be equal to the rate of negative ion formation. Thus, if the boundary layer is frozen to negative ion formation, it will also be frozen to negative ion deionization.

Ambipolar Diffusion Assumption

The ambipolar diffusion assumption arises from the requirement that the plasma maintain charge neutrality in the absence of an external electric field. This assumption of plasma neutrality can only be met if the positively and negatively charged particles diffuse through the plasma at the same rate. If this were not the case, a charge inbalance would occur within the plasma. This would create an electric field which, by affecting the diffusion rates, would restore the charge balance. The ambipolar diffusion rate is determined from the individual particle fluxes as follows.

The positive ion flux rate, j_i, is given by

$$j_i = - D_i \frac{dn_i}{dx} - \bar{\mu}_i n_i \frac{d\phi}{dx} \qquad (2\text{-}21)$$

where $\bar{\mu}_i$ is the positive ion mobility, D_i is the positive ion diffusion coefficient, ϕ is the electric potential caused by charge separation, and the positive ions are assumed to diffuse in the x-direction. The negative particle flux rates are given by

$$j_e = - D_e \frac{dn_e}{dx} + \bar{\mu}_e n_e \frac{d\phi}{dx} \qquad (2\text{-}22)$$

for the electrons and

$$j_n = - D_n \frac{dn_n}{dx} + \bar{\mu}_n n_n \frac{d\phi}{dx} \tag{2-23}$$

for the negative ions.

Multiplying Equation (21) by $\bar{\mu}_e n_e (d\phi/dx) + \bar{\mu}_n n_n (d\phi/dx)$ and multiplying Equations (22) and (23) by $\bar{\mu}_i n_i (d\phi/dx)$ and adding the results gives

$$j_i(\bar{\mu}_e n_e + \bar{\mu}_n n_n) + (j_e + j_n)\bar{\mu}_i n_i = - D_i \frac{dn_i}{dx} (\bar{\mu}_e n_e + \bar{\mu}_n n_n) \tag{2-24}$$

$$- D_e \frac{dn_e}{dx} \bar{\mu}_i n_i$$

$$- D_n \frac{dn_n}{dx} \bar{\mu}_i n_i \ .$$

Since the positively and negatively charged particles diffuse at the same rate

$$j_i = j_e + j_n \tag{2-25}$$

and Equation (24) becomes

$$j_i = \frac{- D_i \frac{dn_i}{dx} (\bar{\mu}_e n_e + \bar{\mu}_n n_n) - D_e \frac{dn_e}{dx} \bar{\mu}_i n_i - D_n \frac{dn_n}{dx} \bar{\mu}_i n_i}{\bar{\mu}_e n_e + \bar{\mu}_n n_n + \bar{\mu}_i n_i} \ . \tag{2-26}$$

Since the plasma remains neutral,

$$n_e = n_i - n_n = \left(1 - \frac{n_n}{n_i}\right) n_i \tag{2-27}$$

and, if it is assumed that n_n/n_i is a constant, Equation (26) becomes

$$j_i = \frac{- D_i\left[\bar{\mu}_e\left(1 - \frac{n_n}{n_i}\right) + \bar{\mu}_n \frac{n_n}{n_i}\right] - D_e\bar{\mu}_i\left(1 - \frac{n_n}{n_i}\right) - D_n \frac{n_n}{n_i}\bar{\mu}_i}{\left[\bar{\mu}_e\left(1 - \frac{n_n}{n_i}\right) + \bar{\mu}_n \frac{n_n}{n_i} + \bar{\mu}_i\right]} \frac{dn_i}{dx} . \tag{2-28}$$

Since the three types of charged particles diffuse through the plasma at the same rate, they can be treated as groups of particles diffusing through the plasma at a rate, j_g, given by

$$j_g = - D_a \frac{dn_g}{dx} \tag{2-29}$$

where n_g is the group number density given by

$$n_g = n_i \tag{2-30}$$

and D_a is the particle group diffusion coefficient known as the ambipolar diffusion coefficient. Substituting Equation (30) into Equation (29) and noting that

$$j_g = j_i \tag{2-31}$$

yields

$$j_i = - D_a \frac{dn_i}{dx} . \tag{2-32}$$

Comparing Equations (28) and (32) yields

$$D_a = \frac{D_i\left[\bar{\mu}_e\left(1 - \frac{n_n}{n_i}\right) + \bar{\mu}_n \frac{n_n}{n_i}\right] + D_e\bar{\mu}_i\left(1 - \frac{n_n}{n_i}\right) + D_n \frac{n_n}{n_i}\bar{\mu}_i}{\bar{\mu}_e\left(1 - \frac{n_n}{n_i}\right) + \bar{\mu}_n \frac{n_n}{n_i} + \bar{\mu}_i} \qquad (2\text{-}33)$$

for the ambipolar diffusion coefficient.

Boundary Layer Equations

The derivation of the boundary layer equations is, with certain exceptions, the work of Lees and Talbot and, as the method of derivation is well known, it will not be presented here. For the benefit of the reader, however, the complete derivation is presented in Appendix A.

With the assumptions of frozen flow and ambipolar diffusion, the boundary layer outside of the sheath surrounding the collecting electrode may be treated as a mixture of neutral molecules and particle groups composed of positive ions, negative ions, and electrons. These charged particles diffuse relatively to the neutral gas at a rate determined by Equation (29).

The charged particle group comcentration is defined as

$$c = \frac{\rho_i + \rho_n + \rho_e}{\rho} = \frac{m_i n_i + m_n n_n + m_e n_e}{m_i n_i + m_n n_n + m_e n_e + m_p n_p} \qquad (2\text{-}34)$$

or

$$c \approx \frac{n_i + \frac{m_n}{m_i} n_n}{n_i + \frac{m_n}{m_i} n_n + n_p} \qquad (2\text{-}35)$$

where m_p and n_p are the uncharged plasma particle masses and number densities. Starting with the customary boundary layer conservation equations for steady, frozen, axisymmetric flow which are

Charged particle concentration

$$\rho\left(u \frac{\partial c}{\partial x} + v \frac{\partial c}{\partial y}\right) = \frac{\partial}{\partial y}\left(\rho D_a \frac{\partial c}{\partial y}\right) \tag{2-36}$$

Continuity

$$\frac{\partial}{\partial x}(\rho u x) + \frac{\partial}{\partial y}(\rho v x) = 0 \tag{2-37}$$

Momentum

$$\rho u \frac{\partial u}{\partial x} + \rho v \frac{\partial u}{\partial y} = - \frac{dp_2}{dx} + \frac{\partial}{\partial y}\left(\mu \frac{\partial u}{\partial y}\right) \tag{2-38}$$

Energy

$$\rho u \frac{\partial h}{\partial x} + \rho v \frac{\partial h}{\partial y} = \frac{\partial}{\partial y}\left(\lambda_T \frac{\partial T}{\partial y}\right) + u \frac{dp_2}{dx} + \mu\left(\frac{\partial u}{\partial y}\right)^2 \tag{2-39}$$

where the subscript 2 denotes conditions in the flow outside of the boundary layer, λ_T is the coefficient of thermal conductivity, and h is the static enthalpy, it can be shown that the equations for the stagnation enthalpy and charged particle concentration in the region near the probe surface are given by

$$\bar{g}(\eta) = 0.50\, \bar{\sigma}^{1/3}\, \eta \tag{2-40}$$

and

$$c(\eta) = c(\eta_o) + c'(\eta_o) \int_{\eta_o}^{\eta} \left[\frac{f''(\eta)}{f''(\eta_o)}\right]^S d\eta \ . \qquad (2\text{-}41)$$

In Equations (40) and (41), S is the Schmidt number, $\bar{\sigma}$ is the Prandtl number, f is the Blasius function, η is a dimensionless coordinate given by

$$\eta = \frac{u_2}{(2s)^{\frac{1}{2}}} \int_o^y x\rho dy \ , \qquad (2\text{-}42)$$

where

$$s = \int_o^x \rho_2 u_2 \mu_2 x^2 dx \ , \qquad (2\text{-}43)$$

and $\bar{g}(\eta)$, given by

$$g(\eta) = \frac{\bar{h}_t(\eta)}{\bar{h}_{t2}} \ , \qquad (2\text{-}44)$$

is the ratio of the stagnation enthalpy at η to the stagnation enthalpy in the free stream.

At the stagnation point of a blunt body

$$u_2 = \bar{\beta} x \qquad (2\text{-}45)$$

and thus Equation (43) becomes

$$s = \frac{\rho_2 \mu_2 \bar{\beta}}{4} x^4 \ . \qquad (2\text{-}46)$$

Substituting Equation (46) into Equation (42) and solving for y yields

$$y = \left(\frac{\mu_2}{2\rho_2\overline{\beta}}\right)^{\frac{1}{2}} \int_0^{\eta} \frac{\rho_2}{\rho(\eta)}\, d\eta \ . \tag{2-47}$$

If the value of η is small and if the ion group concentration in the boundary layer is small, then

$$\frac{\rho_2}{\rho(\eta)} = \overline{g}(\eta) = 0.50\ \overline{\sigma}^{1/3}\ \eta \tag{2-48}$$

and Equation (47) becomes

$$y = 0.18\ \overline{\sigma}^{1/3} \left(\frac{\mu_2}{\rho_2\overline{\beta}}\right)^{1/2} \eta^2 \ , \tag{2-49}$$

where $\overline{\beta}$ is given by Equation (2).

Use of the Boundary Layer Equations

These stagnation point boundary layer equations are used in conjunction with an electrostatic probe theory, which will be developed later, to determine the free stream plasma properties in the following manner. By assuming that the specific heat, $\overline{c}_p$, is constant within the boundary layer, Equation (44) becomes

$$\overline{g}(\eta) = \frac{\overline{h}_t(\eta)}{\overline{h}_{t2}} = \frac{T_\eta}{T_2} \tag{2-50}$$

where T_η and T_2 are the temperature at η and the free stream stagnation temperature respectively. Thus, once the plasma temperature at the

sheath edge is determined, the free stream stagnation temperature can be determined from

$$T_2 = \frac{T_{\eta_d}}{\bar{g}(\eta_d)} \tag{2-51}$$

where η_d is the value of η corresponding to the sheath thickness, d, and is calculated from Equation (49) once the sheath thickness has been determined. The positive ion temperature, but not necessarily the electron temperature, can be assumed to be equal to the plasma temperature at the sheath edge and thus the free stream stagnation temperature can be determined from Equation (51), if an appropriate electrostatic probe theory can be used to calculate the ion temperature at the sheath edge and also to calculate the sheath thickness.

In the electrostatic probe theory, to be presented in Chapter III, the average thermal speed of the positive ions at the sheath edge is given by

$$\bar{c}(\eta_i) = \left[\frac{8kT_{\eta_d}}{\pi m_i}\right]^{\frac{1}{2}} \tag{2-52}$$

where k is the Boltzmann constant and m_i is the mass of a positive ion. In addition, the positive ion saturation current, j_i, is given by

$$j_i = \frac{1}{4} n_i e \bar{c}(\eta_i) \tag{2-53}$$

where e is the electronic charge and n_i is the positive ion number density at the sheath edge. Since the probe theory will permit the calculation of the sheath edge ion temperature directly from the current

voltage characteristic, Equations (51) through (53) can be used to determine the free stream stagnation temperature, T_2, and the sheath edge ion number density, n_i. With the temperature at the sheath edge known and the stagnation pressure determined by some method such as a pitot tube, the total particle density at the sheath edge can be determined and hence the positive ion concentration, c_i, at the sheath edge. Equation (41) can then be used to determine the free stream positive ion concentration if $c'(\eta_d)$ is known. As noted previously, one of the assumptions of the derivation was that the flow was chemically frozen in the boundary layer. Also, one of the assumptions of the electrostatic probe theory is that the probe surface removes a negligible amount of charged particles from the plasma. To be consistent with these two assumptions, there should be no ion concentration gradients in the probe boundary layer outside of the plasma sheath and thus in Equation (41)

$$c'(\eta_d) = 0 \tag{2-54}$$

and consequently the species concentration equation becomes

$$c_2 = c(\eta_d) \ . \tag{2-55}$$

The electrostatic probe theory permits the calculation of the electron temperature from the current-voltage characteristic and the electron number density from the electron saturation current. Since the relaxation time for electron cooling is much larger than the electron transit time through the boundary layer, the electron temperature at the sheath edge is equal to the electron temperature in the free stream. Also, since Equation (55) holds for the electrons as well

as the positive ions, the electron concentration at the sheath edge is equal to the electron concentration in the free stream.

The negative ion temperature and concentration at the sheath edge can be determined from the electrostatic probe theory, and again Equation (55) permits determination of the free stream negative ion concentration.

Thus the electrostatic probe theory can determine the positive ion, negative ion, and electron number densities and temperatures at the sheath edge, and the free stream stagnation temperature and charged particle concentrations can be determined from Equations (51) and (55).

CHAPTER III

ELECTROSTATIC PROBE THEORY

The electrostatic probe theory used in the present work was, with one modification which will be dealt with below, the theory of Hung and Paquette[19] which is the basic Langmuir theory for a collisionless plasma modified for the case of a plasma containing negative ions. This theory was chosen because of its simplicity and ease of application. In addition, as Talbot[12] notes, for the Langmuir theory, this theory may be more accurate than the more complex theories in the present application. The theory of Hung and Paquette is presented briefly in this chapter and is described in greater detail in Appendix B.

Theory of Hung and Paquette

In the present theory, the current density, j, of the charged particles crossing the sheath edge is assumed to be given by

$$j_{i,e,n} = \frac{en_{i,e,n}\bar{c}_{i,e,n}Z_{i,e,n}}{4} \tag{3-1}$$

where the subscripts i, e, and n indicate the positive ion, electron, and negative ion properties respectively, n is the particle number density, $\bar{c}$ is the average particle thermal speed, e is the electronic charge, and Z is the charge number. The current-voltage characteristic, shown in Figure 2, can be separated into four regions. These are the strongly negative, strongly positive, slightly negative, and slightly positive voltage regions.

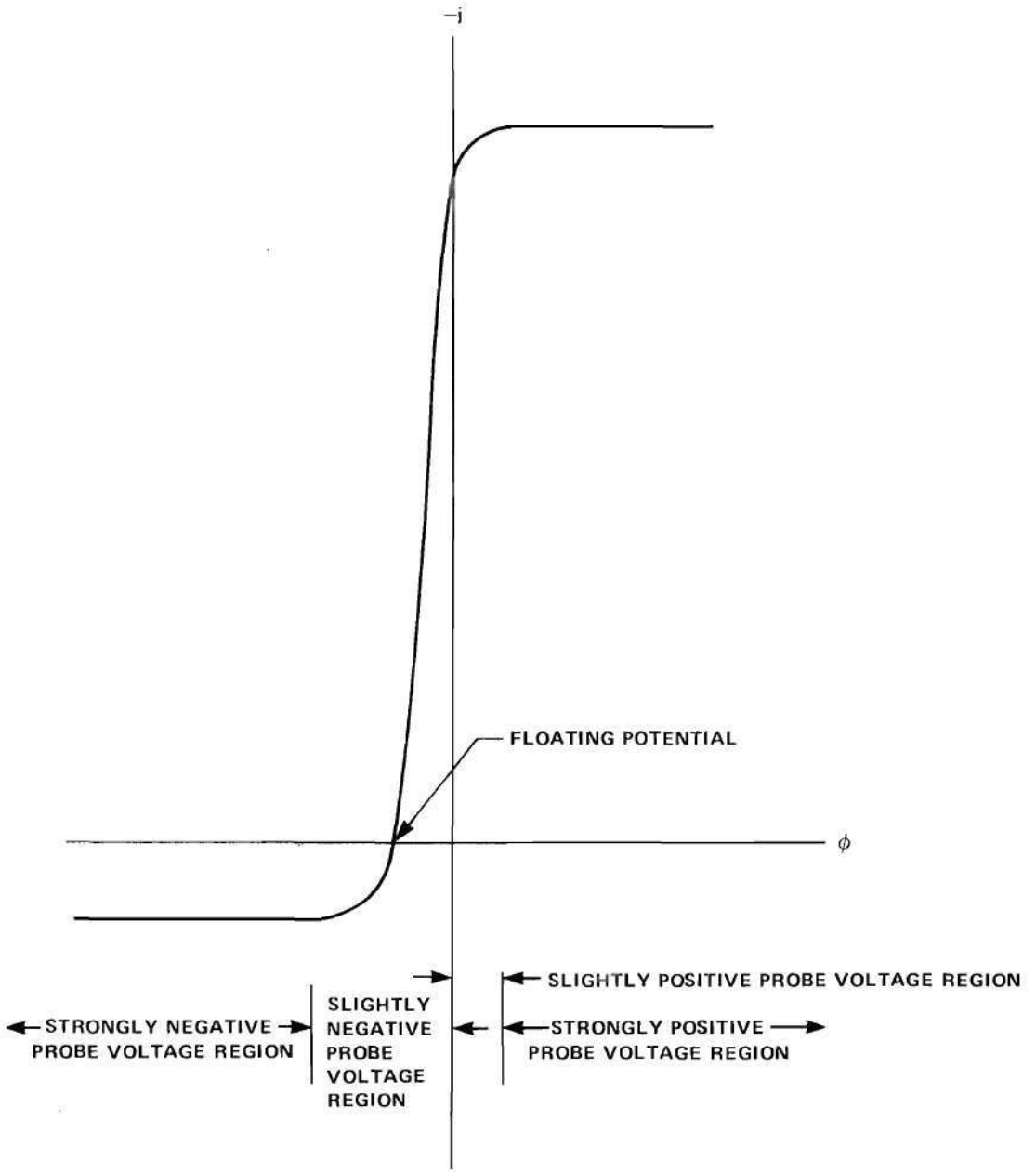

Figure 2. Current-Voltage Characteristic

Strongly Negative Voltage Region

The strongly negative probe voltage region is the case for which $\phi < 0$, and $|\phi|e >> kT_e$ where ϕ is the probe potential, k is the Boltzmann constant, and T_e is the electron temperature. In this case only positively charged ions are collected by the probe, and the current density, known as the positive ion saturation current, is

$$j_i = \frac{i_i}{A_i} \approx \frac{i_i}{A_w} = \frac{en_i\bar{c}_i}{4} \qquad (3\text{-}2)$$

where i_i is the probe current and A_i is the sheath area which is very nearly equal to the probe tip area, A_w, itself since the sheath thickness is small compared to the probe tip diameter.

Strongly Positive Voltage Region

The strongly positive probe voltage region is the case in which $\phi > 0$ and $|\phi|e >> kT_i$ and only electrons and negative ions are collected by the probe. The negative current density, $j_{e,n}$, known as the negative particle saturation current, is given by

$$j_{e,n} = \frac{i_{e,n}}{A_w} = \frac{i_e + i_n}{A_w} = -\frac{e}{4}(n_e\bar{c}_e + n_n\bar{c}_n) \ . \qquad (3\text{-}3)$$

Slightly Negative Voltage Region

The slightly negative probe voltage region is the case in which $\phi < 0$, but $|\phi|e$ is of the order of kT_e. All of the positive ions diffusing into the sheath are collected; and, in addition, those electrons and negative ions diffusing into the sheath and having kinetic energies in excess of $|\phi|e$ are also collected. The net current density is thus

$$j = j_i + j_e + j_n = \frac{e}{4}\left[n_i\bar{c}_i - n_e\bar{c}_e \exp\left(-\frac{e|\phi|}{kT_e}\right) - n_n\bar{c}_n \exp\left(-\frac{e|\phi|}{kT_n}\right)\right]. \tag{3-4}$$

The floating potential, ϕ_f, is defined as the potential at which no net current flows. If this potential is negative, then it is given by

$$\phi_f = \frac{kT_e}{e} \ln\left[\frac{n_i\bar{c}_i}{n_e\bar{c}_e} - \frac{n_n\bar{c}_n}{n_e\bar{c}_e} \exp\left(-\frac{e|\phi_f|}{kT_n}\right)\right]. \tag{3-5}$$

Slightly Positive Voltage Region

The slightly positive probe voltage region is the case in which $\phi > 0$ and $|\phi|e$ is of the order of kT_i. All of the negatively charged particles diffusing into the sheath are collected. In addition, those positive ions diffusing into the sheath and having energies in excess of $|\phi|e$ are also collected. The net current density is thus

$$j = j_i + j_e + j_n = \frac{e}{4}\left[n_i c_i \exp\left(-\frac{e\phi}{kT_i}\right) - n_e c_e - n_n c_n\right]. \tag{3-6}$$

Should the floating potential be positive, it is given by

$$\phi_f = \frac{kT_i}{e}\left[\ln\left(\frac{n_i\bar{c}_i}{n_e\bar{c}_e + n_n\bar{c}_n}\right)\right] \tag{3-7}$$

Sheath Thickness Equation

In the theory of Hung and Paquette, one of the major assumptions made is that the plasma sheath thickness is much less than the charged particle mean free path. This assumption simplifies the analysis and

results in positive and negative saturation currents which are constants and thus independent of the probe potential. For continuum flows, however, this assumption is not valid and it has been experimentally observed that both the positive and negative saturation currents are functions of the probe potential with the absolute value of the saturation currents increasing with the absolute value of the probe potential.

This change in saturation current with probe potential is due to the growth of the plasma sheath into the probe boundary layer with increasing probe potential magnitude. Since most sheath thickness equations have been derived for the case in which the mean free paths of the ions and electrons are greater than the sheath thickness, and the remaining equations either do not account for the presence of negative ions or require extensive computation, a new sheath thickness equation has to be derived. It is assumed that collisions within the sheath do not significantly effect the charged particle velocity distribution function and thus the theory of Hung and Paquette can still be used provided it is used with an appropriate sheath thickness equation.

The derivation of the new sheath thickness equation extends the general outline of the work of Cohen[3] and of Toba and Sayano[20] to express the sheath thickness as a function of the positive ion mean free path and to include the effect of the negative ions. The charged particle flux equations were integrated and the kinetic theory equations for the particle mean free paths and diffusion coefficients were substituted into the integrated equations to produce the sheath thickness equation. A detailed derivation of the sheath thickness equation is presented in Appendix C. When the probe potential is equal to the plasma

potential, the sheath thickness, d, is given by

$$d = \frac{\left(\frac{1 - \alpha}{\varepsilon} + \alpha + 1\right) \frac{3\pi}{4} \lambda}{1.19\left(\frac{1-\alpha}{\varepsilon} + \alpha\right) + (1 - \alpha)\sqrt{2}\,\frac{\bar{Q}_e}{\bar{Q}_i} + 1.68\alpha\left(\frac{m_p}{m_p + m_n}\right)^{\frac{1}{2}} \frac{\bar{Q}_n}{\bar{Q}_i}} \tag{3-8}$$

where m_p and m_n are the masses of the neutral particles and negative ions respectively, $\bar{Q}_e$, $\bar{Q}_i$, and $\bar{Q}_n$ are the cross sections for collisions of the electrons, positive ions, and negative ions respectively with the neutral plasma particles,

$$\alpha = \frac{n_n}{n_i} \tag{3-9}$$

is the ratio of the negative ion number density to the positive ion number density at the sheath edge,

$$\varepsilon = \frac{T_e}{T_i} \tag{3-10}$$

is the ratio of the electron temperature to the ion temperature at the sheath edge, and λ is the positive ion mean free path.

Use of the Electrostatic Probe Theory

As noted in Chapter II, the stagnation point boundary layer equations permit the determination of the free stream plasma conditions once the conditions at the plasma sheath edge have been determined. The use of the electrostatic probe theory to determine the sheath edge conditions is described below.

No Negative Ions in the Plasma

When it is known that no negative ions are present in the plasma, the electron temperature can be determined from Equation (4). By subtracting Equation (2) from Equation (4) and differentiating the logarithm of the result with respect to ϕ, the equation for T_e becomes

$$T_e = \frac{e}{k \dfrac{d\,\ell n|j_e|}{d\phi}} \quad . \tag{3-11}$$

Equation (5) can then be used to determine the ion temperature since

$$\frac{\bar{c}_i}{\bar{c}_e} = \sqrt{\frac{m_e T_i}{m_i T_e}} \tag{3-12}$$

where m_e and m_i are the masses of the electrons and positive ions respectively. The positive ion number density, which is equal to the electron number density in this case, is then determined from Equation (2) where $\bar{c}_i$ is given by

$$\bar{c}_i = \sqrt{\frac{8kT_i}{\pi m_i}} \quad . \tag{3-13}$$

The pressure at the stagnation point, p_o, is determined by some method, such as a pitot tube, and the total particle number density, n, at the sheath edge is determined from

$$n = n_p + n_i + n_e = \frac{p_o}{kT_i} \tag{3-14}$$

where n_p is the neutral gas number density and T_e has been assumed equal to T_i in this equation for simplicity. The magnitude of n_e is

is usually small compared to n_p and thus this approximation does not cause much error. The positive ion concentration at the sheath edge, c_i, is then determined from

$$c_i = \frac{n_i}{n - n_e} = \frac{n_i}{n - n_i} . \tag{3-15}$$

Also, the ion mean free path is determined from

$$\lambda = \frac{1}{\sqrt{2}\, n\bar{Q}_i} . \tag{3-16}$$

Equation (8) with

$$\alpha = 0 \tag{3-17}$$

is then used to determine the sheath thickness, d. With the ion and electron temperatures and concentrations at the sheath edge known and the sheath thickness known, the stagnation point boundary layer equations can then be used to determine the free stream conditions.

Negative Ions in the Plasma

When negative ions are present in the flow, the method of determination of the sheath edge properties is somewhat different. In this case the electron temperature can also be determined using Equation (11). This is due to the much greater mass of the negative ions as compared to the electrons and the consequent result that

$$\bar{c}_n << \bar{c}_e \tag{3-18}$$

and thus, in Equation (4), unless the electron number density is very

much less than the negative ion number density,

$$n_e \bar{c}_e \exp\left(-\frac{e|\phi|}{kT_e}\right) >> n_n \bar{c}_n \exp\left(-\frac{e|\phi|}{kT_n}\right) . \quad (3\text{-}19)$$

The ion number density, however, can no longer be determined from Equation (5) unless the ratio of electrons to positive ions is known.

Nearly Complete Electron Absorption. If the ratio of electrons to positive ions is not known, but the negative particle saturation current is comparable in magnitude to the positive ion saturation current and can be measured accurately, then the ion temperature can be determined by subtracting Equation (3) from Equation (6) and differentiating the logarithm of the result. The positive ion number density can then be determined from Equation (2). Since

$$n_i = n_e + n_n , \quad (3\text{-}20)$$

and since the positive ion and negative ion temperatures should be approximately equal, then the electron and negative ion number densities can be determined from Equation (3) where

$$\bar{c}_e = \sqrt{\frac{8kT_e}{\pi m_e}} \quad (3\text{-}21)$$

and

$$\bar{c}_n = \sqrt{\frac{8kT_n}{\pi m_n}} . \quad (3\text{-}22)$$

The remainder of the analysis proceeds as before, with the exception that α is no longer equal to zero.

Partial Electron Absorption. When the negative particle currents are too large to permit the use of Equation (6) to determine the positive ion temperature, one additional bit of information is needed to solve for the plasma properties at the sheath edge. The nature of this additional bit of information is dependent upon the type of plasma analysis being performed. For the type of analysis in which the ratio of electrons or negative ions to positive ions is known in the plasma, and hence also at the sheath edge, Equation (5) can be used to determine the positive ion temperature at the sheath edge. This is because the second term in the logarithm of Equation (5) is normally negligible compared to the first term. The analysis then proceeds as outlined above. This situation would occur in a plasma in which an electrophilic additive of known effectiveness had been added in order to reduce the electron concentration. This might be done in order to reduce damage to the electrostatic probe or distortion of the current-voltage characteristic caused by high electron saturation currents.

When the ratio of electrons to positive ions is not known, as would be the case when the effectiveness of an electrophilic additive is being analyzed, the additional information must come from the free stream flow properties. The solution is then reached by an iterative process. If, as would normally be the case, the known free stream property is the stagnation temperature, the iteration process proceeds as follows. A ratio of electron number density to positive ion number density is chosen and Equation (5) is then solved for a sheath edge ion temperature. Equations (8), (14), and (16) are then used to determine a sheath edge thickness. The sheath edge temperature, the sheath

thickness, and the stagnation point boundary layer equations are then used to determine a free stream stagnation temperature. This temperature is then compared to the known free stream stagnation temperature. The ratio of electron number density to positive ion number density is then iterated until the calculated free stream stagnation temperature equals the known temperature. Once the ion temperature at the sheath edge has been determined, the remaining sheath edge parameters are determined in the manner outlined above.

CHAPTER IV

EXPERIMENTAL TEST PROGRAM

A test program was undertaken to experimentally evaluate the electrostatic probe theory presented in Chapter III. The test conditions were chosen to approximate those of current interest such as those in a magnetohydrodynamic generator or in a reentry plasma.

Test Conditions

The most likely use of a stagnation point electrostatic probe would be to analyze a plasma flowing at supersonic speeds. In all flow situations, however, the probe itself would remain in a subsonic flow field because at supersonic free-stream speeds a normal shock wave would form in front of the probe and thus produce subsonic flow around the probe. Since the probe remains in subsonic flow for all free stream conditions, it was decided to conduct the experimental tests with the free stream plasma flowing subsonically. The choice of subsonic flow in the free stream made it unnecessary to correct the free stream conditions for the effect of the shock wave in front of the probe and thus eliminated possible sources of error caused by an inexact analysis of the effects of the shock.

The static pressure of the plasma was varied between 15 mm. Hg. and 45 mm. Hg. and the plasma free stream total enthalpy was varied between 4×10^4 k-cal./kg-mole and 6×10^4 k-cal./kg-mole with two data points at 7×10^4 k-cal./kg-mole and two data points at 9×10^4

k-cal./kg-mole. At these pressures and enthalpies, the expected free stream ionizations varied from 0.024 percent to 3.6 percent, the ion mean free path varied from 8.9×10^{-3} to 2.04×10^{-2} cm, and the sheath thickness varied from 1.73×10^{-2} to 5.05×10^{-2} cm. Since the electrostatic probe collecting electrode was 0.15 cm in diameter, the ratio of ion mean free path to electrode diameter was approximately 0.1 and the ratio of sheath thickness to electrode diameter was approximately 0.2. During the experimental investigation, the ratio of the negative ion number density to the positive ion number density was varied from 0 to essentially 1 by the addition of measured amounts of sulphur hexafluoride and uranium hexafluoride. The sulphur hexafluoride number density varied from 0 percent to 0.46 percent of the argon number density and the uranium hexafluoride number density varied from 0 percent to 0.025 percent of the argon number density.

Experimental Apparatus

A continuous flow plasma jet facility, shown in Figure 3, was used for the experiments. The facility uses an L-500 Plasma Torch manufactured by Thermal Dynamics Corporation. The torch is shown in Figure 4. Power is supplied to the facility by five 60 kilowatt welding power supplies arranged in parallel to provide 300 kilowatts of power and a maximum output voltage of 100 volts. The vacuum tank and the heat exchanger are stainless steel and are water cooled. The vacuum pumps are a Stokes Microvac Pump Model No. 412 H-10 capable of pumping 300 $ft.^3$/min of argon and a Stokes Model No. 900-170-22 forepump capable of pumping 1250 $ft.^3$/min of argon. High purity argon is

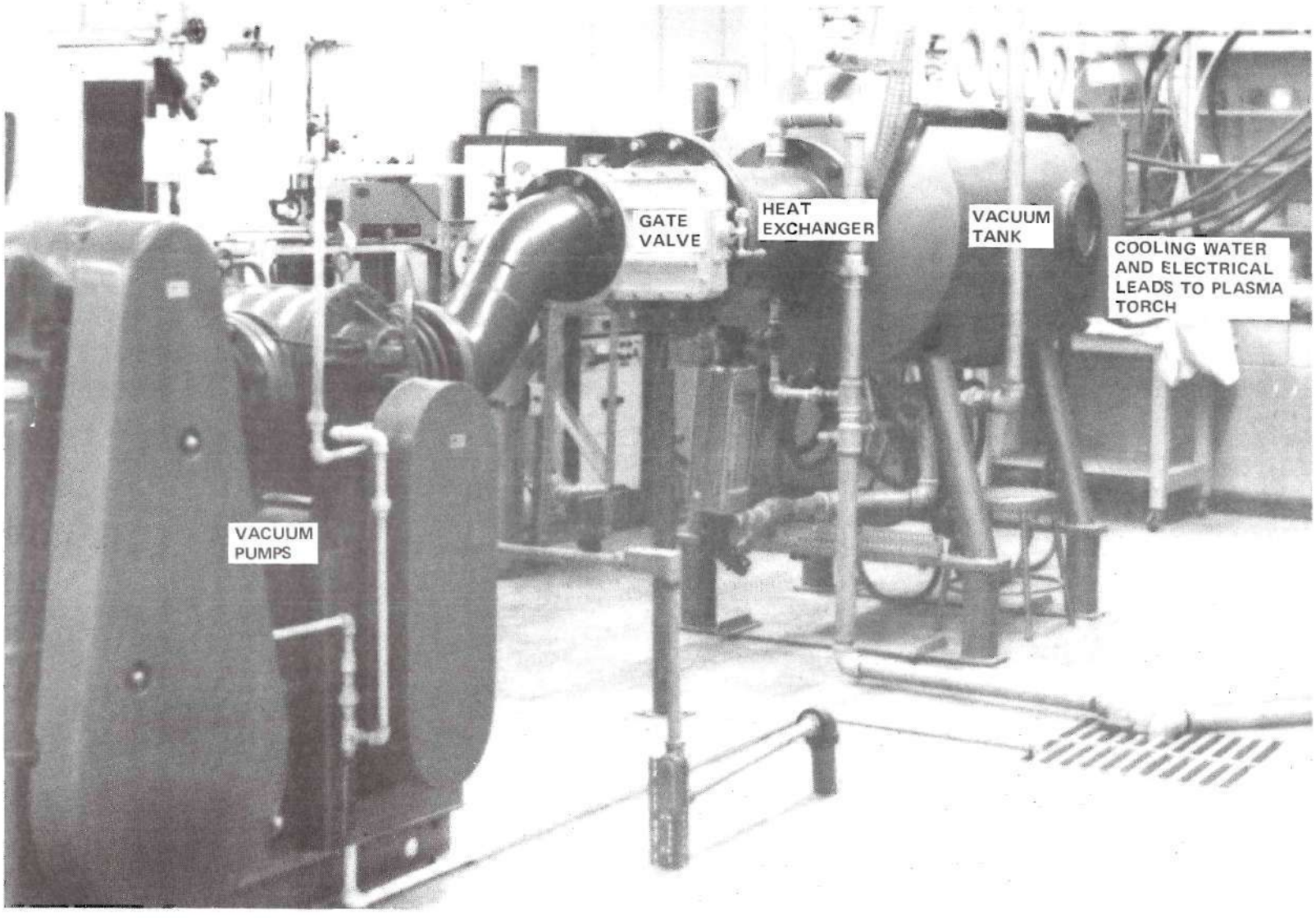

Figure 3. Plasma Torch Facility

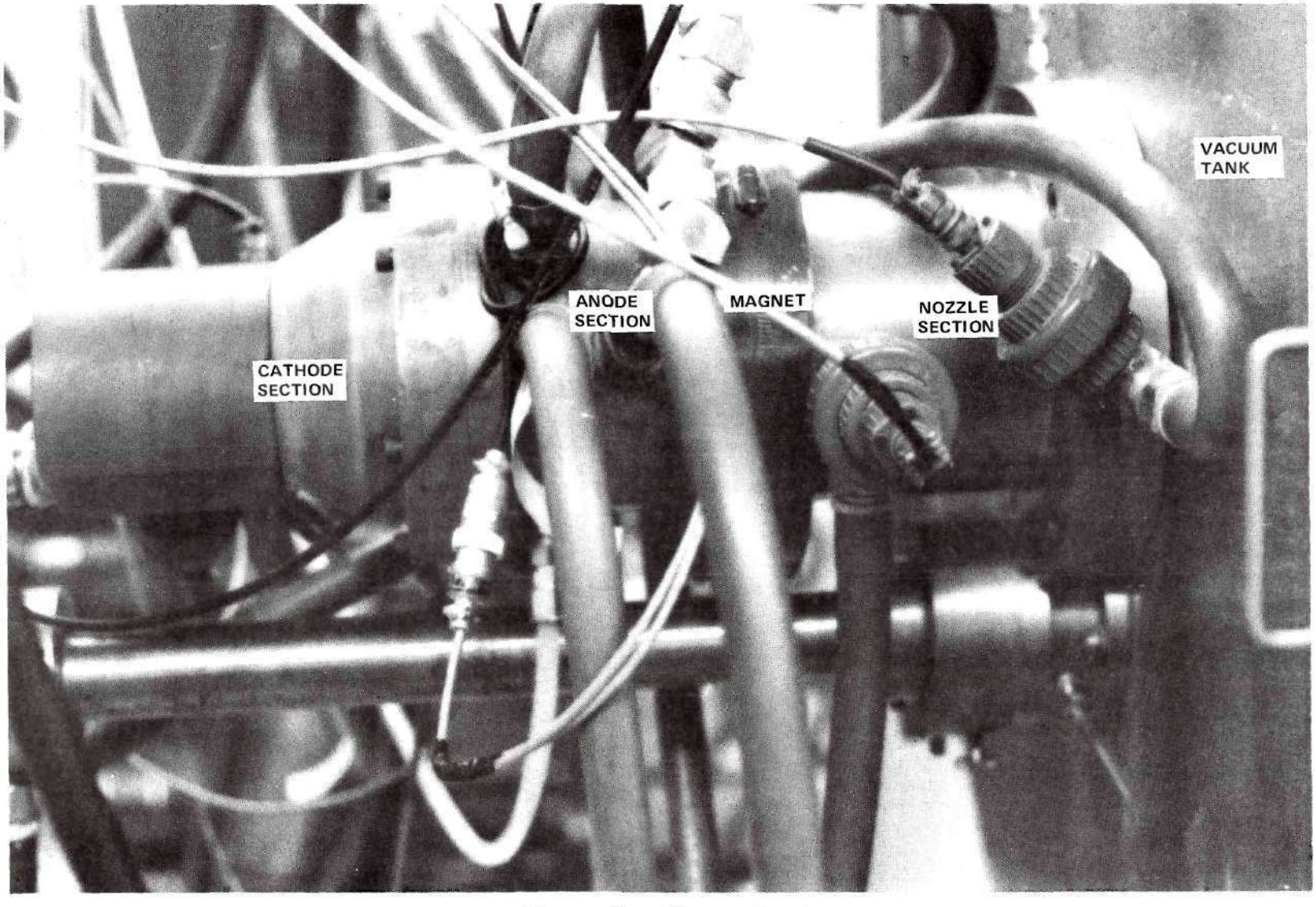

Figure 4. Plasma Torch

supplied from a manifold which can be connected to as many as six bottles of compressed argon at one time.

The electrostatic probe used is shown in Figure 5. The 1.91 cm diameter probe was constructed from copper and mounted on a movable stainless steel sting. The electrode at the probe tip is steel, 0.15 cm in diameter with a glass insulator. The entire probe is water cooled.

Two D.C. power supplies are used to provide the electrical potential to the probe tip. One is a Power Designs, Inc. Model TW5005. This model is a twin power supply which can be wired to supply up to $\pm$50 volts D.C. and up to $\pm$500 ma. current. The other is a Hewlett-Packard, Harrison 6433B D.C. Power Supply. This model can supply up to 40 volts D.C. and 12 amps current.

The negative ions were produced by injecting sulphur hexafluoride or uranium hexafluoride into the plasma. These additives were injected perpendicularly to the plasma flow through two thin tubes as shown in Figure 6. The volume flow rate of the sulphur hexafluoride was measured by determining the pressure drop in a small diameter tube through which the undiluted additive flowed before being injected into the plasma. The flow rate was calibrated by measuring the amount of water displaced in a vessel by the flowing sulphur hexafluoride in a given time for a given pressure differential. The sulphur hexafluoride proved to be a very effective electrophilic additive and this result necessitated smaller than expected additive flow rates. These lower flow rates produced a smaller pressure drop in the thin tube than had originally been expected and consequently instrumentation errors in the pressure measurements became more significant than had initially been anticipated.

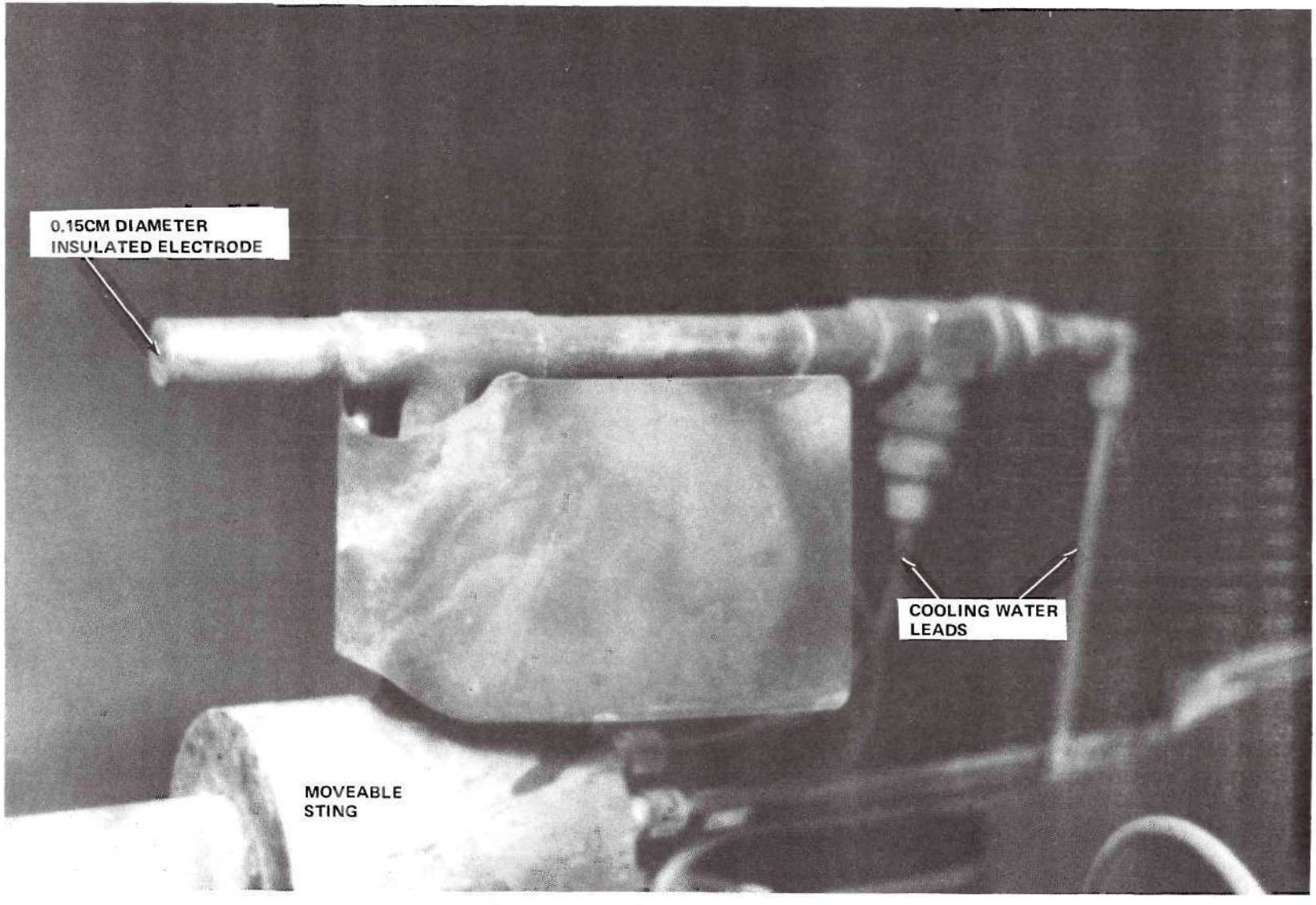

Figure 5. Electrostatic Probe

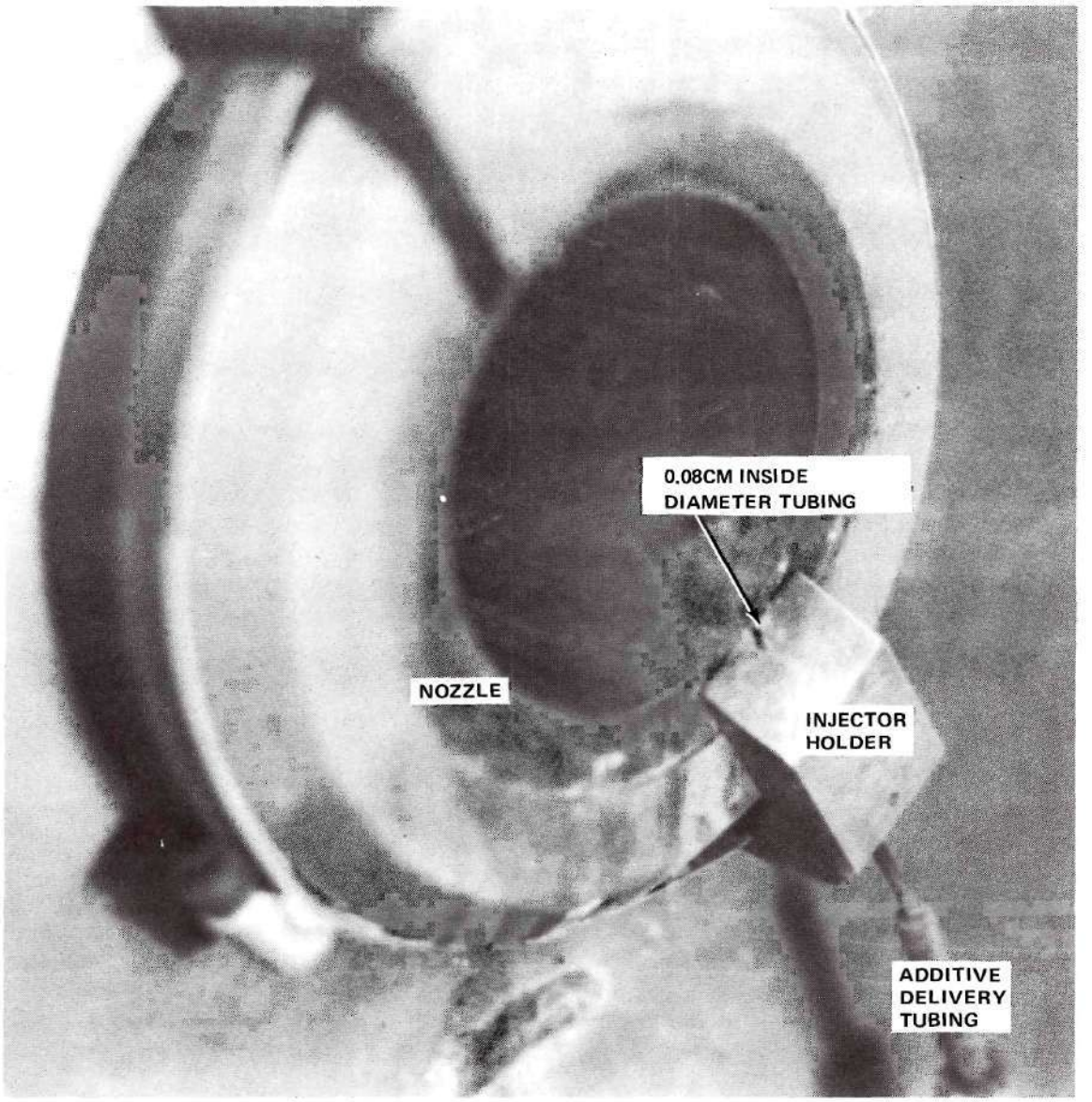

Figure 6. Additive Injector

In the present experiments, the probable error in the sulphur hexafluoride flow rate measurements is estimated to be no larger than ±20 percent. For the higher additive flow rates, the error is probably no larger than ±10 percent. These errors represent the accuracy to which the pressure drop could be read. The flow rate was controlled by a Matheson Model No. 9-590 Pressure Regulator which regulated the upstream pressure in the tube and a valve downstream of the tube which was adjusted to maintain a constant pressure at the downstream end of the tube. The sulphur hexafluoride was injected into the plasma in an undiluted form to minimize possible errors caused by cooling of the plasma when the cooler gas was injected. The uranium hexafluoride flow rate was determined by measuring the rate at which the pressure dropped in a vessel containing a mixture of uranium hexafluoride and argon the volume of which was 458 cm^3 maintained at a constant temperature of 90°C. The uranium hexafluoride and argon were premixed because insufficient uranium hexafluoride was obtainable to permit its use in the undiluted form. Two valves were employed to control the uranium hexafluoride flow. One was used to control the flow rate and the other was used to start or stop the flow as needed. Additional argon was added, as needed, to maintain the pressure of the mixture at a higher level than the pressure of the vacuum tank.

Instrumentation

All data were recorded with an 18 channel Consolidated Electrodynamics Corporation Recording Oscillograph Model No. 5-124A. The quantities measured were the torch voltage and amperage, the pressures of the plenum chamber, nozzle exit, and vacuum tank, the cooling water

flow rates in the cathode, anode, and nozzle as well as the water temperature rise in these cooling circuits. The appropriate pressures to determine the additive flow rates were also measured. In addition, the current and voltage of the electrostatic probe and the stagnation pressure were measured. The stagnation pressure at the location of the electrostatic probe was measured by a pitot tube placed in the plasma stream. The pitot tube had the same dimensions as the electrostatic probe and the pressure tap was located in the same relative position as the collecting electrode. The argon flow rate was measured by a calibrated orifice meter. All of the pressures were measured by strain guage pressure transducers and the water flow rates were measured by orifices connected to differential pressure transducers. The torch current was measured by using a 6000 amp air-cooled shunt and the torch voltage was measured directly. The cooling water temperature rise in each component was measured by two thermistors, one located at the water inlet and the other at the discharge of the cooling water, electrically connected in a balanced Wheatstone bridge.

CHAPTER V

DISCUSSION OF THE HEAT BALANCE TECHNIQUE

The electrostatic probe theory developed in this work was verified by comparing the plasma conditions predicted by the probe theory to known plasma conditions. The probe was placed in a flowing plasma and the current-voltage characteristic curve of the plasma was determined. The probe theory was then used to predict the plasma temperature and the ion number density. The predicted temperature and ion number density were compared to the values predicted by performing a heat balance on the plasma with the assumption that the plasma was in equilibrium.

The heat balance technique was used to determine the plasma enthalpy because of its simplicity. Other investigators have used more complicated methods such as spectroscopy to determine the enthalpy or temperature of the plasma but all of these methods have been more difficult to use and have had experimental errors at least as large as those inherent in the heat balance technique. Use of the heat balance technique thus resulted in no loss of experimental accuracy but did increase the ease of data acquisition.

In the present experiments, the gross energy input to the plasma was calculated by measuring the voltage drop and electrical current through the plasma. The total energy losses were assumed to be confined to losses to the cooling water. These losses were determined by measuring the water flow in the cooling circuits and the water

temperature changes in these circuits. The net energy input to the plasma was assumed to be the difference between the gross energy input and the losses in the cooling water. Losses due to diffusion and radiation were neglected. During the initial stages of the experimental investigation, the plasma jet was traversed radially by the electrostatic probe. The plasma temperature and ionization were found to be uniform throughout the jet cross section. This indicated that the enthalpy distribution in the plasma stream was uniform. To reduce potential errors, care was taken to allow the torch voltage and amperage as well as the water flows and temperatures to stabilize before any data were taken. A discussion of the magnitudes of the experimental error associated with the heat balance technique follows.

Error Caused by Instrumentation

Much of the experimental error associated with the heat balance technique is introduced by the instrumentation and the size of this error must be determined to evaluate the accuracy of the technique. The argon flow rates were measured by orifice meters. These meters were calibrated by comparing their readings to the flow rates measured by a set of high accuracy flow meters. These calibrations were repeated during the experiments and they showed good repeatability indicating that there was negligible drift in the calibrations. The error in determining the argon flow rate is estimated to be about 2 percent. This represents the accuracy to which the meters can be read.

The plasma torch currents and voltages were recorded on an oscillograph using sensitive galvanometers. The voltage calibrations were made by comparing the galvanometer deflections to a known voltage

input. These calibrations were also repeated during the experiments and they showed excellent repeatability. The plasma torch amperage was measured by determining the voltage drop in a low resistance air-cooled shunt. The amperage calibrations were made by comparing the galvanometer deflections to a known voltage input which equaled the voltage drop in the shunt caused by a predetermined current. These calibrations were also repeatable. The errors in determining the plasma torch voltage and amperage are each estimated to be approximately 1 percent. This represents the accuracy to which the galvanometer deflections can be read.

The cooling water flow rates were measured by orifices connected to differential pressure transducers whose output was recorded on the oscillograph. The water flow rates were calibrated using a water weighing technique in which the water flow rate for a given cooling circuit was adjusted to produce a predetermined galvanometer deflection and then the amount of water discharged through the cooling circuit in a measured amount of time was determined by weighing the discharged water. The total amount of water discharged and the time allowed for the water flow were kept large compared to potential errors in starting and stopping the timer and the water flow in order to minimize any calibration errors. These calibrations were repeated during the experiments and also showed little drift. The error in determining the water flow rates is estimated to be about 5 percent. This represents the accuracy to which the galvanometer deflections can be read.

The largest source of instrumentation error occurred in the measurements of the cooling water temperature changes. These temperature changes were measured in each cooling circuit by two high accuracy

thermistors placed in a balanced Whetstone bridge. One thermistor was placed at the inlet of the cooling circuit and the other at the exit. The voltage output of the bridge was proportional to the water temperature differential between the two thermistors. The errors would occur whenever random fluctuations in the inlet water temperatures occurred. To minimize these fluctuations, the cooling water was allowed to run for several minutes before any data were taken. In addition, care was taken to avoid using the extreme values of the temperature differentials and instead to use values which were between the high and low extremes. Because of the care taken to minimize the random fluctuations in the water differential temperature readings, the probable error associated with these readings is believed to be no greater than 5 to 10 percent.

Error Caused by Neglecting Diffusion Effects

Because the effects of diffusion were neglected in the heat balance calculations, the magnitude of these effects should be examined. Care was taken to minimize any effect due to diffusion.

To make the flow as uniform as possible, the plasma was allowed to settle in a plenum chamber and come to an equilibrium condition before exhausting into the test chamber. Further, the probe was placed in the plasma so that it remained within the potential core of the plasma jet. Since the potential core was the brightest part of the jet, it was possible to visually locate the probe within the plasma potential core. In addition to the visual check, other investigators have experimentally determined the length of the potential core as a function of the initial core diameter. Data from several of these experiments are reported by Audeh[21] and show a jet potential core length of 5 to 10 times the initial

jet diameter. For the 15-20 mm. Hg. and the 40-45 mm. Hg. pressure data, the probe was placed 5 inches from the nozzle exit. For the 30 mm. Hg. pressure data, the probe was placed 10 inches from the nozzle exit. Since the initial jet diameter was visually observed to be approximately 2 inches, the expected potential core length of 10 to 20 inches was adequate to insure that the probe tip was within the potential core of the jet and thus unaffected by the diffusion effects. It was thus concluded that diffusion effects were negligible.

Error Caused by Neglecting Losses Due to Radiation

The energy loss due to radiation in an argon plasma has been measured by Menard, Thomas, and Helliwell[22] for an argon number density of 2×10^{17} cm^{-3} and a temperature range of 9000°K to 16,000°K. At a temperature of 10,000°K the radiation loss was found to be 0.1 watt/cm^3-ster. If the radiating portion of the plasma jet is assumed to be a cylinder 1 inch in radius and 10 inches long its volume is

$$V = 514.8 \text{ cm}^3 . \tag{5-1}$$

The highest free stream plasma temperature measured in the experiments was found to be 10,000°K and thus a conservative estimate of the radiation loss rate, $\dot{Q}$, for a 10-inch length section of the jet is given by

$$\dot{Q} = 37 \frac{\text{BTU}}{\text{min}} . \tag{5-2}$$

The rate of heat addition to the plasma varied from 700 BTU/min to 3400 BTU/min. Thus the energy loss due to radiation varied from about

1 to 5 percent of the total energy contained in the plasma. Actually, for the lowest heat addition rates, the probe was only 5 inches from the nozzle exit thus reducing the maximum percentage loss to about 2.6 percent. Since 10,000°K is an upper limit, the actual loss due to radiation is generally much lower than these estimates.

Assumption that the Plasma is in Equilibrium

The plasma reached an initial state of equilibrium in the plenum chamber before being injected into the vacuum tank. In order for the assumption of equilibrium in the free stream plasma to be valid, there must be adequate time in the flow between the plenum chamber and the electrostatic probe to allow the particles to reach a new state of equilibrium. If the free stream plasma temperature in the vacuum tank is assumed to be 10,000°K and the plasma is flowing at its sonic velocity, then the plasma velocity is 2×10^5 cm/sec. The distance from the plenum chamber to the location of the electrostatic probe is 20 cm, or greater, and hence the minimum transit time for the plasma is 10^{-4} seconds.

Since the ionization level is dropping during this time, the appropriate reaction to examine is the ion recombination reaction. Equation (3) of Chapter II gives the recombination equation as

$$\frac{n_i}{n_{i2}} = \frac{1}{1 + \alpha_r n_{i2} t} \qquad (5\text{-}3)$$

where n_i is the positive ion number density after time t, α_r is the recombination coefficient, and n_{i2} is the initial positive ion number density. The value given by Maxwell and Wessling[17] for α_r is

$$\alpha_r = 10^{-10} \text{ cm}^3/\text{sec} \tag{5-4}$$

and the positive ion number density in the plenum chamber was on the order of 10^{16} cm^{-3}. Equation (3) thus gives

$$\frac{n_i}{n_{i2}} = 0.01 \tag{5-5}$$

indicating that, unless the free stream equilibrium positive ion number density is less than 10^{14} cm^{-3}, the plasma will be in equilibrium at the location of the probe. In the present experiments, the free stream equilibrium positive ion number density was greater than 10^{14} cm^{-3}. In addition, the plasma velocity was less than the sonic velocity and hence the time for recombination was actually greater than 10^{-4} seconds.

Overall Estimate of the Error of the Heat Balance Technique

The total estimated error introduced by the instrumentation errors and by the diffusion and radiation assumptions is given by the square root of the sum of the squares of the individual errors. Thus the total estimated experimental error in the heat balance technique is about 7 to 13 percent.

Comparison of the Heat Balance to Other Methods

The experimental errors of other plasma diagnostic techniques have been evaluated by other authors and should be examined in order to determine if the experimental error of the heat balance is acceptable. Swift and Schwar[23] have examined the experimental error associated with the microwave transmission technique. The technique makes use of the

fact that when a high frequency electromagnetic wave is passed through a plasma it is attenuated and also undergoes a phase shift. The magnitudes of the attenuation and phase shift are dependent upon the plasma electron density. One method of using the technique is to vary the frequency of the wave passing through the plasma until the wave ceases to penetrate the plasma. The frequency at which the wave propagation ceases is known as the cut-off frequency and it is directly proportional to the square root of the electron number density. Swift and Schwar note that this method shows little experimental error for plasma pressures below 10^{-2} mm. Hg. but that above this pressure the error increases rapidly. At a plasma pressure of 5×10^{-2} mm. Hg. the experimental error is 30 percent.

The second method of using the microwave transmission technique is to measure the phase shift which occurs as the microwaves pass through the plasma. Swift and Schwar note that this method has an experimental error of approximately 25 percent.

For both methods, the microwave wavelength, δ, must satisfy the relation

$$\delta < 3.3 \times 10^{6} \, n_e^{-\frac{1}{2}} \text{ cm} \qquad (5\text{-}6)$$

in order for the waves to be transmitted through the plasma. Swift and Schwar note that because of the difficulties involved in working at wavelengths below 4 mm. these methods are limited to electron densities below 10^{14} cm^{-3}. It should be further noted that while these methods permit the determination of the electron number density they do not permit the determination of the electron, positive ion, or

negative ion temperatures; nor, if negative ions are present in the plasma, do they permit the determination of the positive and negative ion number densities.

Additional methods of plasma diagnostics have been discussed by Huddlestone and Leonard.[24] The methods include magnetic probes, spectrographic methods, optical interferometry techniques, microwave techniques, and particle measurement techniques. Of these methods, only the spectrographic, optical interferometry, and microwave methods are applicable to the present experiments. The microwave techniques presented are similar to those discussed by Swift and Schwar and they are subject to the same limitations.

The spectrographic methods discussed involved studies of spectral intensities and line broadening using optical and ultraviolet techniques, x-ray spectroscopy, and far-infrared techniques. The spectral intensity method involves an examination of the relative, as well as absolute, intensities of spectral lines produced by the plasma. These spectral lines are produced by the transitions of electrons within the plasma from one energy state to another and the interpretation of these spectral lines is dependent upon the molecular model used in the analysis. Huddlestone and Leonard described several plasma models and estimate that their experimental error varies from 30 percent to 300 percent. An additional consideration in the use of the spectral intensity method is the accuracy of the intensity calibration of the spectroscopic instrumentation. Huddlestone and Leonard have noted that, in the visible and near-ultraviolet regions, calibration against a tungsten filament lamp or carbon arc is possible with a precision of a few percent but that for higher

frequency radiation the calibration is less precise. In the soft x-ray region, they note that the calibration error is about 40 percent.

The line broadening method differs from the spectral intensity method in that the width of the spectral line rather than its intensity is used to determine the plasma properties. The two dominant causes of line broadening are the Doppler effect and the Stark effect. The Doppler broadening of the spectral lines is caused by the motion of the radiating body relative to the spectrograph, while the Stark broadening is caused by the interactions of the charged particles within the plasma which cause perturbations in the radiation frequency. The degree of line broadening from the Doppler effect is dependent upon the plasma temperature while the degree of line broadening from the Stark effect is dependent upon the electron density as well as the plasma temperature. As an example of the magnitude of the line broadening effects, Huddlestone and Leonard note that for argon at a temperature of 2×10^4°K with an electron number density of 10^{15} cm^{-3} the line broadening half width for the 4806 Å line is 0.0014 Å for the Stark effect and 0.08 Å for the Doppler effect. In addition, they note that an experimental resolution of better than 0.1 Å is quite difficult to achieve. With this degree of resolution, the experimental error would be expected to be on the order of 100 percent. If the proper equipment is used, however, the experimental error can be reduced. Huddlestone and Leonard report that in a study of an argon plasma in which the temperature was 1.1×10^4°K and the electron number density was 10^{15} cm^{-3} the experimental error, averaged over 13 lines, was 5 percent; but, for the individual lines, errors of up to 30 percent were encountered. In addition to the previously noted difficulties in achieving adequate spectral

resolution, other problems with the line broadening method were noted. These problems included the necessity for the plasma properties to remain constant for a time sufficient to record the spectrum and also the distortion to the line profile caused by other broadening mechanisms or self-absorption within the plasma. In concluding their analysis of the line broadening method, Huddlestone and Leonard estimated that, if precise line profiles can be obtained and if the results from several lines are averaged, the method will give results which are accurate to within 15 percent.

The optical interferometry technique makes use of the fact that the refractive index of the plasma varies with the electron number density. By measuring the changes produced in the interference pattern when light is passed through the plasma, the electron number density can be deduced. The technique requires that the light path be sufficiently long so that only the macroscopic properties of the plasma influence the refraction. The light source must also be brighter than the plasma so that it can be observed and, additionally, the plasma must be optically thin so that little of the light is absorbed by the plasma. In an experiment in which the electron concentration in a hydrogen plasma was determined by the optical interferometry technique, an examination of the continuum radiation intensity, and the line broadening method, Huddlestone and Leonard report that the results for the optical interferometry method agreed with the results of the line broadening method, differed from the results of the continuum radiation examination by 22 percent, and exhibited an experimental uncertainty of ± 9 percent.

The diagnostic techniques described above exhibit experimental errors which are equal to or greater than those of the heat balance technique. In addition they are more difficult to use and require more complex experimental equipment. Also, since the heat balance technique gives the plasma enthalpy directly, all of the equilibrium plasma properties can be determined using that technique while the other techniques, in general, yield this information less directly. For these reasons, the experimental error of the heat balance is considered to be acceptable for the present experiments.

CHAPTER VI

RESULTS AND DISCUSSION

The electrostatic probe theory was evaluated for its ability to determine the plasma temperature and degree of ionization. The free stream stagnation temperatures and ionization percentages predicted by the electrostatic probe theory were compared to the values predicted by the heat balance technique. In addition, the electrophilic additives sulphur hexafluoride and uranium hexafluoride were injected into the plasma and the effectiveness of these additives was measured.

Analysis of the Probe Results for Temperature Predictions

The electrostatic probe can be used to predict free stream plasma temperatures only when the ion temperature at the plasma sheath can be determined or when the ratio of electrons to positive ions is known or can be determined. When analyzing a plasma to which an electrophilic compound has been added, the ratio of electrons to positive ions can be determined if the effectiveness of the additive is known. In the present experiments, this effectiveness was not known and was in fact one of the parameters under investigation. Thus, verification of the probe theory was limited to test conditions which permitted a determination of the positive ion temperature at the sheath edge. These test conditions occurred when there was no electrophilic additive present in the plasma, and hence no electron absorption, and also when there was sufficient additive present to absorb virtually all of the electrons, thus making

it possible to observe the change in positive ion current with changes in probe potential. Data were taken for each of these two conditions and the plasma temperatures predicted by the probe theory were compared to the plasma temperatures predicted by the heat balance.

Results for No Electron Absorption

Seven data points were obtained in which no electrophilic additive was present in the plasma. These data points were taken over a static pressure range of 15 to 45 mm. Hg. and an enthalpy range of 4×10^4 to 9×10^4 k-cal./kg.-mole. The low number of data points is due to the high electron densities and the growth of the plasma sheath with increasing probe potential which made it very difficult to achieve electron saturation. In addition, the high currents at the collecting electrode often severely damaged the electrode, thus preventing a determination of the electron saturation current.

The free-stream stagnation temperatures predicted using the probe theory and the heat balance are plotted in Figure 7. The probe results agree with the heat balance results to within the experimental error of the heat balance. In view of the experimental error associated with other plasma diagnostic techniques, this agreement is considered to be quite good.

Results for Virtually Complete Electron Absorption

Twelve data points were obtained for which sufficient electrons were absorbed by the electrophilic additive to make it possible to observe the change in positive ion current with probe potential. The pressure and enthalpy ranges for the data were the same as in the case without electron absorption. At some of the pressure-enthalpy

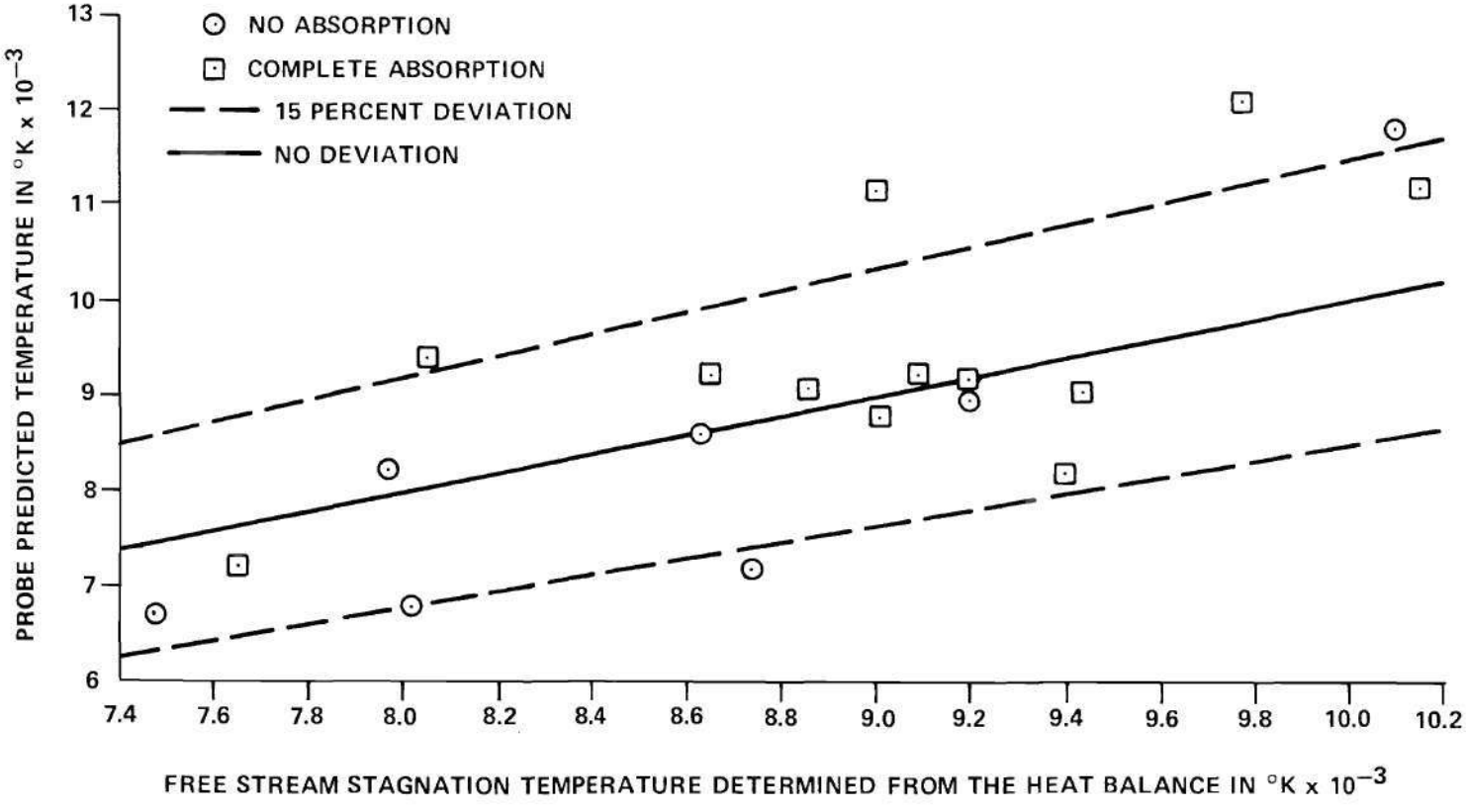

Figure 7. Electrostatic Probe Predicted Temperature as a Function of Free Stream Stagnation Temperature

combinations, data were not obtained because of difficulty in absorbing enough of the higher energy electrons to allow the effect of positive ion retardation to be shown. Sulphur hexafluoride has a high capture cross section for low energy electrons, but this cross section decreases rapidly as the electron energy increases. Thus, even though nearly all of the free electrons can be absorbed by the sulphur hexafluoride, the remaining electrons are normally high velocity electrons which can produce electron currents which are high enough to mask the effect of positive ion retardation.

The free stream stagnation temperatures predicted by the probe theory and the heat balance are also shown in Figure 7. These results also show good agreement with the heat balance results.

Combined Results for the Two Cases

The results for both the no absorption and the nearly complete absorption cases are tabulated in Table 1 with the free-stream pressure and stagnation enthalpy associated with each data point. The table shows the percentage of the deviation of the probe results from the heat balance results for each data point. A comparison of the data obtained for both cases shows that for each pressure-enthalpy combination at which data were obtained for the no electron absorption case there were also data obtained for the nearly complete absorption case. The data for the complete absorption case generally showed deviations from the data for the no absorption case. This deviation is comparable to the experimental uncertainty of the heat balance and it was concluded that, for the range of experimental conditions investigated, the ability of the probe theory to predict plasma free stream stagnation

Table 1. Error Percentage with Pressure and Enthalpy

Enthalpy - $\frac{\text{K-cal.}}{\text{Kg.-mole}}$	4×10^4	5×10^4	6×10^4	7×10^4	9×10^4
No Absorption					
Pressure-mm. Hg.					
15-20	-10.4% -15.2%	-17.6%			
30	3.7%		-2.50%		
40-45		-0.04%			15.3%
Complete Absorption					
Pressure-mm. Hg.					
20	-5.9%	6.9%			
30	16.7%		23.7% 1.73% -0.16% -12.8%	-4.1% 23.8%	
40-45		2.3%	-2.3%		10.3%

temperatures is unaffected by the presence of negative ions.

With the limited amount of data available, and with the amount of scatter exhibited, no trend in the magnitude of the deviation with changes in plasma enthalpy or pressure which might exist could be observed. In addition, at three pressure enthalpy combinations, the tests were repeated. In general, the errors were of similar magnitude but for two of the combinations, the errors differed in sign, thus indicating at least some randomness to the errors.

Because the electrostatic probe theory gave equally good results in predicting the plasma free stream stagnation temperature for both the no electron absorption and the complete electron absorption cases, and because the probe results agreed with the heat balance results to within the experimental error of the heat balance, it was concluded that, within the range of the experimental conditions, the experimental error associated with the probe theory temperature predictions is not sensitive to variations in additive concentration, and that the magnitude of the error is acceptable.

Analysis of the Probe Results for Ionization Predictions

Data were taken for the case of no electrophilic additive present in the plasma and also for increasing amounts of additive up to nearly complete electron absorption and the electrostatic probe theory was used to predict the free stream ionization level. These predicted ionization levels were compared to the ionization levels predicted by the heat balance technique.

Comparison of Probe Ionization Calculations to the Free Stream Equilibrium Ionization

With the exception of two points, all of the data showed ionization predictions which were significantly below the free stream equilibrium values predicted by the heat balance method.

A comparison of the ionization levels predicted by the probe theory to the ionization levels which would have resulted if the plasma had been in equilibrium at the sheath edge (at the temperature and pressure predicted by the probe theory) showed the predicted ionization to always be larger than the sheath edge equilibrium ionization but to approach the equilibrium value with increasing static or stagnation pressure. This indicated that the flow was not completely frozen.

As noted in Chapter II, the equation for ion recombination is given by

$$\frac{n_i}{n_{i2}} = \frac{1}{1 + \alpha_r n_{i2} t} \qquad (6\text{-}1)$$

where n_i is the positive ion number density after time t, n_{i2} is the initial positive ion number density, and α_r is the recombination coefficient. The recombination coefficient was calculated for each of the data points which exhibited evidence of recombination and the results of these calculations are shown in Figure 8 as a function of the free stream static temperature. Implicit in the derivation of Equation (1) is the assumption that the rate of ionization is negligible compared to the rate of recombination. This assumption is valid in the probe boundary layer except for the cases in which the actual ionization level at the plasma sheath edge is near the equilibrium value. To minimize

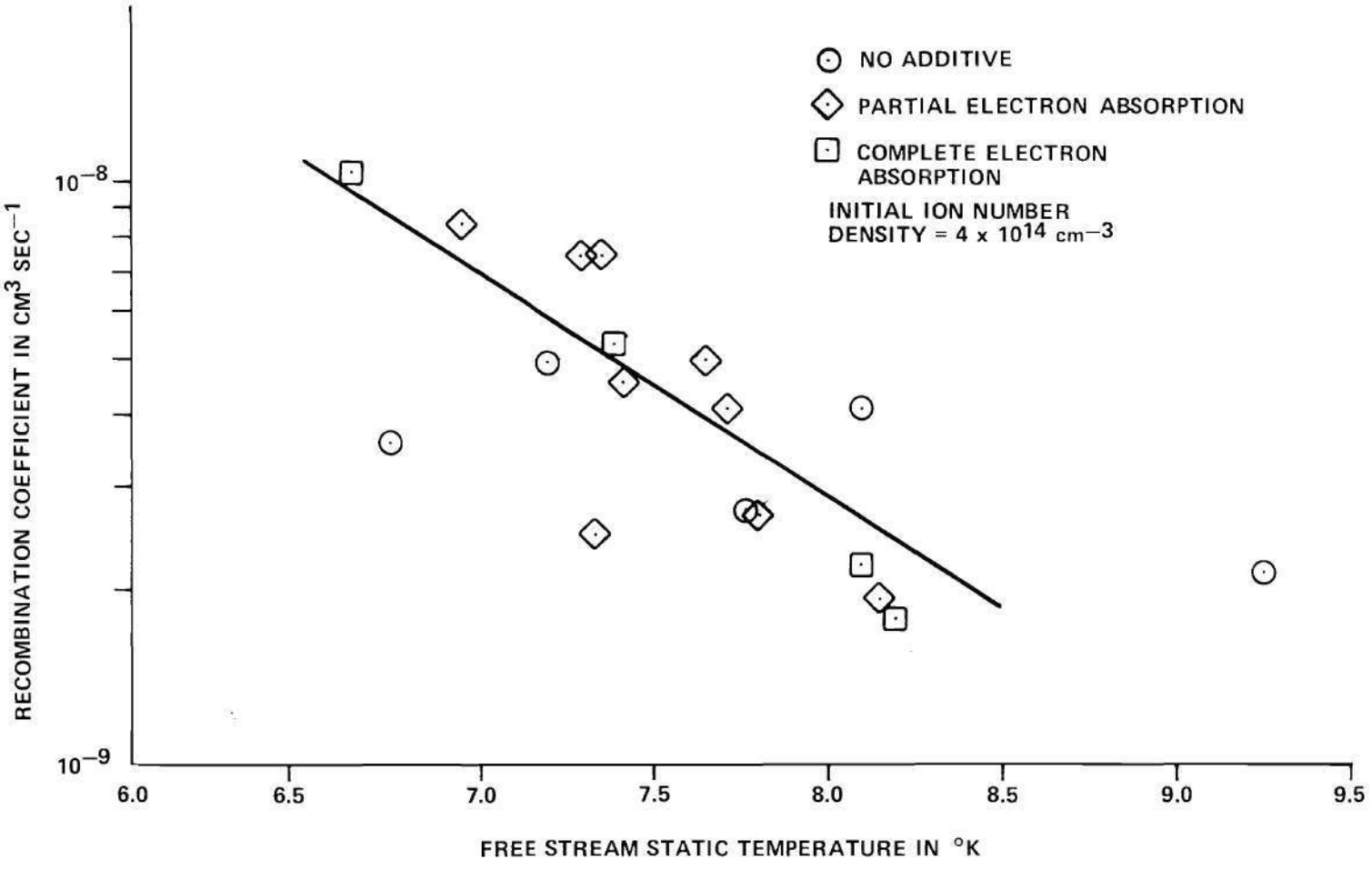

Figure 8. Argon Recombination Coefficient

the effect of the ionization rate upon the recombination coefficient calculations, only the data for which the value of n_i is greater than 5 percent of the value of n_{i2} is shown in Figure 8. The recombination coefficient is normally given as a function of the electron temperature. This was not possible in the present case since the lower energy electrons are removed from the plasma at a faster rate than are the higher energy electrons by the electrophilic additive and the recombination process. This gives a fictitiously high electron temperature at the edge of the plasma sheath. A comparison of the electron temperatures determined by the electrostatic probe for the data in which no electrophilic additives were present in the plasma with the free stream static temperature determined from the heat balance indicated that the free stream static temperature is a good approximation to the electron temperature in the free stream. Since the free stream plasma is expected to be in equilibrium, this result is reasonable. For these reasons, instead of the sheath edge electron temperature the free stream static temperature was used in Figure 8. The values for the recombination coefficient shown in Figure 8 are well within the range of values for the coefficient reported by Loeb.[16]

An increase in the value of the recombination coefficient was noted with the addition of sulphur hexafluoride. The variation of the recombination coefficient with the ratio of the sulphur hexafluoride number density to the sheath edge positive ion number density for a free stream static temperature of 8,000°K is shown in Figure 9. The increase in the recombination coefficient with increasing sulphur hexafluoride ratios indicates that the additive acts as a catalyst towards the

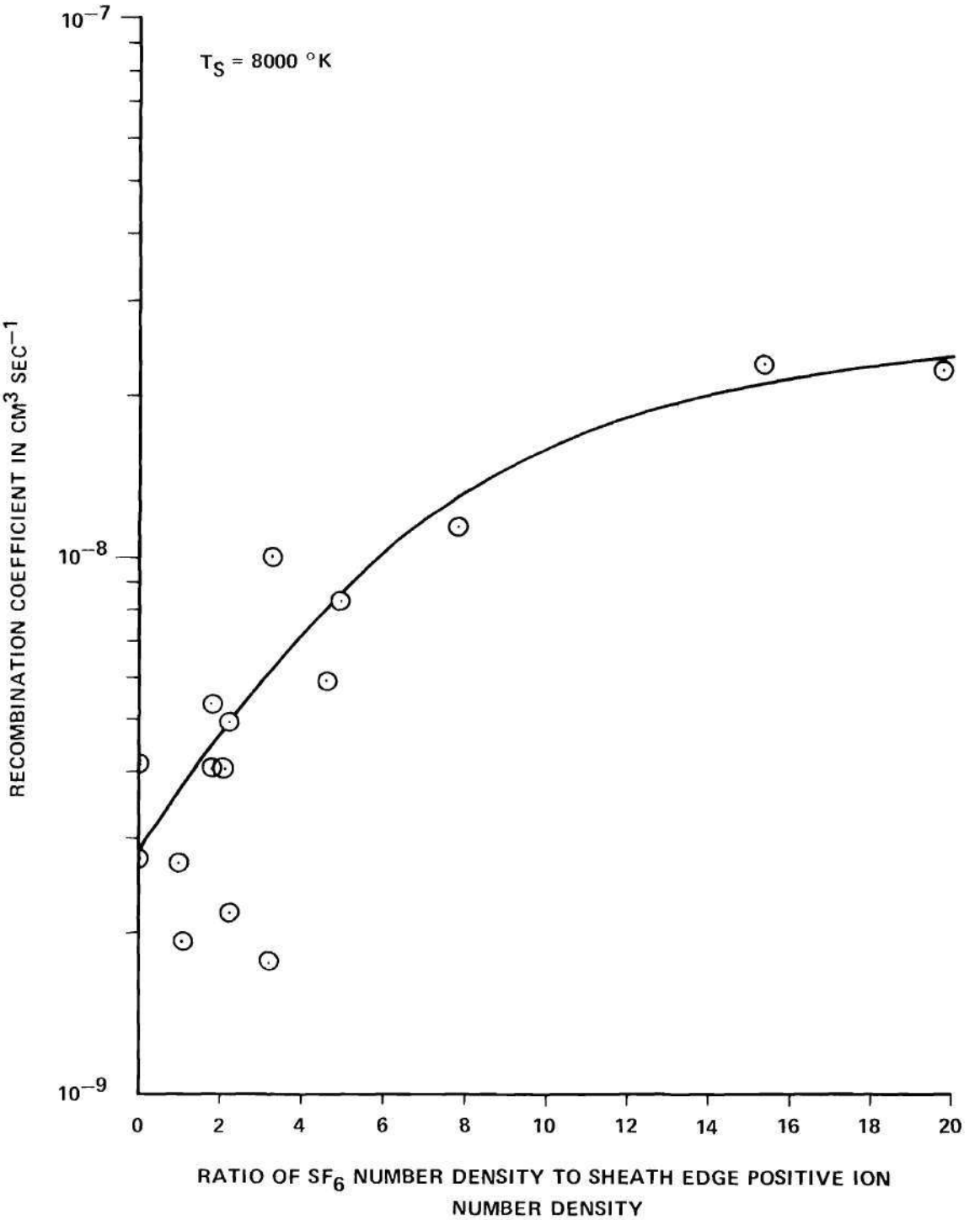

Figure 9. Change in Recombination Coefficient with Sulphur Hexafluoride Addition

recombination reaction.

Effect of the Non-Frozen Flow on the Temperature Predictions of the Probe Theory

By assuming frozen flow in the probe boundary layer it was possible to neglect any heat of recombination in the boundary layer. For the temperature predictions of the theory to remain correct when there is recombination within the boundary layer, the heat addition due to this recombination must be small enough to remain negligible. In the present experiments, 75 percent of the data points had free stream equilibrium ionization levels of less than 1 percent and 50 percent of the data points had free stream equilibrium ionization levels which were less than one-half of 1 percent. The ionization potential of argon is 15.68 volts, thus the energy released when one argon ion recombines is 15.68 electron-volts. This is equivalent to a temperature of 180,000°K. Thus, if an argon plasma were 1 percent ionized and all of these ions were to recombine, the plasma temperature would increase by 1,800°K. The lowest plasma stagnation temperature for which the free stream ionization was 1 percent was 9,000°K. The lower temperature plasmas were significantly less ionized. The temperature increase due to recombination in these cases is thus no more than 20 percent of the stagnation temperature of the plasma. Further, some of the energy released in argon due to recombination is in the form of electronic excitation or in the form of radiation which may not be reabsorbed by the plasma until it has traveled some distance from the point of recombination. This reduces some of the heat addition in the boundary layer due to recombination.

For these reasons, the heat of recombination in the boundary layer remained small enough to be acceptable insofar as the temperature

predictions are concerned. Further, an examination of the data reveals no trend towards larger errors in the temperature predictions with increased recombination, thus further supporting the assumption that the effect of recombination on the temperature predictions was small.

The effect of the non-frozen flow on the ionization predictions, however, is severe in the present experiments. Nevertheless, it is possible to compensate for these effects. By reducing the diameter of the probe, the pressure gradient in the probe boundary layer is increased. This has the effect of decreasing the time of passage of the ions through the boundary layer and thus reducing the amount of recombination. If the probe diameter is reduced sufficiently, the effect of recombination can be made negligible. In addition, if the value of the recombination coefficient is known, the degree of recombination within the boundary layer can be determined and thus the probe results can be corrected to the free stream values.

Use of the Probe Theory to Study the Effect of Electrophilic Additives

The electrostatic probe was used to measure the effectiveness of sulphur hexafluoride and uranium hexafluoride as electrophilic compounds. One of the additives would be injected into the flowing plasma and the probe theory would be used to determine, at the plasma sheath edge, the ratio of the remaining free electron number density to the positive ion number density. This ratio would be a measure of the effectiveness of the additive. The lower the ratio the greater the percentage of free electrons being absorbed. The concentration of the additive was the ratio of the additive number density to the sheath edge positive ion

number density. The additive concentration was varied and the change in the ratio, at the plasma sheath edge, of the free electron number density to the positive ion number density was determined as a function of the additive concentration.

The number of free electrons removed from the plasma is a function of the electron capture coefficient of the electrophilic additive. The sulphur hexafluoride data were taken at test conditions under which the electrostatic probe boundary layer was not frozen, and this circumstance made it possible to determine the electron capture coefficient for sulphur hexafluoride.

The usefulness of the electrostatic probe theory is expanded by knowledge of the value of the electron capture coefficient. If, in a plasma being analyzed, the electron current to the electrostatic probe is unacceptably high, this electron current can be reduced by the addition of a measured amount of an electrophilic additive. If the value of the electron capture coefficient is known, the reduction in the electron number density can be determined, and hence the electrostatic probe theory can be used to determine the plasma properties.

Sulphur Hexafluoride as an Additive

The data taken for the sulphur hexafluoride experiments were taken at plasma enthalpies of 4×10^4, 5×10^4, and 6×10^4 k-cal./kg-mole. The data for the plasma enthalpy of 6×10^4 k-cal./kg-mole were taken primarily at free stream static pressures of 20 and 45 mm. Hg. The data for the plasma enthalpies of 4×10^4 and 5×10^4 k-cal./kg-mole were taken at a static pressure of 20 mm. Hg. The ratio at the plasma sheath edge of the electron number density to the positive

ion number density was determined in the manner described in Chapter III, and the electron capture coefficient of sulphur hexafluoride was determined in the following manner.

Within the boundary layer, the rate of electron reduction is given by

$$\frac{dn_e}{dt} = - Kn_e n_a - \alpha_r n_i n_e \tag{6-2}$$

where n_e and n_a are the electron and unionized additive number densities, K is the electron capture coefficient, and t is the time of the reaction. As electrons are absorbed by the additive, negative ions are formed and the ionized additive number density decreases as

$$n_a = n_{ao} - (n_n - n_{no}) \tag{6-3}$$

where the subscript o denotes the initial value. Since the plasma must remain neutral,

$$n_n = n_i - n_e \tag{6-4}$$

and Equation (2) becomes

$$\frac{dn_e}{dt} = n_e[(K - \alpha_r)n_i - K(n_{ao} + n_{no})] - Kn_e^2 . \tag{6-5}$$

The rate of positive ion reduction is given by

$$\frac{dn_i}{dt} = - \alpha_r n_i n_e - \alpha_n n_i n_n \tag{6-6}$$

where α_n is the charge exchange coefficient between the negative ions and the positive ions. Substituting Equation (4) into Equation (6) yields

$$\frac{dn_i}{dt} = (\alpha_n - \alpha_r)n_i n_e - \alpha_n n_i^2 \ . \qquad (6\text{-}7)$$

An attempt to find an exact analytical solution to Equations (5) and (7) was unsuccessful. A finite difference computer program was written to solve these equations for the value of K in the electrostatic probe boundary layer. Realistic values of α_r and α_n were used and the value of K was iterated until a numerical integration of Equations (5) and (7) gave results for n_e and n_i at the plasma sheath edge which matched the values for n_e and n_i determined by the electrostatic probe. The results showed that, for the range of experimental conditions investigated in the present work, the value of K was close to the value of α_r. This result permitted an approximate solution to Equation (5).

If the term $(K - \alpha_r)n_i$ in Equation (5) is assumed to be small compared to the term $K(n_{ao} + n_{no})$, then Equation (5) can be approximated by

$$\frac{dn_e}{dt} = - K(n_{ao} + n_{no})n_e - Kn_e^2 \qquad (6\text{-}8)$$

which becomes

$$\frac{1}{n_{ao} + n_{no}} \ln\left[\left(\frac{n_e}{n_{eo}}\right)\left(\frac{n_{eo} + n_{ao} + n_{no}}{n_e + n_{ao} + n_{no}}\right)\right] = - Kt \ . \qquad (6\text{-}9)$$

Solving Equation (9) for n_e/n_i yields

$$\frac{n_e}{n_i} = \frac{\dfrac{n_{eo}}{n_{eo} + n_{ao} + n_{no}} \left(\dfrac{n_{ao} + n_{no}}{n_i}\right) e^{-K(n_{ao}+n_{no})t}}{1 - \dfrac{n_{eo}}{n_{eo} + n_{ao} + n_{no}} e^{-K(n_{ao}+n_{no})t}} \tag{6-10}$$

and solving Equation (10) for K yields

$$K = \frac{1}{\beta n_i t} \ell n \left[\frac{\beta + \dfrac{n_e}{n_i}}{\left(\dfrac{n_e}{n_i}\right)\left(\dfrac{n_{eo} + n_{ao} + n_{no}}{n_{eo}}\right)} \right] \tag{6-11}$$

where

$$\beta = \frac{n_{ao} + n_{no}}{n_i} \tag{6-12}$$

To use Equation (11) to determine the value of K, the values of n_{ao} and n_{no} at the edge of the probe boundary layer must be known. In the present experiments, the sulphur hexafluoride was injected into the free stream plasma in small enough quantities so that, in the free stream, the sulphur hexafluoride number density, n_{SF_6}, was always less than the positive ion number density. In addition, the sulphur hexafluoride proved to be a sufficiently good electron absorbing agent and the time required for the particles to travel from the point of injection to the location of the probe boundary layer was sufficiently long so that, at the edge of the probe boundary layer, good approximations to n_{ao} and n_{no} were

$$n_{ao} = 0 \tag{6-13}$$

and

$$n_{no} = n_{SF_6} \quad . \tag{6-14}$$

Since

$$n_{io} = n_{eo} + n_{no} \quad , \tag{6-15}$$

Equation (11) becomes

$$K = \frac{1}{\beta n_i t} \ln \left[\frac{\beta + \frac{n_e}{n_i}}{\frac{n_e}{n_i} \frac{n_{io}}{n_{eo}}} \right] \tag{6-16}$$

The values for K determined by Equation (16) are shown in Figure 10. The free stream equilibrium ionization percentages were used to determine n_{io} and the values used for n_i and n_e in Equations (12) and (16) were the values determined for the plasma sheath edge by the electrostatic probe theory. The value of t was determined from

$$t = \frac{1.05}{\overline{\beta}} \tag{6-17}$$

where $\overline{\beta}$ is the boundary layer pressure gradient parameter introduced previously. For reasons identical to those for the recombination coefficient data, the value of K is shown as a function of the free stream static temperature instead of the sheath edge electron temperature.

Since, in deriving Equation (16), the assumption was made that the term $(K - \alpha_r)n_i$ in Equation (5) is small compared to the term

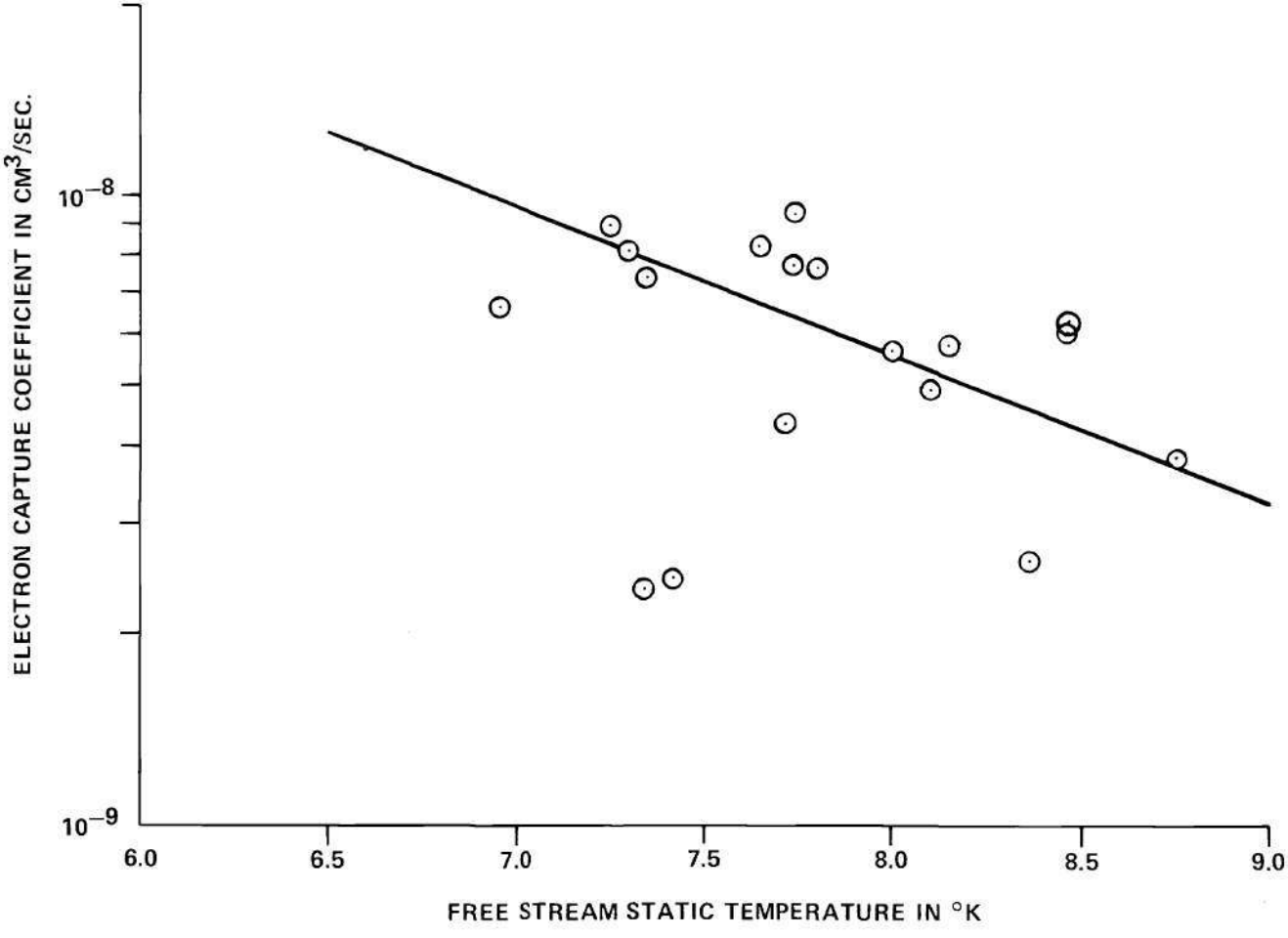

Figure 10. Sulphur Hexafluoride Electron Capture Coefficient

$K(n_{ao} + n_{no})$, this assumption should be checked. At the boundary layer edge, with a free stream static temperature of 8,000°K, typical values for n_i, n_{no}, and K were

$$n_i = n_{io} = 4 \times 10^{14} \text{ cm}^{-3} , \tag{6-18}$$

$$n_{no} = 4 \times 10^{13} \text{ cm}^{-3} , \tag{6-19}$$

and

$$K = 6 \times 10^{-9} \text{ cm}^3/\text{sec} . \tag{6-20}$$

The values determined for the recombination coefficient α_r, are shown in Figure 8. The value for α_r at 8,000°K is

$$\alpha_r = 3 \times 10^{-9} \text{ cm}^3/\text{sec} . \tag{6-21}$$

The ratio of the two terms in Equation (5) is thus

$$\frac{(K - \alpha_r)n_i}{K(n_{ao} + n_{no})} = 5 \tag{6-22}$$

at the boundary layer edge. Thus, initially, the assumption is not valid. At the edge of the plasma sheath, however, a typical value of n_i is

$$n_i = 1 \times 10^{13} \text{ cm}^{-3} \tag{6-23}$$

and the ratio of the two terms is thus

$$\frac{(K - \alpha_r)n_i}{K(n_{ao} + n_{no})} = 0.125 \tag{6-24}$$

and the assumption is valid. By substituting an averaged value for α_r and α_n into Equation (6), the value of n_i as a function of time can be shown to be

$$n_i = \frac{n_{io}}{1 + \bar{\alpha} n_{io} t} \tag{6-25}$$

where $\bar{\alpha}$ is the averaged value for the recombination coefficient. The time required for the value of n_i to drop to 4×10^{13} cm^{-3}, where the ratio $(K - \alpha_r)n_i / K(n_{ao} + n_{no})$ is equal to 0.5 is thus

$$t = \frac{9}{\bar{\alpha} n_{io}} \tag{6-26}$$

while the time required for the value of n_i to drop to the sheath edge value of 1×10^{13} cm^{-3} is

$$t = \frac{39}{\bar{\alpha} n_{io}} \tag{6-27}$$

and thus for only 25 percent of the range of integration is the assumption that $(K - \alpha_r)n_i$ is small compared to $K(n_{ao} + n_{no})$ invalid. A further test of the validity of the assumption is to compare the term $(K - \alpha_r)n_i n_e$ to the term Kn_e^2 in Equation (5). At the plasma sheath edge, Equations (15), (18), and (19) give

$$n_{eo} = 3.6 \times 10^{14} \text{ cm}^{-3} \tag{6-28}$$

and hence

$$\frac{(K - \alpha_r)n_i n_e}{Kn_e^2} = 0.56 \ . \tag{6-29}$$

Thus, even though the neglected term in Equation (5) is not initially small compared to the second term, it is small compared to the third term. Equation (16) should, therefore, give a good approximation to the value of K.

The electron capture cross section, σ, is related to the reaction rate constant, K, by

$$K = \sigma \bar{c}_e \tag{6-30}$$

where $\bar{c}_e$ is the average thermal speed of the electrons. Substituting Equation (30) into Equation (16) and solving for σ yields

$$\sigma = \frac{1}{\bar{c}_e \beta n_i t} \ln \frac{\beta + \frac{n_e}{n_i}}{\frac{n_e}{n_i} \frac{n_{io}}{n_{eo}}} \quad . \tag{6-31}$$

The calculated values of the electron absorption coefficient of sulphur hexafluoride as a function of the free stream static temperature are shown in Figure 11. The value for the sulphur hexafluoride electron capture cross section as a function of the electron temperature, as determined by Asundi and Craggs[18] for monoenergetic electrons passing through a sulphur hexafluoride gas at room temperature, is also presented in Figure 11. Although there is some scatter in the present data, their agreement with the data of Asundi and Craggs is quite good. The scatter in the data is attributed to the combined errors associated with the heat balance enthalpy measurements, the electrostatic probe measurements, and the sulphur hexafluoride flow rate measurements.

The equations used in determining the degree of electron number

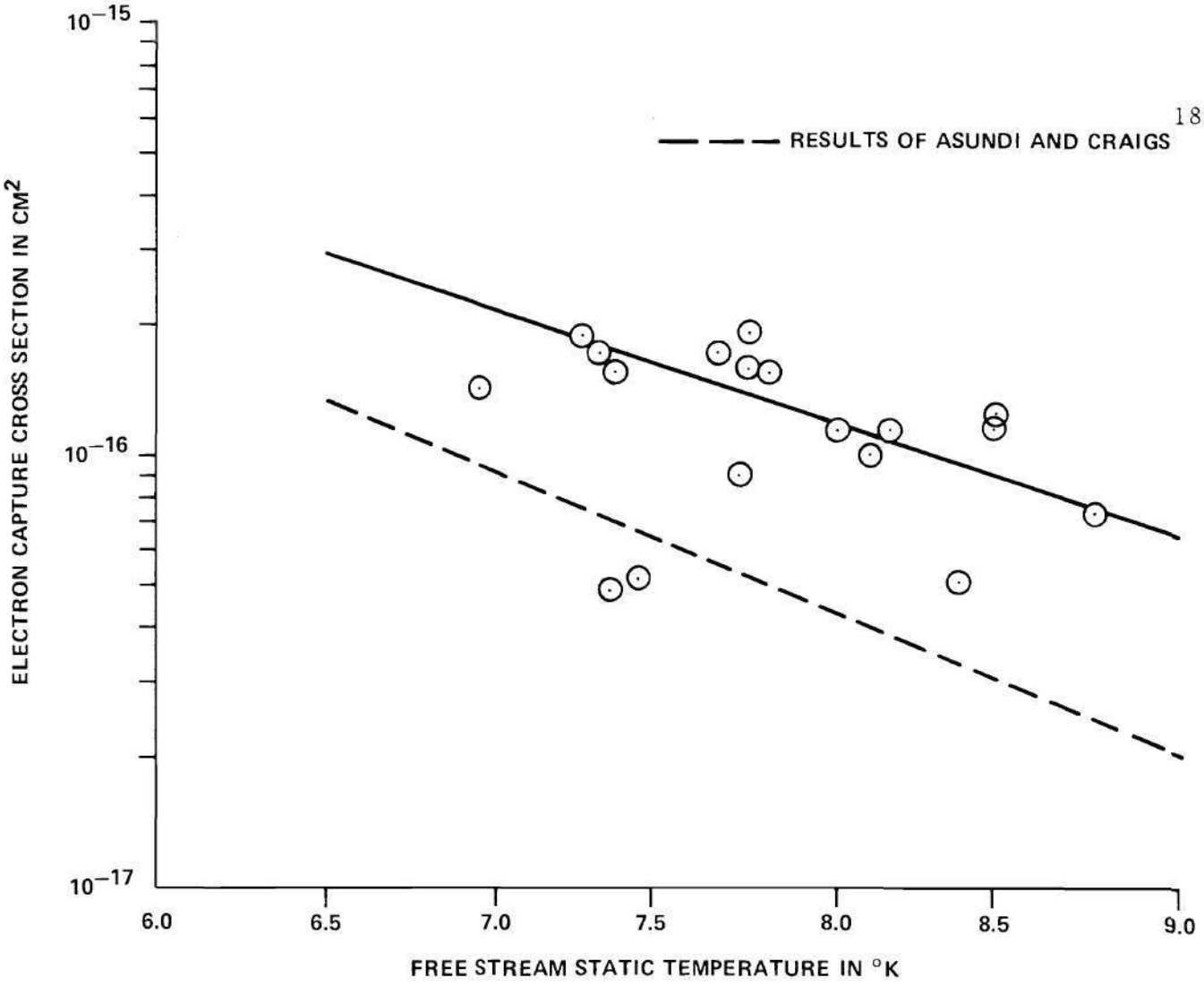

Figure 11. Sulphur Hexafluoride Electron Capture Cross Section

density reduction are dependent upon the experimental test conditions. In experiments similar to those conducted in the present work, Equation (10) would be used to determine the reduction in electron number density. If the experimental conditions were sufficiently different so that no deionization would occur within the plasma, then Equation (2) reduces to

$$\frac{dn_e}{dt} = - Kn_e n_a \tag{6-32}$$

which can be solved exactly to give

$$\frac{n_e}{n_{eo}} = \frac{\left(\frac{n_{ao}}{n_{eo}} - 1\right) e^{-K\left(\frac{n_{ao}}{n_{eo}} - 1\right) n_{eo} t}}{\frac{n_{ao}}{n_{eo}} - e^{-K\left(\frac{n_{ao}}{n_{eo}} - 1\right) n_{eo} t}} \tag{6-33}$$

This equation is similar to Equation (9) of Chapter II and it was derived in the same manner.

As noted previously, the argon recombination coefficient exhibited an increase in value with increasing amounts of sulphur hexafluoride, thus indicating a tendency towards greater recombination with sulphur hexafluoride addition. The variations in sheath edge positive ion number density with sulphur hexafluoride addition for the free stream stagnation enthalpies of 4×10^4, 5×10^4, and 6×10^4 k-cal./kg-mole are shown in Figures 12, 13, and 14 respectively. The positive ion number density is shown as a function of the ratio of the sulphur hexafluoride number density to the sheath edge positive ion number

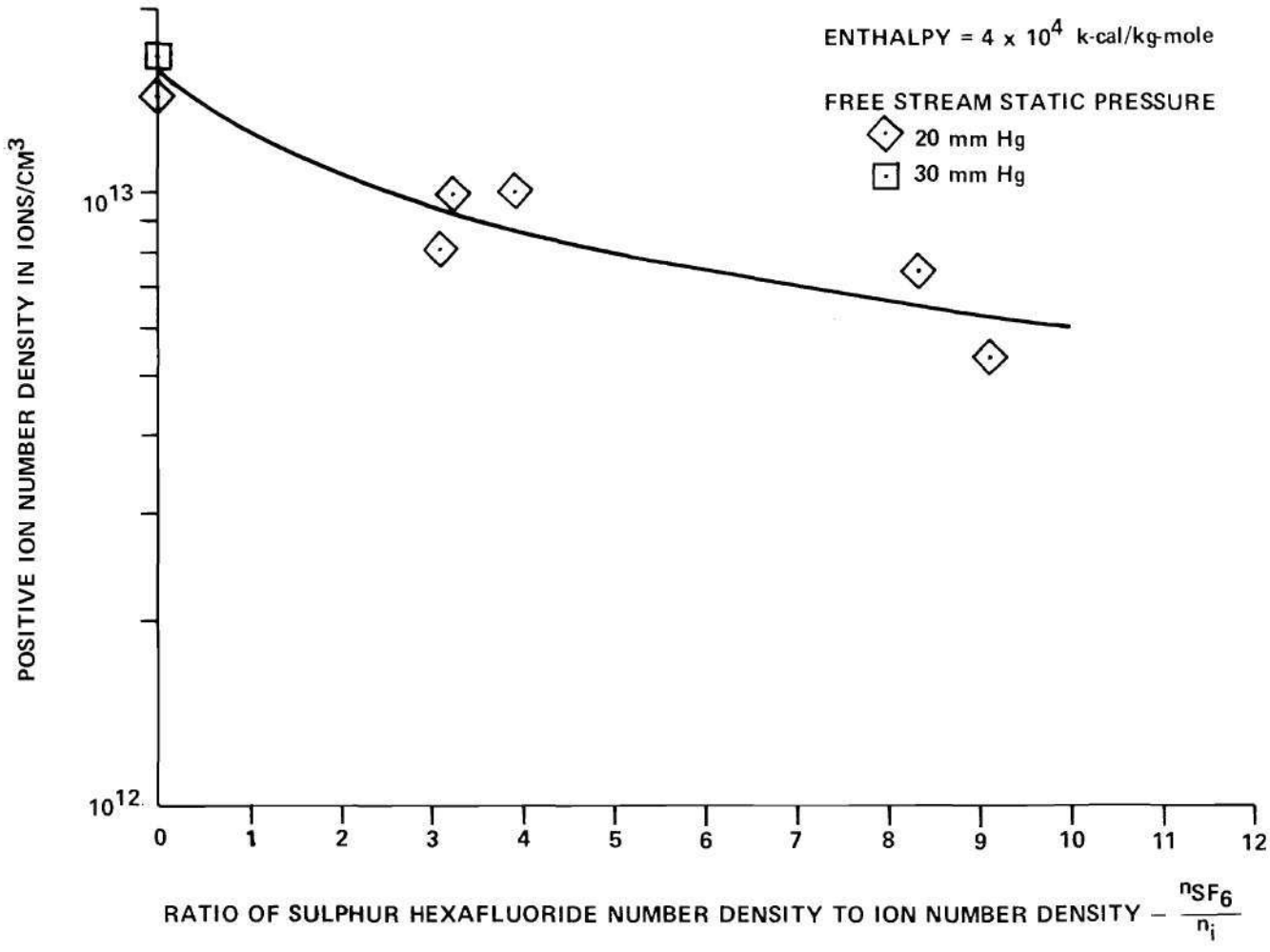

Figure 12. Decrease in Sheath Edge Positive Ion Number Density with Sulphur Hexafluoride Addition for a Plasma Stagnation Enthalpy of 4×10^4 k-cal/kg-mole

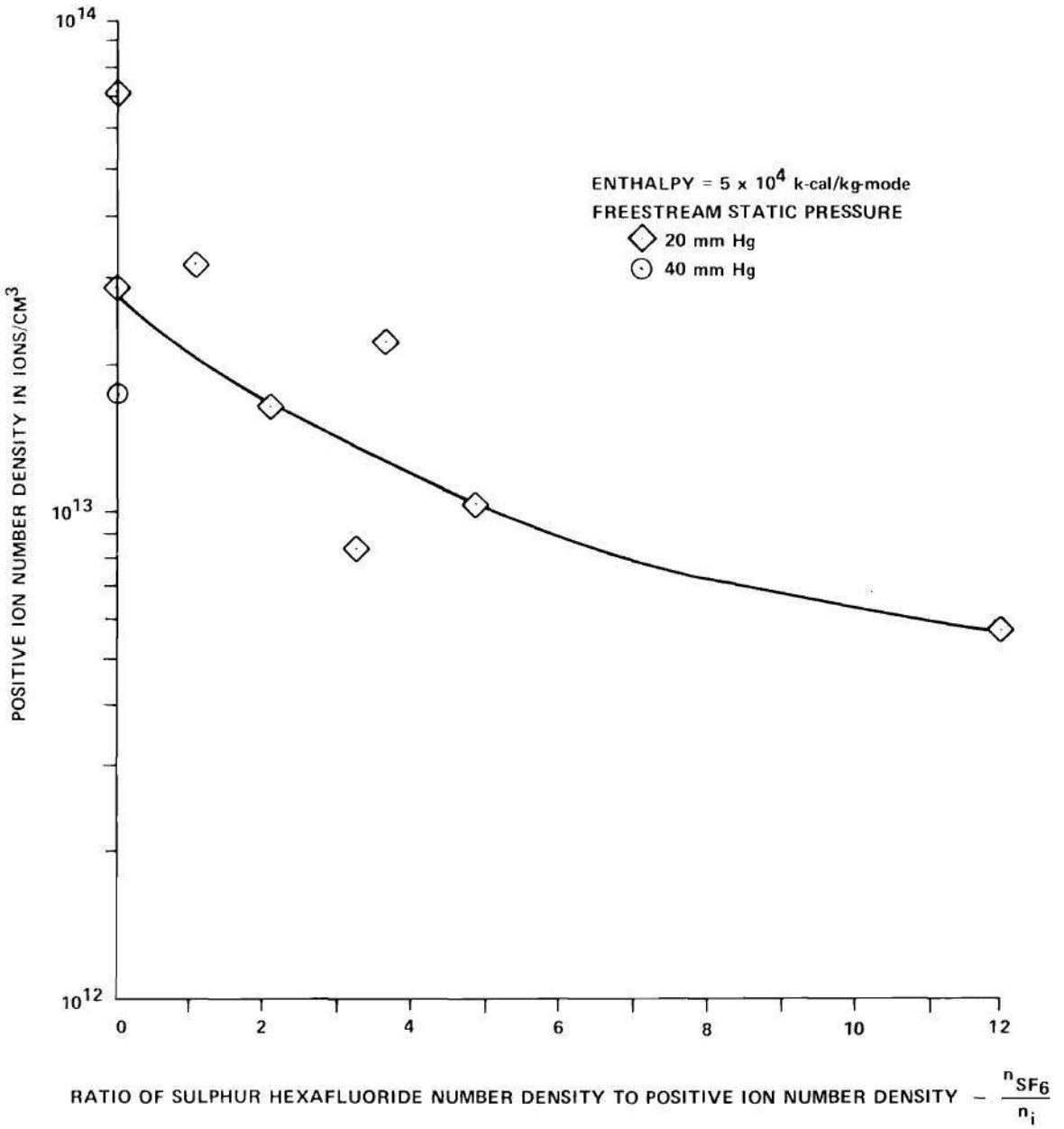

Figure 13. Decrease in Sheath Edge Positive Ion Number Density with Sulphur Hexafluoride Addition for a Plasma Stagnation Enthalpy of $5 \times 10^4 \frac{\text{k-cal.}}{\text{kg.-mole}}$

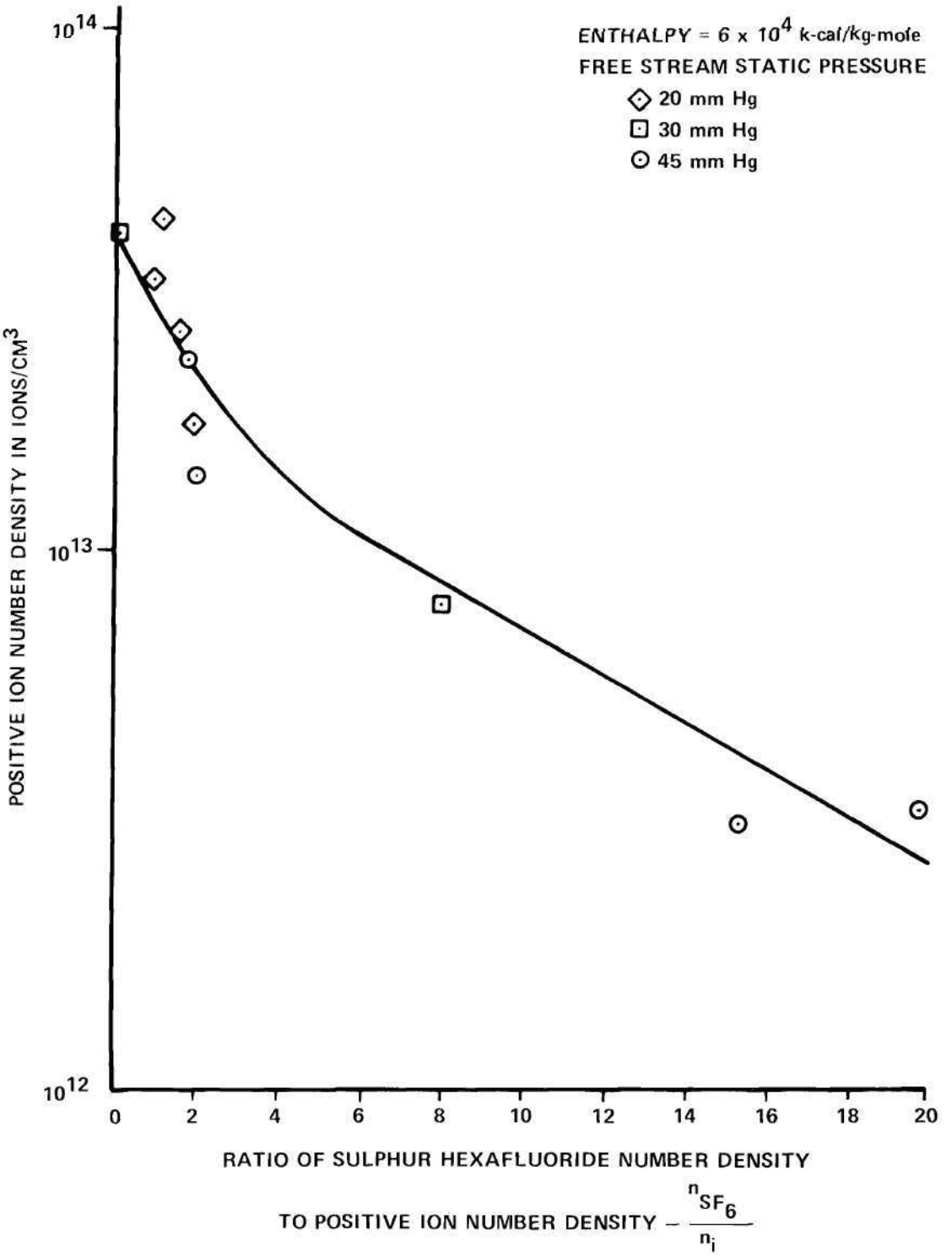

Figure 14. Decrease in Sheath Edge Positive Ion Number Density with Sulphur Hexafluoride Addition for a Plasma Stagnation Enthalpy of $6 \times 10^4 \frac{\text{k-cal.}}{\text{Kg.-mole}}$

density, n_{SF_6}/n_i. For all three enthalpies, the sheath edge positive ion number density decreased with increasing amounts of sulphur hexafluoride, thus, further demonstrating the effectiveness of sulphur hexafluoride in promoting recombination.

As expected, the sheath edge positive ion number density at a given value of n_{SF_6}/n_i increases with increasing enthalpy. While the data for the 5×10^4 k-cal./kg-mole enthalpy level were too scattered for accurate analysis, the remaining data showed an increase with increasing plasma enthalpy in the rate of sheath edge positive ion number density reduction with sulphur hexafluoride addition. This result is expected since the rate of positive ion recombination is directly proportional to the positive ion number density as well as to the recombination coefficient.

The experimental results thus show the effect of the sulphur hexafluoride to be twofold. When the ionization rate is low compared to the deionization rate, the sulphur hexafluoride can accelerate the rate of deionization and thereby cause a reduction of 50 percent, or more, in the free electron number density. The electron absorption effect causes an additional reduction in the electron number density of up to 99 percent.

Use of Uranium Hexafluoride as an Additive

In certain proposed gas core nuclear reactors, an MHD generator has been proposed as a topping device to a conventional steam generator. In order for this generator to operate efficiently, the plasma must contain sufficient free electrons for the plasma to be a good electrical conductor. Uranium hexafluoride has been suggested as a potential fuel

for the reactor; however, the presence of a halogen in the molecule indicates that uranium hexafluoride is likely to be an electrophilic compound. For these reasons, the electrophilic properties of uranium hexafluoride warranted investigation.

In this study, the data were taken for a free stream stagnation enthalpy of 2×10^4 k-cal./kg-mole and at a free stream static pressure of 15 mm. Hg.

The data analysis method for the uranium hexafluoride tests differed somewhat from the sulphur hexafluoride method due to problems caused by the choice of a lower test enthalpy. The lower enthalpy was chosen because the higher enthalpies at which the sulphur hexafluoride data were taken often produced sufficient ionization to cause a burnout of the collecting electrode when the electron saturation current was obtained with little or no electron absorption. As very little uranium hexafluoride was available, it was decided to minimize possible problems and delays by running the tests at a lower enthalpy level. A further advantage of the lower enthalpy was that the plasma temperature was lowered to about 5,000°K which is the approximate operating temperature proposed for the MHD generator topping device. Thus the lower enthalpy made it possible to more closely match the actual conditions under which the uranium hexafluoride would be used.

Unfortunately, the cooling effect of the probe at the chosen enthalpy was greater than expected and caused the ion temperature at the sheath edge to be close to 1,000°K for all but the greatest electron absorption cases. At this temperature the collision cross section (upon which the sheath thickness depends) of argon varies quite strongly with

temperature and sufficiently accurate information was unavailable in the literature to permit the usual data reduction procedure. In the cases in which the electron absorption was great enough to permit the determination of the ion temperature at the sheath edge by observing the ion current, the calculated ion temperatures were used to determine the remaining parameters. When this was not possible, the ion temperature was assumed to be 1,000°K. This temperature was chosen because data taken with no uranium hexafluoride in the plasma showed that the ion temperature at the sheath edge was very close to this value. Once the ion temperature at the sheath edge was determined, or assumed, the normal data reduction procedure was followed except that the ratio of the electron saturation current to the ion saturation current was used rather than the floating potential to determine the value of the ratio $(n_e\sqrt{T_e})/(n_i\sqrt{T_i})$. This change was required because the uranium hexafluoride produced a coating on the collecting electrode which tended to distort the current-voltage characteristic curve. The distortion did not affect the magnitude of the saturation currents but it did produce a fictitious increase in the floating potential.

The results of the uranium hexafluoride study are quite similar to the results for the sulphur hexafluoride study. The electron number density showed a significant decrease with increasing uranium hexafluoride number density. The ratio of the number density of the free electrons to the positive ion number density at the sheath edge, as a function of the ratio of the uranium hexafluoride number density to the positive ion number density at the sheath edge, is shown in Figure 15. The electron number density showed a more rapid decrease with uranium

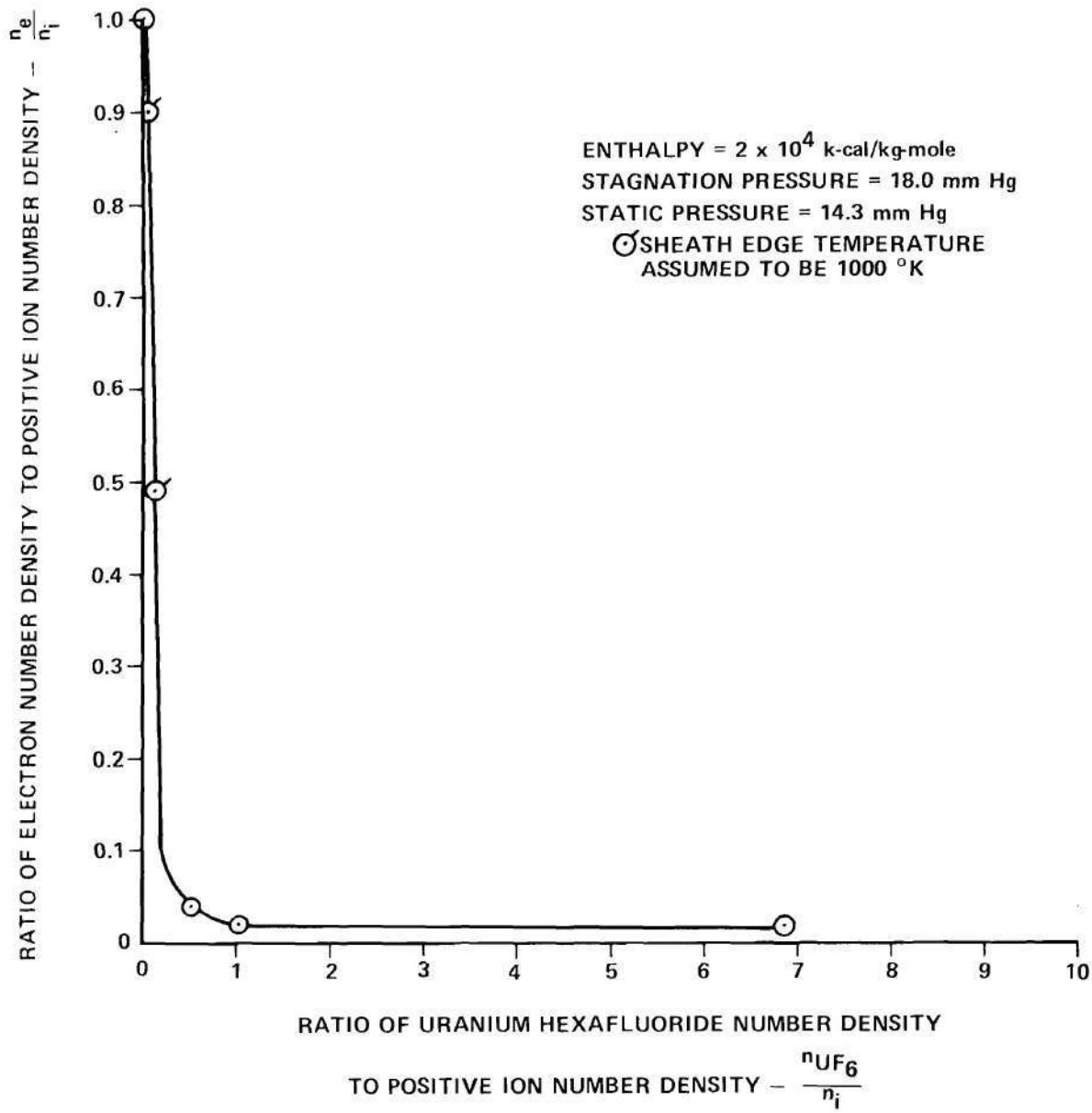

Figure 15. Free Electron Reduction with Uranium Hexafluoride Addition

hexafluoride addition than with sulphur hexafluoride addition. This was probably caused by the fact that at elevated temperatures uranium hexafluoride breaks down into uranium tetrafluoride and fluorine thus creating more election absorbing agents. The uranium hexafluoride was also effective in promoting recombination in the plasma. The sheath edge positive ion number density as a function of the ratio of the uranium hexafluoride number density to the positive ion number density at the sheath edge is shown in Figure 16. The results show a decrease in positive ion number density of up to 80 percent with the addition of uranium hexafluoride.

The recombination coefficient for argon, with uranium hexafluoride present, could not be calculated because, for reasons noted previously, the data were taken at a lower free stream pressure and stagnation enthalpy than were the data for the sulphur hexafluoride addition. At this lower pressure and enthalpy, the probe boundary layer becomes more nearly frozen. If equilibrium in the flow is assumed, the free stream ionization would be expected to be 1×10^{-3} percent and, for the stagnation conditions, the equilibrium ionization would be expected to be 4×10^{-3} percent. The actual sheath edge ionization measured by the electrostatic probe averaged 4.7×10^{-3} percent indicating little, if any, recombination within the boundary layer. The fact that the measured ionization was somewhat higher than the calculated free stream ionization can be attributed to the imprecision in determining the positive ion temperature at the sheath edge and to some residual ionization within the plasma caused by initially much higher ionization levels within the plasma jet.

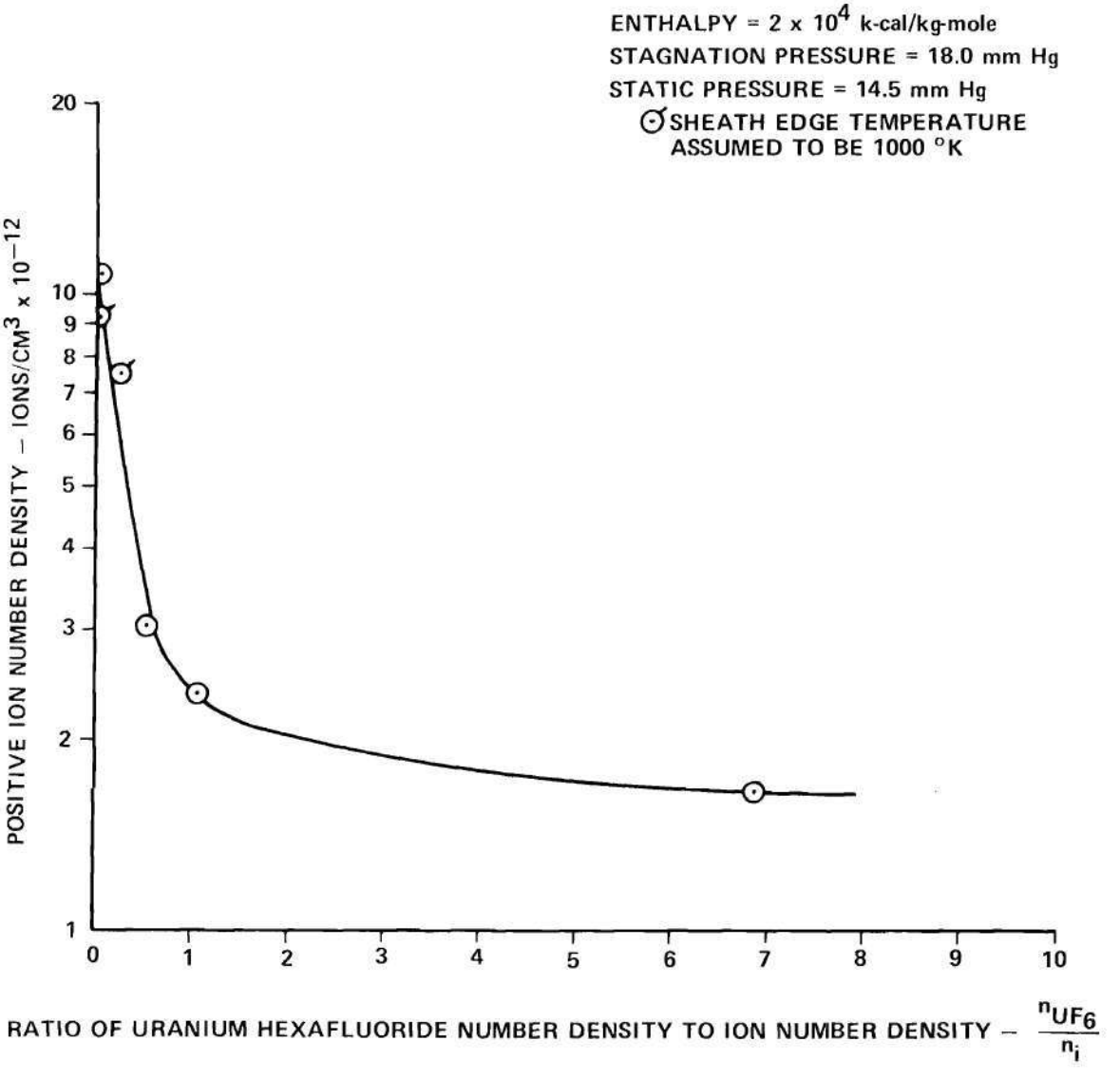

Figure 16. Ion Number Density Decrease with Uranium Hexafluoride Addition

The electron capture cross section for uranium hexafluoride could not be determined since the time for electron absorption in the plasma was sufficiently long and the effectiveness of the additive was sufficiently high to prevent an accurate determination of this parameter.

Uranium hexafluoride thus has the same twofold effect as the sulphur hexafluoride. The recombination effect causes as much as an 80 percent reduction in the electron number density and the electron absorption effect causes a further reduction in electron number density of up to 99 percent.

CHAPTER VII

CONCLUSIONS AND RECOMMENDATIONS

The ability of the electrostatic probe theory to determine plasma free stream stagnation temperatures has been experimentally demonstrated for the enthalpy range of 4×10^4 k-cal./kg-mole to 9×10^4 k-cal./kg-mole and pressure range of 15 mm. Hg. to 45 mm. Hg.

Under these test conditions, however, the probe theory was unable to give accurate predictions for the free stream ionization because of the recombination within the probe boundary layer. However, if the plasma is in equilibrium, then the free stream ionization can be deduced from the free stream temperature determined by the probe. For the experimental conditions examined, the argon recombination coefficient as a function of the free stream static temperature was found to vary from 1×10^{-8} cm^3/sec at a static temperature of 6,600°K to 1.9×10^{-9} cm^3/sec at a static temperature of 8,500°K. The recombination within the probe boundary layer had a negligible effect on the accuracy of the probe temperature predictions because the free stream ionization was generally small. If the free stream ionization is increased, however, the recombination effect on the temperature predictions would be expected to increase.

The experimental data indicate that both sulphur hexafluoride and uranium hexafluoride are highly effective electrophilic compounds. The sulphur hexafluoride electron capture cross section as a function of the free stream static temperature was found to vary from 3×10^{-16} cm^2 at

6,500°K to 6.5 x 10^{-17} cm^2 at 9,000°K for the experimental conditions examined. The uranium hexafluoride data were taken under experimental conditions which were sufficiently different from those of the sulphur hexafluoride to prevent the determination of the uranium hexafluoride electron capture cross section. The data for the uranium hexafluoride indicate, however, that it is at least as effective as an electrophilic compound as is sulphur hexafluoride. This is probably due in part to dissociation of uranium hexafluoride into uranium tetrafluoride and atomic fluorine at high temperatures and thus the creation of additional electron absorbing particles.

In addition to being strongly electrophilic, both sulphur hexafluoride and uranium hexafluoride tend to promote recombination within the plasma. In the absence of any tendency towards reionization in the plasma, the injection of either compound into the plasma can cause a reduction in the positive ion number density to as much as 90 percent below the ion number density which would exist if no additive were present.

For future studies, it is recommended that the ability of the electrostatic probe theory to predict free stream temperatures and ionization levels at additional pressures and enthalpies be studied in order to determine the complete range of applicability of the electrostatic probe theory. For the cases in which recombination within the probe boundary layer becomes unacceptable, it is recommended that the diameter of the probe be reduced. This will decrease the time of passage through the probe boundary layer for the ions and thus reduce the amount of recombination which occurs.

In addition to determining the range of applicability of the electrostatic probe theory, the range of temperatures for which the argon recombination coefficient is known can be extended in future studies. This can be done by measuring the recombination within the probe boundary layer, as was done in the present experiments, or by measuring the rate of decrease in the free stream ionization as the ionization approaches its equilibrium value from the highly ionized state which exists within the plasma jet.

The range of temperatures for which the electron capture cross section of sulphur hexafluoride is known can also be extended. For free stream temperatures above 9,000°K, where the capture cross section is expected to be small, it is recommended that the cross section be determined by measuring the electron concentration at several axial stations in the plasma jet. These measurements will yield the electron concentrations as a function of time and thus permit the calculation of the electron capture cross section. For free stream temperatures below 7,000°K, the electron capture cross section is expected to be sufficiently large to virtually deplete the electron population in a time period which is too short to permit an accurate determination of the capture cross section by the above method. It is therefore recommended that, for free stream temperatures below 7,000°K, the method employed in the present research be used to determine the sulphur hexafluoride electron capture cross section.

It is also recommended that the electron capture cross section of uranium hexafluoride be determined. Since this cross section appears to be quite large at plasma temperatures near 5,000°K, the method used in

the present research to determine the sulphur hexafluoride electron capture cross section should be used when the plasma temperature is lower than 5,000°K. For higher plasma temperatures, it may be possible to determine the capture cross section by measuring the electron concentration at various axial stations within the plasma jet.

The electrophilic effects of other additives can be investigated using the electrostatic probe. Of special interest would be other proposed uranium carrying gases for gas core nuclear reactors as well as gases which might also be highly electrophilic. Also of interest would be gases which increase rather than decrease the electron concentration within a plasma. A gas of this type would be useful in a magnetohydrodynamic generator where a high electron concentration is important.

In addition to the studies outlined above, it is recommended that additional refinements be made to the present theory in order to improve its accuracy and extend its range of applicability. This can be done by rederiving the electrostatic probe equations eliminating the assumptions made in the theory. The solution would involve simultaneous solutions of the flow equations, the electrostatic equations, the chemical reaction rate equations, and possibly a more exact analysis of the plasma sheath thickness equations. The electrostatic probe theory can also be extended to include supersonic flow by accounting for the effects of the normal shock upstream of the probe on the ionization level and the pressure gradient parameter at the probe surface.

APPENDIX A

DERIVATION OF THE STAGNATION POINT FLOW EQUATIONS

The solutions to the stagnation point flow equations are presented in Chapter II along with an explanation of their use. In this appendix a detailed solution to the stagnation point flow equations is presented. The solution is essentially that of Lees[13] and Talbot[12] and is presented here for the benefit of the reader. When the present derivation differs from those of Lees and Talbot, the difference will be noted. Since the assumptions that were made in solving the equations have been discussed in detail in Chapter II, they will not be examined extensively here.

A completely general solution to the problem of an ionized stagnation-point flow containing negative ions would have to consider at least a four-component gas containing positive ions, negative ions, electrons, and neutral particles and include the rates of reaction and interdiffusion between these species. However, if it is assumed that (a) the flow in the boundary layer is completely frozen and that (b) ambipolar diffusion is the diffusion mechanism outside of the plasma sheath then the solution can be simplified considerably.

The condition for frozen flow is that the transit time for a particle through the boundary layer must be much less than the relevant time for recombination.

Ambipolar diffusion implies that, in the absence of an external electric field, the positive ions, negative ions, and electrons all

diffuse through the plasma at the same rate. This must be the case if the plasma condition $n_i = n_e + n_n$ is to hold. The term ambipolar diffusion is normally used to describe the diffusion process in a plasma in which the only charged particles are positive ions and electrons. The definition has been extended in this work to include plasmas which contain negative ions. Thus, in the boundary layer, outside the sheath, the gas may be treated as a mixture of neutral molecules and positive ion-negative ion-electron groups which diffuse relative to the neutral gas at a rate determined by the ambipolar diffusion coefficient

$$D_a = \frac{D_i\left|\left(1 - \frac{n_n}{n_i}\right)\bar{\mu}_e + \frac{n_n}{n_i}\bar{\mu}_n\right| + D_e\left(1 - \frac{n_n}{n_i}\right)\bar{\mu}_i + D_n\frac{n_n}{n_i}\bar{\mu}_i}{\left(1 - \frac{n_n}{n_i}\right)\bar{\mu}_e + \frac{n_n}{n_i}\bar{\mu}_n + \bar{\mu}_i} \qquad \text{(A-1)}$$

which was derived in Chapter II and where $\bar{\mu}_i$, $\bar{\mu}_n$, $\bar{\mu}_e$ are the positive ion, negative ion, and electron mobilities, and D_i, D_n, and D_e are the diffusion coefficients.

The stagnation point boundary layer flow can thus be considered to be a flow composed of a mixture of neutral gas molecules, positive ions, negative ions, and electrons where because of charge neutrality

$$n_i = n_e + n_n \, . \qquad \text{(A-2)}$$

The charged particle group concentration can be defined as

$$c = \frac{\rho_i + \rho_n + \rho_e}{\rho} = \frac{m_i n_i + m_n n_n + m_e n_e}{m_i n_i + m_n n_n + m_e n_e + m_p n_p} \approx \frac{n_i + \frac{m_n}{m_i} n_n}{n_i + \frac{m_n}{m_i} n_n + n_p} \qquad \text{(A-3)}$$

where m_p and n_p are the masses and number densities of the neutral molecules. Following the work of Lees[13] and using the customary boundary-layer notation shown in Figure 17 the conservation equations for steady axisymmetric flow can be written as:

Charged particle concentration

$$\rho\left(u\,\frac{\partial c}{\partial x} + v\,\frac{\partial c}{\partial y}\right) = \frac{\partial}{\partial y}\left(\rho D_a\,\frac{\partial c}{\partial y}\right) \tag{A-4}$$

Continuity

$$\frac{\partial}{\partial x}\,(\rho u x) + \frac{\partial}{\partial y}\,(\rho v x) = 0 \tag{A-5}$$

Momentum

$$\rho u\,\frac{\partial u}{\partial x} + \rho v\,\frac{\partial u}{\partial y} = -\,\frac{dp_2}{dx} + \frac{\partial}{\partial x}\left(\mu\,\frac{\partial u}{\partial y}\right) \tag{A-6}$$

Energy

$$\rho u\,\frac{\partial h}{\partial x} + \rho v\,\frac{\partial h}{\partial y} = \frac{\partial}{\partial y}\left(\lambda_T\,\frac{\partial T}{\partial y}\right) + u\,\frac{dp_2}{dx} + \mu\left(\frac{\partial u}{\partial y}\right)^2 \tag{A-7}$$

where the subscript 2 denotes conditions in the inviscid flow external to the boundary layer. The static enthalpy, h, is defined in terms of the frozen specific heat $\bar{c}_p$, by

$$dh = \bar{c}_p\,dT\ . \tag{A-8}$$

It is convenient to also define a "frozen total enthalpy," $\bar{h}_t$, by

$$d\bar{h}_t = \bar{c}_p\,dT + d\left(\frac{u^2}{2}\right) \tag{A-9}$$

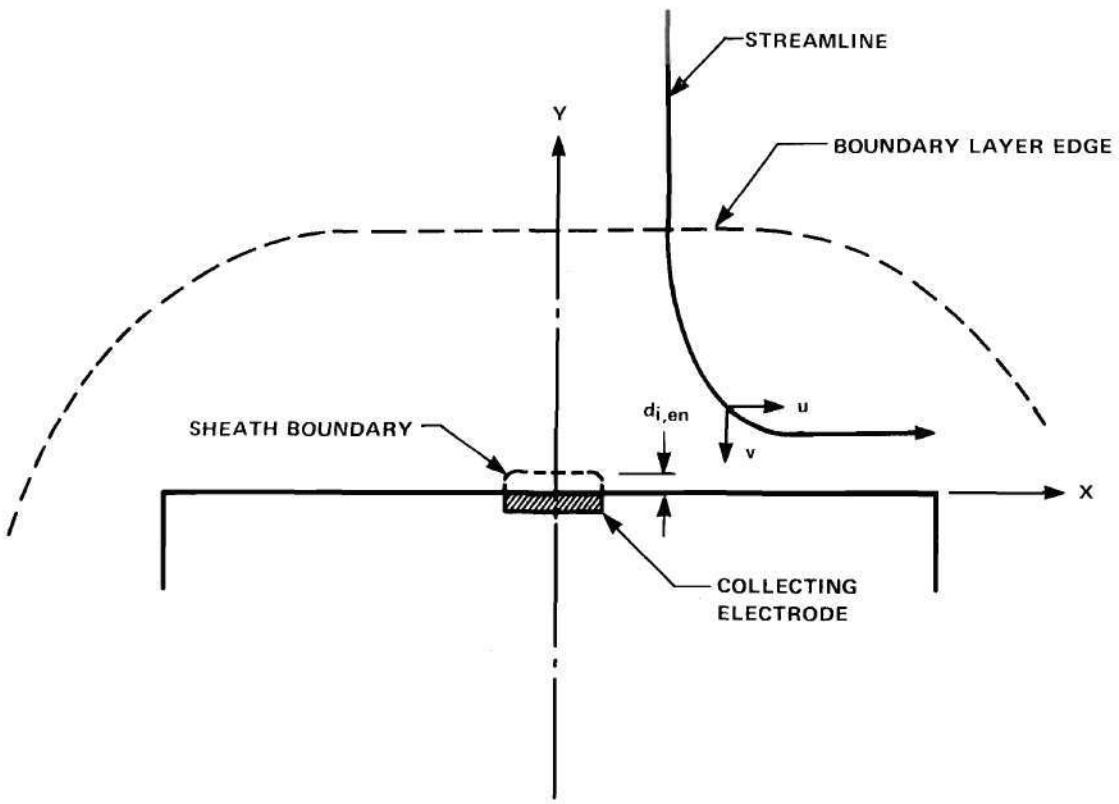

Figure 17. Boundary Layer Notation

which is analogous to the total enthalpy of a perfect unionized gas.

When the momentum equation is multiplied by u and added to the energy equation, the terms involving the concentration c drop out when the charged particle concentration equation is substituted. Thus Equation (7) becomes

$$\rho u \frac{\partial \bar{h}_t}{\partial x} + \rho v \frac{\partial \bar{h}_t}{\partial y} = \frac{\partial}{\partial y}\left(\frac{\lambda_T}{\bar{c}_p}\frac{\partial \bar{h}_t}{\partial y}\right) - \frac{\partial}{\partial y}\left[\mu\left(\frac{1}{\bar{\sigma}} - 1\right)\frac{\partial}{\partial y}\left(\frac{u^2}{2}\right)\right] \tag{A-10}$$

in which

$$\bar{\sigma} = \frac{\mu \bar{c}_p}{\lambda_T} \tag{A-11}$$

is the Prandtl number. To simplify the equations, two new coordinates,

$$\eta = \frac{u_2}{(2s)^{\frac{1}{2}}} \int_o^y x\rho \, dy \tag{A-12}$$

and

$$s = \int_o^x \rho_2 u_2 \mu_2 x^2 dx \ , \tag{A-13}$$

a stream function ψ which satisfies the continuity equation by

$$\frac{\partial \psi}{\partial y} = \rho u x \tag{A-14}$$

and

$$\frac{\partial \psi}{\partial x} = - \rho v x \ , \tag{A-15}$$

and a nondimensional stream function

$$f = \frac{\psi}{(2s)^{\frac{1}{2}}} \tag{A-16}$$

which is chosen such that

$$\frac{u}{u_2} = \frac{\partial f}{\partial \eta} \equiv f' \tag{A-17}$$

and

$$v = - \frac{1}{\rho x} \frac{ds}{dx} \left[\frac{f}{(2s)^{\frac{1}{2}}} + (2s)^{\frac{1}{2}} f' \left(\frac{\partial \eta}{\partial s} \right) \right] \tag{A-18}$$

are introduced. The relationships

$$\frac{\partial}{\partial x} = \frac{\partial}{\partial \eta} \frac{\partial \eta}{\partial s}\bigg|_y \frac{ds}{dx} + \frac{\partial}{\partial s}\bigg|_y \frac{ds}{dx} = \frac{ds}{dx} \left[\frac{\partial \eta}{\partial s} \frac{\partial}{\partial \eta} + \frac{\partial}{\partial s}\bigg|_y \right] \tag{A-19}$$

and

$$\frac{\partial}{\partial y} = \frac{\partial}{\partial \eta} \frac{\partial \eta}{\partial y} + \frac{\partial}{\partial s} \frac{\partial s}{\partial y} = \frac{u_2 \, x \rho}{(2s)^{\frac{1}{2}}} \frac{\partial}{\partial \eta} \tag{A-20}$$

and the definitions

$$z = \frac{c}{c_2} \tag{A-21}$$

and

$$\overline{g} = \frac{\overline{h}_t}{\overline{h}_{t2}} \tag{A-22}$$

are also introduced. Substitution of Equation (21) into the species conservation equation, Equation (4), gives

$$\rho\left(u\frac{\partial zc_2}{\partial x} + v\frac{\partial zc_2}{\partial y}\right) = \frac{\partial}{\partial y}\left(\rho D_a \frac{\partial zc_2}{\partial y}\right) \tag{A-23}$$

which becomes

$$\rho\left(u\frac{\partial zc_2}{\partial x} + v\frac{\partial zc_2}{\partial y}\right) = \rho D_a \frac{\partial^2 zc_2}{\partial y^2} + \frac{\partial zc_2}{\partial y} D_a \frac{\partial \rho}{\partial y} \tag{A-24}$$

where D_a is assumed to be independent of y. Substituting Equations (17), (18), (19), and (20) into Equation (24) yields

$$f'\frac{ds}{dx}\frac{\partial zc_2}{\partial s} - \frac{ds}{dx}\frac{f}{2s}\frac{\partial zc_2}{\partial \eta} = D_a \frac{u_2 x^2 \rho^2}{2s}\left(\frac{\partial^2 zc_2}{\partial \eta^2} + \frac{1}{\rho}\frac{\partial zc_2}{\partial \eta}\frac{\partial \rho}{\partial \eta}\right). \tag{A-25}$$

Since

$$\frac{ds}{dx} = \rho_2 u_2 \mu_2 x^2 , \tag{A-26}$$

Equation (25) becomes

$$2sf'\rho_2\mu_2\frac{\partial zc_2}{\partial s} - f\rho_2\mu_2\frac{\partial zc_2}{\partial \eta} = D_a\rho^2\left(\frac{\partial^2 zc_2}{\partial \eta^2} + \frac{1}{\rho}\frac{\partial \rho}{\partial \eta}\frac{\partial zc_2}{\partial \eta}\right) \tag{A-27}$$

where c_2 is a constant. Also since

$$\rho = \frac{(2s)^{\frac{1}{2}}}{u_2 x}\frac{\partial \eta}{\partial y} , \tag{A-28}$$

$\partial\rho/\partial\eta$ is given by

$$\frac{\partial \rho}{\partial \eta} = \frac{\partial}{\partial \eta}\left[\frac{(2s)^{\frac{1}{2}}}{u_2 x}\right]\frac{\partial \eta}{\partial y} + \frac{(2s)^{\frac{1}{2}}}{u_2 x}\frac{\partial^2 \eta}{\partial y \partial \eta} = \frac{\partial \eta}{\partial y}\frac{(2s)^{-\frac{1}{2}}}{u_2 x}\frac{\partial s}{\partial \eta} = 0 \qquad \text{(A-29)}$$

and Equation (27) becomes

$$2s\frac{\partial z}{\partial s} f' - fz' - \frac{D_a \rho^2}{\mu_2 \rho_2}\frac{\partial^2 z}{\partial \eta^2} = 0 \qquad \text{(A-30)}$$

which simplifies to

$$2s\frac{\partial z}{\partial s} f' - fz' - \left(\frac{\ell}{S} z'\right)' = 0 \qquad \text{(A-31)}$$

where the definitions

$$\ell = \frac{\rho \mu}{\rho_2 \mu_2} \qquad \text{(A-32)}$$

and

$$S = \frac{\mu}{\rho D_a} \qquad \text{(A-33)}$$

are used. The term ℓ is the Chapman-Rubesin factor and S is the Schmidt number.

Before substituting the new coordinates into the momentum equation, Equation (6), it should be noted that

$$\frac{dp_2}{dx} = -\rho_2 u_2 \frac{\partial u_2}{\partial x} . \qquad \text{(A-34)}$$

Hence Equation (6) becomes

$$u \frac{\partial u}{\partial x} + v \frac{\partial u}{\partial y} = \frac{\rho_2}{\rho} u_2 \frac{\partial u_2}{\partial x} + \frac{1}{\rho} \frac{\partial}{\partial y} \left(\mu \frac{\partial u}{\partial y} \right) \tag{A-35}$$

or, after the substitutions,

$$f' \frac{\partial u_2 f'}{\partial s} - \frac{f}{2s} \frac{\partial u_2 f'}{\partial \eta} = \frac{\rho_2}{\rho} \frac{\partial \eta}{\partial s} \frac{\partial u_2}{\partial \eta} + \frac{\rho_2}{\rho} \frac{\partial u_2}{\partial s} \tag{A-36}$$

$$+ \frac{x}{(2s)^{\frac{1}{2}}} \frac{1}{\frac{ds}{dx}} \mu \frac{u_2 x \rho}{(2s)^{\frac{1}{2}}} \frac{\partial^2 (u_2 f')}{\partial \eta^2} + \frac{x}{(2s)^{\frac{1}{2}}} \frac{\partial u_2 f'}{\partial \eta} \frac{\partial \left[\frac{\mu u_2 x \rho}{(2s)^{\frac{1}{2}}} \right]}{\partial \eta} \frac{1}{\frac{ds}{dx}} .$$

Since

$$\frac{ds}{dx} = \rho_2 u_2 \mu_2 x^2 , \tag{A-37}$$

Equation (36) becomes

$$f' \frac{\partial u_2 f'}{\partial s} - \frac{f}{2s} \frac{\partial u_2 f'}{\partial \eta} = \frac{\rho_2}{\rho} \frac{\partial \eta}{\partial s} \frac{\partial u_2}{\partial \eta} + \frac{\rho_2}{\rho} \frac{\partial u_2}{\partial s} + \frac{\rho}{\rho_2} \frac{\mu}{\mu_2} \frac{1}{2s} \frac{\partial^2 (u_2 f')}{\partial \eta^2} \tag{A-38}$$

$$+ \frac{1}{(2s)^{\frac{1}{2}} u_2 \mu_2 x \rho_2} \frac{\partial u_2 f'}{\partial \eta} \frac{\partial \left[\frac{\mu u_2 x \rho}{(2s)^{\frac{1}{2}}} \right]}{\partial \eta} .$$

Since f is not a function of s and u_2 is not a function of η, Equation (38) becomes

$$\frac{2s}{u_2} (f')^2 \frac{\partial u_2}{\partial s} - ff'' = \frac{2s\rho_2}{u_2 \rho} \frac{\partial u_2}{\partial s} + \left(\frac{\rho \mu}{\rho_2 \mu_2} f'' \right)' \tag{A-39}$$

and substituting the Chapman-Rubesin factor, ℓ, gives

$$(\ell f'')' + ff'' = -\frac{2s}{u_2}\frac{\partial u_2}{\partial s}\left[\frac{\rho_2}{\rho} - f'^2\right] \tag{A-40}$$

for the transformed momentum equation.

The energy equation to be transformed is in the form of Equation (10). Before making the transformation the relationship

$$\bar{g} = \frac{\bar{h}_t}{\bar{h}_{t2}} \tag{A-41}$$

where $\bar{h}_{t2}$ is the free stream stagnation enthalpy, is substituted into Equation (10) to give

$$\rho u \frac{\partial \bar{h}_{t2}\bar{g}}{\partial x} + \rho v \frac{\partial \bar{h}_{t2}\bar{g}}{\partial y} = \frac{\partial}{\partial y}\left(\frac{\lambda_T}{\bar{c}_p}\frac{\partial \bar{h}_{t2}\bar{g}}{\partial y}\right) - \frac{\partial}{\partial y}\left[\mu\left(\frac{1}{\bar{\sigma}} - 1\right)\frac{\partial}{\partial y}\left(\frac{u^2}{2}\right)\right] \tag{A-42}$$

and substituting the new coordinate system yields

$$f'\frac{ds}{dx}\frac{\partial \bar{h}_{t2}\bar{g}}{\partial s} - \frac{ds}{dx}\frac{f}{2s}\frac{\partial \bar{h}_{t2}\bar{g}}{\partial \eta} = \frac{x^2 u_2}{2s}\frac{\partial}{\partial \eta}\left[\frac{\lambda_T}{\bar{c}_p}\rho\frac{\partial \bar{h}_{t2}\bar{g}}{\partial \eta}\right] \tag{A-43}$$

$$- \frac{x^2 u_2^3}{2s}\frac{\partial}{\partial \eta}\left[\mu\left(\frac{1}{\bar{\sigma}} - 1\right)\rho\frac{\partial}{\partial \eta}\left(\frac{f'^2}{2}\right)\right] .$$

Substituting Equation (34) into Equation (43) yields

$$f'\rho_2 u_2 \mu_2 x^2 \frac{\partial \bar{h}_{t2}\bar{g}}{\partial s} - \rho_2 u_2 \mu_2 x^2 \frac{f}{2s} \frac{\partial \bar{h}_{t2}\bar{g}}{\partial \eta} = \tag{A-44}$$

$$\frac{x^2 u_2}{2s} \frac{\partial}{\partial \eta} \left[\frac{\bar{\lambda}_T}{\bar{c}_p} \rho \frac{\partial \bar{h}_{t2}\bar{g}}{\partial \eta} \right] - \frac{x^2 u_2^3}{2s} \frac{\partial}{\partial \eta} \left[\mu \left(\frac{1}{\bar{\sigma}} - 1 \right) \rho \frac{\partial}{\partial \eta} \left(\frac{f'^2}{2} \right) \right] .$$

With $\bar{h}_{t2}$ a constant and $\bar{g}$ a function of η only, Equation (44) becomes

$$f\bar{g}' = - \left[\frac{\rho\mu}{\rho_2 \mu_2 \bar{\sigma}} \bar{g}' \right]' + \frac{u_2^2}{2\bar{h}_{t2}} \left[2 \frac{\rho\mu}{\rho_2 \mu_2} \left(\frac{1}{\bar{\sigma}} - 1 \right) f'f'' \right]' . \tag{A-45}$$

Thus the three transformed conservation equations become:

Species conservation

$$2s \frac{\partial z}{\partial s} f' - fz' - \left(\frac{\ell}{S} z' \right)' = 0 \tag{A-46}$$

Momentum

$$(\ell f'')' + ff'' = - \frac{2s}{u_2} \frac{\partial u_2}{\partial s} \left(\frac{\rho_2}{\rho} - f'^2 \right) \tag{A-47}$$

and Energy

$$f\bar{g}' + \left(\frac{\ell}{\bar{\sigma}} \bar{g}' \right)' = - \frac{u_2^2}{2\bar{h}_{t2}} \left[2\ell \left(1 - \frac{1}{\bar{\sigma}} \right) f'f'' \right]' . \tag{A-48}$$

The boundary conditions on f and $\bar{g}$ are

$$f(o) = f'(o) = 0 , \tag{A-49}$$

$$f'(\infty) = 1 , \tag{A-50}$$

$$\bar{g}(\infty) = 1 \ , \tag{A-51}$$

and for the cold wall case

$$\bar{g}(o) << 1 \ . \tag{A-52}$$

The approximations made by Lees are sufficiently accurate for the Langmuir probe case and will be introduced here. The approximations are to take

$$\ell = 1 \ , \tag{A-53}$$

$$\bar{\sigma} = \text{constant} \ , \tag{A-54}$$

and to neglect the pressure gradient terms on the right-hand side of the momentum and energy equations. Then, the momentum equation reduces to the Blasius equation

$$f''' + ff'' = 0 \tag{A-55}$$

and the energy equation becomes

$$\bar{\sigma} f \bar{g}' + \bar{g}'' = 0 \ . \tag{A-56}$$

In the vicinity of the stagnation point ($s << 1$), the ion group conservation equation with S assumed constant becomes

$$z'' + Sfz' = 0 \ . \tag{A-57}$$

In general, the approximations inherent in any Langmuir probe theory can be expected to introduce errors more serious than those of this simplified boundary layer theory, so it is clearly justified to use the

Lees approximations which permit explicit solutions of the problem.

The solution to the momentum equation is the Blasius function, which is tabulated in the literature.

To solve the energy equation, the momentum equation is written in the form

$$f = - \frac{f'''}{f''} \tag{A-58}$$

and the energy equation becomes

$$\frac{\bar{g}''}{\bar{g}'} = \bar{\sigma} \frac{f'''}{f''} . \tag{A-59}$$

Integrating with respect to η gives

$$\ell n \left[\frac{\bar{g}'(\eta)}{\bar{g}'(\eta_o)} \right] = \bar{\sigma} \ell n \left[\frac{f''(\eta)}{f''(\eta_o)} \right] \tag{A-60}$$

or

$$\bar{g}'(\eta) = \bar{g}'(\eta_o) \left[\frac{f''(\eta)}{f''(\eta_o)} \right]^{\bar{\sigma}} \tag{A-61}$$

and integrating once again

$$\bar{g}(\eta) = \bar{g}(\eta_o) + \bar{g}'(\eta_o) \int_{\eta_o}^{\eta} \left[\frac{f''(\eta)}{f''(\eta_o)} \right]^{\bar{\sigma}} d\eta . \tag{A-62}$$

Likewise for the ion group conservation equation

$$z(\eta) = z(\eta_o) + z'(\eta_o) \int_{\eta_o}^{\eta} \left[\frac{f''(\eta)}{f''(\eta_o)} \right]^{S} d\eta . \tag{A-63}$$

In both equations η_o is arbitrary and not necessarily the same for each equation.

For the energy equation, if it is assumed that the temperature distribution within the boundary layer is undisturbed by the presence of the sheath, the lower boundary condition may be applied at $\eta = 0$. The temperature of the wall is assumed to be known and according to Cohen and Reshotko[25] the enthalpy gradient $\bar{g}'(0)$ is represented quite accurately by

$$\bar{g}'(0) = 0.50\ \bar{\sigma}^{1/3} \quad . \tag{A-64}$$

Lees and Talbot use a value of 0.47 for the coefficient in Equation (64). This represents the enthalpy gradient when there is no pressure gradient in the boundary layer. In this case, there is a pressure gradient in the boundary layer and the value of 0.50 is more correct. Equation (62) thus becomes

$$\bar{g}(\eta) = \bar{g}(0) + 0.50\ \bar{\sigma}^{1/3} \int_o^{\eta} \left[\frac{f''(\eta)}{f''(0)}\right]^{\bar{\sigma}} d\eta \quad . \tag{A-65}$$

For the ion group conservation equation, the choices for η_o are the transformed sheath thicknesses d_i or $d_{e,n}$ depending upon the type of particles being absorbed at the probe. The probe surface cannot be used for η_o because the assumed conditions of plasma neutrality and ambipolar diffusion do not apply for $\eta < \eta_{i;e,n}$. If the sheath thicknesses η_i and $\eta_{e,n}$ are denoted by the common symbol η_d, Equation (63) becomes

$$z(\eta) = z(\eta_d) + z'(\eta_d) \int_{\eta_d}^{\eta} \left[\frac{f''(\eta)}{f''(\eta_d)}\right]^S d\eta \ . \qquad \text{(A-66)}$$

For

$$\eta = \infty \qquad \text{(A-67)}$$

the value of $z(\eta)$ becomes

$$z(\eta) = 1 \qquad \text{(A-68)}$$

thus

$$z(\eta_d) = 1 - z'(\eta_d) \int_{\eta_d}^{\infty} \left[\frac{f''(\eta)}{f''(\eta_d)}\right]^S d\eta \ . \qquad \text{(A-69)}$$

This equation may be interpreted as follows. If both the charge concentration and concentration gradient at the edge of the sheath are known or can be determined, and the transformed sheath thickness is calculated, then this equation can be used to determine the charge concentration c_2 at the outer edge of the boundary layer.

Talbot uses a value for $z'(\eta_d)$ of $0.47\ S^{1/3}$. This value was arrived at by assuming that the sheath is thin enough so that its thickness may be neglected and that, because the charged particles undergo a large acceleration in the sheath, the charge concentration at the probe surface is very small. With these two assumptions, Equation (66) becomes identical in form to Equation (65) and thus, by similarity, $z'(\eta_d)$ will have the same form as $\overline{g}'(0)$. In the present case, however, the sheath is not negligibly thin compared to the boundary layer thickness and

thus the above argument is not applicable and the charge concentration gradient at the sheath edge will have to be determined in another manner.

The gradient $\left.\frac{\partial c}{\partial \eta}\right|_{\eta=\eta_d}$ at the edge of the sheath can, in principle, be found by making measurements with varying probe potential to determine the variation of c with η in the vicinity of a particular η_d. It should be noted that, if the ionization is appreciable, the calculations may be quite involved because the transformation giving $d_{i,e}$ in terms of η_d involves the density ρ which itself is a function of the concentration. However, once these parameters are determined, c_2 may be calculated by the relationship

$$c_2 = c(\eta_d) + c'(\eta_d) \int_{\eta_d}^{\infty} \left[\frac{f''(\eta)}{f''(\eta_d)}\right]^S d\eta \ . \qquad \text{(A-70)}$$

Some additional approximations are necessary to simplify the solution. As noted by Talbot, these approximations introduce errors no worse than those already introduced and thus are consistent with the rest of the analysis.

In the energy equation, Equation (65), the term $\left[\frac{f''(\eta)}{f''(0)}\right]^{\bar{\sigma}}$ may be taken equal to unity since $f''(\eta)$ varies slowly and the limits of integration are 0 and η_d (which is assumed to be small). Also $\bar{g}(0)$ is assumed to be small enough to be neglected. Using these two assumptions the energy equation becomes

$$\bar{g}(\eta_d) = 0.50\ \bar{\sigma}^{-1/3}\ \eta_d \ . \qquad \text{(A-71)}$$

At the stagnation point of a blunt body

$$u_2 = \overline{\beta} x \ . \tag{A-72}$$

Putting this relationship into the transformation equations gives

$$s = \int_o^x \rho_2 \overline{\beta} x \mu_2 x^2 dx \tag{A-73}$$

or

$$s = \frac{\rho_2 \mu_2 \overline{\beta}}{4} x^4 \tag{A-74}$$

and

$$\eta = \frac{\overline{\beta} x}{\left(\frac{\rho_2 \mu_2 \overline{\beta}}{2} x^4 \right)^{\frac{1}{2}}} \int_o^y x \rho dy \tag{A-75}$$

or

$$\eta = \frac{\sqrt{2}\ \overline{\beta}^{\frac{1}{2}}}{\sqrt{\rho_2 \mu_2}} \int_o^y \rho dy \ . \tag{A-76}$$

Taking the derivative of η with respect to y gives

$$\frac{d\eta}{dy} = \frac{\sqrt{2}\ \overline{\beta}^{\frac{1}{2}}}{\sqrt{\rho_2 \mu_2}} \rho = \sqrt{\frac{2\ \rho_2 \overline{\beta}}{\mu_2}} \frac{\rho}{\rho_2} \tag{A-77}$$

and solving for y gives

$$y = \left(\frac{\mu_2}{2\ \rho_2 \overline{\beta}} \right)^{\frac{1}{2}} \int_o^\eta \frac{\rho_2}{\rho} d\eta \ . \tag{A-78}$$

If the value of η is small and if the ion group concentration in the boundary layer is small, then

$$\frac{\rho_2}{\rho(\eta)} = \bar{g}(\eta) \ . \tag{A-79}$$

Thus, Equation (78) becomes

$$y = \left(\frac{\mu_2}{2\ \rho_2\bar{\beta}}\right)^{\frac{1}{2}} \int_o^{\eta} \bar{g}(\eta)\, d\eta \tag{A-80}$$

and if $\bar{g}(\eta)$ is assumed to be given by

$$\bar{g}(\eta) = \bar{g}'(0)\eta = 0.50\ \bar{\sigma}^{1/3}\eta \ , \tag{A-81}$$

Equation (80) becomes

$$d_{i;e,n} = \left(\frac{\mu_2}{2\ \rho_2\bar{\beta}}\right)^{\frac{1}{2}} \int_o^{\eta_d} 0.50\ \bar{\sigma}^{1/3}\eta d\eta \tag{A-82}$$

and integrating

$$d_{i;e,n} = 0.18\ \bar{\sigma}^{1/3} \left(\frac{\mu_2}{\rho_2\bar{\beta}}\right)^{\frac{1}{2}} \eta^2_{i;e,n} \ . \tag{A-83}$$

For the value of $\bar{\beta}$, Probstein's[26] expression for the supersonic case which gives

$$\bar{\beta} = \frac{8v_1}{3\pi D_o}\left[\frac{\rho_1}{\rho_2}\left(2 - \frac{\rho_1}{\rho_2}\right)\right]^{\frac{1}{2}} \tag{A-84}$$

may be used where v_1 is the velocity before the shock, D_o is the diameter of the probe, and ρ_1 and ρ_2 are the gas densities before and after the

shock respectively. For the subsonic case the relationship

$$-\frac{d\,\frac{p}{\rho}}{dx} = \frac{d}{dx}\left(\frac{u_2^2}{2}\right) = \frac{d}{dx}\left(\frac{\bar{\beta}^2 x^2}{2}\right) \tag{A-85}$$

is integrated to give

$$\bar{\beta} = \frac{\sqrt{2\left(\frac{p_o}{\rho_o} - \frac{p}{\rho}\right)}}{x} \tag{A-86}$$

where p and ρ are the pressure and density at a distance x from the center of the probe. If it is assumed that the flow at the edge of the boundary layer is a constant density flow, and that the pressure drops radially from the stagnation pressure p_o at x = o to the free stream static pressure p_2 at $x = D_o/2$; i.e., at the edge of the probe, then Equation (86) becomes

$$\bar{\beta} = \frac{2}{D_o}\sqrt{2\,\frac{p_o - p_2}{\rho_o}} \quad . \tag{A-87}$$

Equations (70), (71), (83), and either Equation (84) or Equation (87) are used in the manner described in Chapter II to determine the free stream stagnation temperature and ionization level once the plasma temperature and ionization at the edge of the plasma sheath has been determined. The electrostatic probe theory which was used to determine the sheath edge plasma temperature and ionization will be developed in Appendix B.

APPENDIX B

DERIVATION OF THE ELECTROSTATIC PROBE EQUATIONS

In Chapter III, the electrostatic probe theory was briefly summarized and the rational for selecting a simple and easily used theory was presented. A more detailed derivation of the electrostatic probe theory will be presented in this appendix.

The basic theory is that of Hung and Paquette[19] which is a modification of the theory originally developed by Langmuir.[1] According to Langmuir's original theory, the plasma can be divided into two distinct regions, a sheath adjacent to the probe surface where charged particles of predominately one sign are present, and the undisturbed plasma which maintains its charge neutrality. The current collected by the probe is supplied by gas kinetic diffusion across the plasma-sheath interface and is space-charge limited within the sheath. It was further assumed that the sheath thickness is small compared to an ionic or electron mean free path, so that the velocities of the charged particles are given by the free fall relations and no ionization, recombination, or charge exchange occurs within the sheath.

The present problem is that of a plane probe in a steady continuum flow in which the electric field points only in the x-direction and is given by

$$E = - \frac{d\phi}{dx} \tag{B-1}$$

where E is the electric field in the x-direction and ϕ is the electric potential which is assumed to be zero in the plasma. It is also assumed that although the sheath thickness is larger than the particle mean free path no ionization, recombination, or charge exchange occurs within the sheath. For this particular case, the Boltzmann equation is given by

$$u \frac{\partial \overline{f}}{\partial x} - \frac{eZ}{m} \frac{d\phi}{dx} \frac{\partial \overline{f}}{\partial u} = 0 \qquad \text{(B-2)}$$

where u is the particle velocity in the x-direction, e is the electronic charge, Z is the number of net electronic charges per particle, m is the particle mass, and $\overline{f}$ is the particle distribution function. If the function $\overline{f}$ is assumed to be given by

$$\overline{f} = \overline{f}_x(x,u)\overline{f}_y(y,v)\overline{f}_z(z,w) \qquad \text{(B-3)}$$

where v and w are the particle velocities in the y and z directions respectively, then equation (2) becomes

$$u \frac{\partial \overline{f}_x}{\partial x} - \frac{eZ}{m} \frac{d\phi}{dx} \frac{\partial \overline{f}_x}{\partial u} = 0 \ . \qquad \text{(B-4)}$$

In addition, if $\overline{f}_x(x,u)$ is assumed to be given by

$$\overline{f}_x(x,u) = F(u)G(x) \qquad \text{(B-5)}$$

then Equation (4) becomes

$$uF \frac{dG}{dx} - \frac{eZ}{m} \frac{d\phi}{dx} \frac{dF}{du} G = 0 \qquad \text{(B-6)}$$

or

$$\frac{\frac{dG}{dx}}{eZG\,\frac{d\phi}{dx}} = \frac{1}{mu}\,\frac{dF}{du}\,\frac{1}{F}\ . \qquad \text{(B-7)}$$

Since G and F are independent, Equation (7) can hold only if both sides of the equation are equal to a constant. Thus

$$\frac{1}{eZG\,\frac{d\phi}{dx}}\,\frac{dG}{dx} = -b \qquad \text{(B-8)}$$

and

$$\frac{1}{mu}\,\frac{dF}{du}\,\frac{1}{F} = -b\ . \qquad \text{(B-9)}$$

Equation (8) becomes

$$\frac{1}{G}\,\frac{dG}{dx} = -\,beZ\,\frac{d\phi}{dx} \qquad \text{(B-10)}$$

or

$$\ell n\ G = -\,beZ\phi\ -\ \ell n\,\frac{1}{a_1} \qquad \text{(B-11)}$$

where a_1 is a constant. Equation (11) becomes

$$G = a_1 e^{-beZ\phi}\ . \qquad \text{(B-12)}$$

Equation (9) becomes

$$\frac{dF}{F} = -\,bmudu \qquad \text{(B-13)}$$

or

$$\ell nF = - bm \frac{u^2}{2} - \ell n \frac{1}{a_2} \tag{B-14}$$

where a_2 is a constant. Equation (14) becomes

$$F = a_2 e^{-b\left(\frac{mu^2}{2}\right)} . \tag{B-15}$$

Substituting Equations (12) and (15) into Equation (5) yields

$$\overline{f}_x(x,u) = a_3 e^{-b(\frac{mu^2}{2} + eZ\phi)} \tag{B-16}$$

where

$$a_3 = a_1 a_2 . \tag{B-17}$$

In the other directions, there is no contribution from the electric field and thus $\overline{f}_y(y,v)$ and $\overline{f}_z(z,w)$ are Maxwellian distributions. Equation (3) thus becomes

$$\overline{f} = ae^{-b(\frac{mu^2}{2}) - \frac{1}{2}(\frac{m}{kT})(v^2 + w^2) - beZ\phi} \tag{B-18}$$

where a is the combined value of a_3 and the constants from $\overline{f}_y(y,v)$ and $\overline{f}_z(z,w)$.

When there is no electrical potential between the probe surface and the plasma,

$$\phi = 0 \tag{B-19}$$

and the distribution function is Maxwellian. Hence

$$b = \frac{1}{kT} \tag{B-20}$$

and

$$a = n_o\left(\frac{m}{2\pi kT}\right)^{3/2} \tag{B-21}$$

thus giving

$$\bar{f} = n_o\left(\frac{m}{2\pi kT}\right)^{3/2} e^{-\left(\frac{m\bar{V}^2 + 2eZ\phi}{2kT}\right)} \tag{B-22}$$

where k is the Boltzmann constant, T is the temperature of the particles, n_o is the undisturbed particle number density, and

$$\bar{V}^2 = u^2 + v^2 + w^2 \ . \tag{B-23}$$

Equation (22) is a general equation for the particle distribution function. If the plasma is assumed to be singly ionized and to contain positive and negative ions as well as electrons, then the distribution functions for each species become

$$\bar{f}_e = n_{oe}\left(\frac{m_e}{2\pi kT_e}\right)^{3/2} e^{\frac{-\left(\frac{1}{2} m_e \bar{V}_e^2 - e\phi\right)}{kT_e}} , \tag{B-24}$$

$$\bar{f}_i = n_{oi}\left(\frac{m_i}{2\pi kT_i}\right)^{3/2} e^{\frac{-\left(\frac{1}{2} m_i \bar{V}_i^2 + e\phi\right)}{kT_i}} , \tag{B-25}$$

and

$$\bar{f}_n = n_{oi}\left(\frac{m_n}{2\pi kT_n}\right)^{3/2} e^{\frac{-(\frac{1}{2} m_n \bar{V}_n^2 - e\phi)}{kT_n}} \qquad \text{(B-26)}$$

where the subscripts e, i, and n indicate properties of the electrons, positive ions, and negative ions respectively.

Within the sheath, the particle number density is obtained by integrating the particle distribution functions over all possible velocities. The electron number density becomes

$$n_e = \int_{-\infty}^{\infty}\int_{-\infty}^{\infty}\int_{-\infty}^{\infty} \bar{f}_e \, du \, dv \, dw \qquad \text{(B-27)}$$

or

$$n_e = \int_{-\infty}^{\infty}\int_{-\infty}^{\infty}\int_{-\infty}^{\infty} n_{oe} \frac{m_e}{2\pi kT_e}^{3/2} e^{\frac{-(\frac{1}{2} m_e \bar{V}_e^2 - e\phi)}{kT_e}} du \, dv \, dw \qquad \text{(B-28)}$$

which integrates to

$$n_e = n_{oe} e^{\frac{e\phi}{kT_e}} . \qquad \text{(B-29)}$$

Likewise, the positive and negative ion number densities within the sheath are given by

$$n_i = n_{oi} e^{-\frac{e\phi}{kT_i}} \qquad \text{(B-30)}$$

and

$$n_n = n_{on} e^{\frac{e\phi}{kT_n}} . \qquad \text{(B-31)}$$

The electrical current to the probe surface is obtained by integrating the product of the particle distribution, the charge per particle, and the particle velocity over all possible velocities towards the probe. The electron flux thus obtained is given by

$$j_e = - e \int_{-\infty}^{\infty} \int_{-\infty}^{\infty} \int_{-\infty}^{0} u \, \overline{f}_e \, du \, dv \, dw \qquad \text{(B-32)}$$

or

$$j_e = - e \int_{-\infty}^{\infty} \int_{-\infty}^{\infty} \int_{-\infty}^{0} u \, n_{oe} \left(\frac{m_e}{2\pi k T_e} \right)^{3/2} e^{\frac{-(\frac{1}{2} m_e \overline{V}_e^{\,2} - e\phi)}{k T_e}} \, du \, dv \, dw \qquad \text{(B-33)}$$

which integrates to

$$j_e = - n_{oe} \frac{e}{4} \sqrt{\frac{8kT_e}{\pi m_e}} \, e^{\frac{e\phi}{kT_e}} \, . \qquad \text{(B-34)}$$

Likewise, the positive and negative ion currents are given by

$$j_i = n_{oi} \frac{e}{4} \sqrt{\frac{8kT_i}{\pi m_i}} \, e^{- \frac{e\phi}{kT_i}} \qquad \text{(B-35)}$$

and

$$j_n = - n_{on} \frac{e}{4} \sqrt{\frac{8kT_n}{\pi m_n}} \, e^{\frac{e\phi}{kT_n}} \, . \qquad \text{(B-36)}$$

Equations (29) through (31) and (34) through (36) are correct for the case in which the probe surface is insulated and no charged particles are absorbed by the probe. In actuality, however, any charged particle

contacting the probe surface will be neutralized and hence there will be maximum values for the particle number densities and the magnitudes of the particle currents. These maximum values are the values at the plasma sheath edge. The sheath edge is defined as the location closest to the collecting electrode in which the electrical potential is equal to the plasma potential. For the purpose of this derivation the plasma potential has been assumed to be equal to zero. The limiting current values, known as the saturation currents, are thus given by

$$j_{es} = - n_{oe} \frac{e}{4} \sqrt{\frac{8kT_e}{\pi m_e}} = - \frac{n_{oe} e \bar{c}_e}{4} , \qquad \text{(B-37)}$$

$$j_{is} = n_{oi} \frac{e}{4} \sqrt{\frac{8kT_i}{\pi m_i}} = \frac{n_{oi} e \bar{c}_i}{4} , \qquad \text{(B-38)}$$

and

$$j_{ns} = - n_{on} \frac{e}{4} \sqrt{\frac{8kT_n}{\pi m_n}} = - \frac{n_{on} e \bar{c}_n}{4} \qquad \text{(B-39)}$$

where $\bar{c}_e$, $\bar{c}_i$, and $\bar{c}_n$ are the average speeds of the electrons, positive ions, and negative ions respectively and are given by

$$\bar{c}_{e,i,n} = \sqrt{\frac{8kT_{e,i,n}}{\pi m_{e,i,n}}} . \qquad \text{(B-40)}$$

For any given probe potential, the net current to the probe is given by the sum of the individual particle currents at the probe surface. Since the magnitudes of the particle currents cannot exceed the magnitudes of the currents which flow when the probe potential is equal

to the plasma potential, the equations for the net current to the probe surface depend upon whether the probe potential is positive or negative.

For the case in which the probe potential is negative, the net current to the probe, j, is given by

$$j = \frac{n_{oi}\, e\, \bar{c}_i}{4} - \frac{n_{oe}\, e\, \bar{c}_e}{4}\, e^{\frac{e\phi_p}{kT_e}} - \frac{n_{on}\, e\, \bar{c}_n}{4}\, e^{\frac{e\phi_p}{kT_n}} \qquad \text{(B-41)}$$

where ϕ_p is the probe potential. When the value of $e\phi_p/kT_e$ is strongly negative, Equation (41) becomes

$$j = \frac{n_{oi}\, e\, \bar{c}_i}{4} = j_{is} \,. \qquad \text{(B-42)}$$

Thus, for strongly negative probe potentials, only the positive ion saturation current reaches the probe surface. For less negative probes, the electron and negative ion contribution to the net current begins to increase and to cancel the positive ion contribution to the current. At some probe potential, called the floating potential, the electron and negative ion contribution to the net current exactly cancels the positive ion contribution and no net current flows to the probe. If the floating potential is negative, then Equation (41) becomes

$$0 = \frac{n_{oi}\, e\, \bar{c}_i}{4} - \frac{n_{oe}\, e\, \bar{c}_e}{4}\, e^{\frac{e\phi_f}{kT_e}} - \frac{n_{on}\, e\, \bar{c}_n}{4}\, e^{\frac{e\phi_f}{kT_n}} \qquad \text{(B-43)}$$

or

$$\phi_f = \frac{kT_e}{e}\, \ell n \left[\frac{n_{oi}\, \bar{c}_i}{n_{oe}\, \bar{c}_e} - \frac{n_{on}\, \bar{c}_n}{n_{oe}\, \bar{c}_e}\, e^{\frac{e\phi_f}{kT_n}} \right] \qquad \text{(B-44)}$$

where ϕ_f is the floating potential. Subtracting Equation (38) from Equation (41) yields

$$j + j_{is} = - \frac{n_{oe}\, e\, \bar{c}_e}{4} e^{\frac{e\phi_p}{kT_e}} - \frac{n_{on}\, e\, \bar{c}_n}{4} e^{\frac{e\phi_p}{kT_n}} \qquad \text{(B-45)}$$

and taking the absolute value and then the natural logarithm of Equation (45) yields

$$\ell n|j-j_{is}| = \ell n \frac{n_{oe}\, e\, \bar{c}_e}{4} + \ell n \left[e^{\frac{e\phi_p}{kT_e}} + \frac{n_{on}\, \bar{c}_n}{n_{oe}\, \bar{c}_e} e^{\frac{e\phi_p}{kT_n}} \right] . \qquad \text{(B-46)}$$

Taking the derivative of Equation (46) with respect to ϕ_p yields

$$\frac{d\, \ell n|j-j_{is}|}{d\phi_p} = \frac{d}{d\phi_p} \left[\ell n \left(e^{\frac{e\phi_p}{kT_e}} + \frac{n_{on}\, \bar{c}_n}{n_{oe}\, \bar{c}_e} e^{\frac{e\phi_p}{kT_n}} \right) \right] . \qquad \text{(B-47)}$$

For the case in which the probe potential is positive, the net current to the probe is given by

$$j = n_{oi} \frac{e}{4} \bar{c}_i e^{-\frac{e\phi_p}{kT_i}} - \frac{n_{oe}\, e\, \bar{c}_e}{4} - \frac{n_{on}\, e\, \bar{c}_n}{4} . \qquad \text{(B-48)}$$

When the value of $e\phi_p/kT_i$ is strongly positive, Equation (48) becomes

$$j = - \left[\frac{n_{oe}\, e\, \bar{c}_e}{4} + \frac{n_{on}\, e\, \bar{c}_n}{4} \right] = j_{es} + j_{ns} . \qquad \text{(B-49)}$$

Thus, for strongly positive probe potentials, only the electron and

negative ion saturation currents reach the probe surface. For less positive probe potentials, the positive ion current increases and partially cancels the electron and negative ion current. Normally the positive ion current does not become large enough to completely cancel the electron and negative ion saturation currents, but when this occurs the floating potential is given by

$$\phi_f = \frac{kT_i}{e}\left[\ell n\left(\frac{n_{oi}\ \bar{c}_i}{n_{oe}\ \bar{c}_e + n_{on}\ \bar{c}_n}\right)\right] . \qquad \text{(B-50)}$$

Subtracting Equations (37) and (39) from Equation (48) yields

$$j - j_{es} - j_{ns} = \frac{n_{oi}\ e\ \bar{c}_i}{4}\, e^{-\frac{e\phi_p}{kT_i}} \qquad \text{(B-51)}$$

and taking the natural logarithm of Equation (51) gives

$$\ell n(j - j_{es} - j_{ns}) = \ell n\ \frac{n_{oi}\ e\ \bar{c}_i}{4} - \frac{e\phi_p}{kT_i} . \qquad \text{(B-52)}$$

Taking the derivative of Equation (52) with respect to ϕ_p gives

$$\frac{d}{d\phi_p}\ \ell n(j - j_{es} - j_{ns}) = -\frac{e}{kT_i} . \qquad \text{(B-53)}$$

Solving Equation (53) for T_i yields

$$T_i = -\frac{e}{k}\left[\frac{d}{d\phi_p}\ \ell n(j - j_{es} - j_{ns})\right]^{-1} . \qquad \text{(B-54)}$$

In theory, once an electrostatic probe has been used to determine

the plasma current-voltage characteristic, Equations (41), (47), (48), and (54) along with the assumption that

$$T_i = T_n \ , \tag{B-55}$$

within the plasma, and the relationship

$$n_{oi} = n_{oe} + n_{on} \tag{B-56}$$

can be used to solve for n_{oi}, n_{oe}, n_{on}, T_i, T_e, and T_n at the sheath edge. In practice, this is often not possible because of the very low mass of the electrons compared to the masses of the positive and negative ions. This very low mass causes the average electron speed to be much higher than the average speed of either the positive or negative ions. Thus, unless the positive ion number density is very much greater than the electron number density, the electron saturation current is several times that of the positive ions. When this occurs, determining the value of the term $j - j_{es} - j_{ns}$ found in Equation (54) is practically impossible and thus Equation (54) cannot be used in the solution. When this occurs, one additional equation is needed to solve for the plasma conditions at the sheath edge.

When it is known that no negative ions exist within the plasma, the additional equation needed is

$$n_{on} = 0 \tag{B-57}$$

and Equation (56) becomes

$$n_{oi} = n_{oe} \ . \tag{B-58}$$

The positive ion temperature is then obtained from Equation (44) which in the absence of negative ions becomes

$$\phi_f = \frac{kT_e}{e} \ln\left(\frac{\bar{c}_i}{\bar{c}_e}\right) \tag{B-59}$$

where $\bar{c}_i$ and $\bar{c}_e$ are given by Equation (40).

When negative ions are present within the plasma, the temperature or particle number density of either the positive or negative ions must be known in order to determine the remaining parameters. This information must be obtained independently from the electrostatic probe theory.

In general, the electrostatic probe theory presented in this appendix permits a solution for the six unknowns at the sheath edge n_{oi}, n_{oe}, n_{on}, T_i, T_e, and T_n through the use of Equations (41), (47), (48), (55), and (56) together with either Equations (54) or (57) or independently determined values for the positive or negative ion temperatures or number densities.

APPENDIX C

DERIVATION OF THE SHEATH THICKNESS EQUATIONS

In Chapter III, the sheath thickness was introduced into the electrostatic probe theory as an important parameter. The current-voltage characteristic of the electrostatic probe yields the plasma conditions at the sheath edge and these conditions must be corrected for the effects of the probe boundary layer before the free stream conditions can be determined. Since the plasma conditions within the probe boundary layer change rapidly with distance from the probe surface, knowledge of the actual sheath thickness is important.

The sheath thickness equation derivation presented in this appendix is based upon the works of Cohen[3] and of Toba and Sayano.[20] Cohen derived the sheath thickness equations for a spherical probe in a continuum plasma in which a variation between the electron and positive ion temperatures was permitted. Toba and Sayano derived the equations for a planar probe in which the electron and positive ion temperatures were identical. Both works assumed that no negative ions were present in the plasma and both works divided the sheath into an ambipolar diffusion region in which charge neutrality was maintained and a space charge region in which charge neutrality was no longer maintained. In both cases, the solutions to the equations in the ambipolar diffusion region were obtained in a closed form while the solutions to the equations in the space charge region required detailed numerical trial and error techniques.

The derivation presented in this appendix is for a planar probe and accounts for the presence of negative ions in the plasma sheath but neglects the thickness of the space charge region. Since numerical calculations by Cohen and Toba and Sayano show the space charge region thickness to be no more than 5 percent of the total sheath thickness, the thickness of this region can be neglected without greatly affecting the accuracy of the sheath thickness calculations. By neglecting the space charge region, however, an excessive amount of computation can be eliminated in the calculation of the electrostatic probe sheath thickness.

In the absence of charged particle production, the basic flux equations are, for the positive ions

$$\frac{d}{dx}\left(-D_i \frac{dn_i}{dx} - \bar{\mu}_i n_i \frac{d\phi}{dx}\right) = \frac{d}{dx}\Gamma_i = 0 \ , \qquad \text{(C-1)}$$

for the electrons

$$\frac{d}{dx}\left(-D_e \frac{dn_e}{dx} + \bar{\mu}_e n_e \frac{d\phi}{dx}\right) = \frac{d}{dx}\Gamma_e = 0 \ , \qquad \text{(C-2)}$$

and for the negative ions

$$\frac{d}{dx}\left(-D_n \frac{dn_n}{dx} + \bar{\mu}_n n_n \frac{d\phi}{dx}\right) = \frac{d}{dx}\Gamma_n = 0 \qquad \text{(C-3)}$$

where the subscripts i, e, and n indicate properties of the positive ions, electrons, and negative ions respectively. The diffusion and mobility coefficients are given by D and $\bar{\mu}$ respectively, Γ is the net

particle flux, n is the particle number density, ϕ is the electric field potential, and x is the distance normal to the probe surface. The diffusion and mobility coefficients are related by the Einstein relation which gives

$$D = \frac{kT}{e} \bar{\mu} \tag{C-4}$$

The particle number densities are related to the electric field potential by Poisson's equation which gives

$$\frac{\partial^2 \phi}{\partial x^2} = - \frac{e}{K_o} (n_i - n_e - n_n) \tag{C-5}$$

where K_o is the permittivity of a vacuum.

The flux equations may be integrated once to give

$$- D_i \frac{dn_i}{dx} - \bar{\mu}_i n_i \frac{d\phi}{dx} = \Gamma_i \ , \tag{C-6}$$

$$- D_e \frac{dn_e}{dx} + \bar{\mu}_e n_e \frac{d\phi}{dx} = \Gamma_e \ , \tag{C-7}$$

and

$$- D_n \frac{dn_n}{dx} + \bar{\mu}_n n_n \frac{d\phi}{dx} = \Gamma_n \ . \tag{C-8}$$

To simplify these equations, the following substitutions are made. Let

$$\varepsilon = \frac{T_o}{T_i} \ , \tag{C-9}$$

$$\lambda_d = \left(\frac{K_o \; k \; T_i}{n_i e^2} \right)^{\frac{1}{2}} , \qquad \text{(C-10)}$$

$$y = - \frac{e\phi}{kT_i} , \qquad \text{(C-11)}$$

$$N_i = \frac{n_i}{n_o} , \qquad \text{(C-12)}$$

$$N_e = \frac{n_e}{(1-\alpha) n_o} , \qquad \text{(C-13)}$$

$$N_n = \frac{n_n}{\alpha \; n_o} , \qquad \text{(C-14)}$$

and

$$\zeta = \frac{x}{a} \qquad \text{(C-15)}$$

where λ_d is the Debye length based upon the positive ion temperature, n_o is the positive ion number density at the sheath edge, and a is the positive ion mean free path. The coefficient α is the ratio of the negative ion number density at the sheath edge n_{no}, to the positive ion number density at the sheath edge and is given by

$$\alpha = \frac{n_{no}}{n_o} . \qquad \text{(C-16)}$$

Substituting these parameters into Equation (6) yields

$$- D_i \frac{d(n_o N_i)}{d(a\zeta)} - \mu_i n_o N_i \frac{d\left[\frac{-kT_i y}{e}\right]}{d(a\zeta)} = \Gamma_i , \qquad \text{(C-17)}$$

or

$$- \frac{D_i n_o}{a} \frac{dN_i}{d\zeta} + \frac{n_o}{a} \frac{\mu_i \, k \, T_i}{e} N_i \frac{dy}{d\zeta} = \Gamma_i \qquad \text{(C-18)}$$

and substituting Equation (4) into Equation (18) yields

$$- \frac{dN_i}{d\zeta} + N_i \frac{dy}{d\zeta} = \Gamma_i \frac{a}{D_i n_o} . \qquad \text{(C-19)}$$

Substituting Equation (4) and Equations (9) through (15) into Equation (7) yields

$$(1-\alpha) \frac{dN_e}{d\zeta} + \frac{1-\alpha}{\varepsilon} N_e \frac{dy}{d\zeta} = - \Gamma_e \frac{a}{D_e n_o} . \qquad \text{(C-20)}$$

Substituting Equation (4) and Equations (9) through (15) into Equation (8) yields

$$\frac{D_n \, \alpha \, n_o}{a} \frac{dN_n}{d\zeta} + \frac{eD_n}{kT_n} \frac{\alpha \, n_o N_n}{a} \frac{kT_i}{e} \frac{dy}{d\zeta} = - \Gamma_n . \qquad \text{(C-21)}$$

If it is assumed that

$$T_n = T_i \qquad \text{(C-22)}$$

Equation (21) becomes

$$\alpha \frac{dN_n}{d\zeta} + \alpha N_n \frac{dy}{d\zeta} = - \Gamma_n \frac{a}{D_n n_o} . \qquad \text{(C-23)}$$

Substitution into Poisson's equation yields

$$\left(\frac{\lambda_d}{a}\right)^2 \frac{d^2y}{d\zeta^2} = [N_i - (1-\alpha)N_e - \alpha N_n] \ . \qquad \text{(C-24)}$$

In the continuum case with ion temperatures less than 10^{4}°K

$$\left(\frac{\lambda_d}{a}\right)^2 << 1 \ . \qquad \text{(C-25)}$$

Equation (24) thus becomes

$$N_i - (1-\alpha)N_e - \alpha N_n = 0 \qquad \text{(C-26)}$$

and hence the quasi-neutral solution is

$$N_i = N_e = N_n = N \ . \qquad \text{(C-27)}$$

Adding Equations (20) and (23) and substituting Equation (27) gives

$$\frac{dN}{d\zeta} + \left(\frac{1-\alpha}{\varepsilon} + \alpha\right) N \frac{dy}{d\zeta} = - \left(\frac{\Gamma_e a}{D_e n_o} + \frac{\Gamma_n a}{D_n n_o}\right) \ . \qquad \text{(C-28)}$$

Substituting Equation (27) into Equation (19) yields

$$\frac{dN}{d\zeta} - N \frac{dy}{d\zeta} = - \frac{\Gamma_i a}{D_i n_o} \ . \qquad \text{(C-29)}$$

Multiplying Equation (29) by $(\frac{1-\alpha}{\varepsilon} + \alpha)$ and adding the result to Equation (28) yields

$$\frac{dN}{d\zeta} = \frac{-1}{\frac{1-\alpha}{\varepsilon} + \alpha + 1} \left[\left(\frac{1-\alpha}{\varepsilon} + \alpha\right) \frac{\Gamma_i a}{D_i n_o} + \frac{\Gamma_e a}{D_e n_o} + \frac{\Gamma_n a}{D_n n_p}\right]. \qquad \text{(C-30)}$$

At the probe surface, $\zeta = 0$, the boundary condition is that

$$N = 0 \tag{C-31}$$

and thus Equation (30) can be integrated to give

$$\int_0^N dN = \int_0^\zeta \frac{-1}{\frac{1-\alpha}{\varepsilon} + \alpha + 1} \left[\left(\frac{1-\alpha}{\varepsilon} + \alpha \right) \frac{\Gamma_i a}{D_i n_o} + \frac{\Gamma_e a}{D_e n_o} + \frac{\Gamma_n a}{D_n n_o} \right] d\zeta \tag{C-32}$$

which becomes

$$N = \frac{-1}{\frac{1-\alpha}{\varepsilon} + \alpha + 1} \left[\left(\frac{1-\alpha}{\varepsilon} + \alpha \right) \frac{\Gamma_i a}{D_i n_o} + \frac{\Gamma_e a}{D_e n_o} + \frac{\Gamma_n a}{D_n n_o} \right] \zeta \ . \tag{C-33}$$

When the probe potential is equal to the plasma potential, the particle fluxes Γ_{io}, Γ_{eo}, and Γ_{no} are given by

$$\Gamma_{io} = - \frac{1}{4} n_o \bar{c}_i \ , \tag{C-34}$$

$$\Gamma_{eo} = - \frac{1-\alpha}{4} n_o \bar{c}_e \ , \tag{C-35}$$

and

$$\Gamma_{no} = - \frac{\alpha}{4} n_o \bar{c}_n \tag{C-36}$$

where $\bar{c}_i$, $\bar{c}_e$, and $\bar{c}_n$ are the average particle velocities of the positive ions, electrons, and negative ions respectively at the sheath edge. The positive ion mean free path is given by

$$a = \frac{1}{\sqrt{2}\, n_p\, \bar{Q}_i} \tag{C-37}$$

where $\overline{Q}_i$ is the average collision cross section between the positive ions and the neutral particles and n_p is the average number density of the neutral particles within the sheath. Collisions between the charged particles can be neglected for low ionization levels, as in the current experiments; however, at higher ionization levels the collision cross section must include the effect of collisions between the charged particles. Within a plasma or a plasma sheath, the determination of the diffusion coefficients is complicated by the presence of the charged particles. The diffusion coefficients are dependent upon the number densities and binary diffusion coefficients of all of the charged species present within the plasma. For plasmas of low ionization levels, however, the diffusion coefficients are very close in value to the binary diffusion coefficients for each species. Equations for the diffusion coefficients have been determined by Devoto[27] for approximations up to the fourth level; however, in keeping with the previous approximations made in this work, only the first approximations to the binary diffusion coefficients will be used in this derivation. The diffusion coefficients are thus given by

$$D_i = \frac{3}{16 n_p} \left(\frac{2\pi k T_i}{\overline{m}_i} \right)^{1/2} \frac{1}{\overline{Q}_i} \quad , \tag{C-38}$$

$$D_e = \frac{3}{16 n_p} \left(\frac{2\pi k T_e}{\overline{m}_i} \right)^{1/2} \frac{1}{\overline{Q}_e} \quad , \tag{C-39}$$

and

$$D_n = \frac{3}{16 n_p} \left(\frac{2\pi k T_n}{\overline{m}_n} \right)^{1/2} \frac{1}{\overline{Q}_n} \tag{C-40}$$

where $\overline{m}_i$, $\overline{m}_e$, $\overline{m}_n$ are the reduced masses for collisions between the neutral particles and the positive ions, electrons, and negative ions respectively and $\overline{Q}_e$ and $\overline{Q}_n$ are the average collision cross sections between the neutral particles and the electrons and negative ions respectively. Equation (33) implies that the diffusion coefficients are constants within the sheath since they are taken outside of the integration. However, as shown by Equations (38) through (40) the diffusion coefficients vary with the neutral particle number density and collision cross section. Since the temperature varies throughout the boundary layer, the diffusion coefficients would be expected to vary within the sheath and consequently an average value for the diffusion coefficients must be used. Since n_p, $\overline{Q}_i$, $\overline{Q}_e$, and $\overline{Q}_n$ are defined as average quantities, an average particle temperature should also be used. The positive and negative ion temperatures are assumed to be equal to the neutral particle temperature within the sheath while the electrons are assumed to maintain a constant temperature because their low mass causes a reduction in the energy transfer during the collision process. Consequently, the average electron temperature used in Equation (39) will be the electron temperature at the sheath edge and the average temperatures T_{ia} and T_{na} used in Equations (38) and (40) will be the plasma temperature found at one-half of the sheath thickness.

For the positive ions, the reduced mass is given by

$$\overline{m}_i = \frac{m_i m_p}{m_i + m_p} \tag{C-41}$$

where m_p is the mass of a neutral particle. When the masses of the positive ions are equal to the masses of the neutral particles, Equation

(41) becomes

$$\bar{m}_i = \frac{m_i^2}{2m_i} = \frac{m_i}{2} \quad . \tag{C-42}$$

Thus Equation (38) becomes

$$D_i = \frac{3\pi}{16\sqrt{2}\, n_p} \left(\frac{8kT_i}{\pi\, m_i}\right)^{1/2} \frac{1}{\bar{Q}_i} \left(\frac{T_{ia}}{T_i}\right)^{1/2} \tag{C-43}$$

where T_i is the positive ion temperature at the sheath edge. Since

$$\bar{c}_i = \left(\frac{8kT_i}{\pi\, m_i}\right)^{1/2} , \tag{C-44}$$

Equation (43) becomes

$$D_i = \frac{3\pi\, \bar{c}_i}{16\sqrt{2}\, n_p} \frac{1}{\bar{Q}_i} \left(\frac{T_{ia}}{T_i}\right)^{1/2} \tag{C-45}$$

and hence

$$\frac{a}{D_i n_o} = \frac{\dfrac{1}{\sqrt{2}\, n_p\, \bar{Q}_i}}{\dfrac{3\pi\, \bar{c}_i}{16\sqrt{2}\, n_p \bar{Q}_i} \left(\dfrac{T_{ia}}{T_i}\right)^{1/2} n_o} = \frac{16}{3\pi\, \bar{c}_i\, n_o} \left(\frac{T_i}{T_{ia}}\right)^{1/2} . \tag{C-46}$$

For the electrons, the reduced mass is given by

$$\bar{m}_e = \frac{m_e m_p}{m_e + m_p} . \tag{C-47}$$

Since the neutral particles are very much more massive than the

electrons, Equation (47) becomes

$$\bar{m}_e = m_e \tag{C-48}$$

and thus Equation (39) becomes

$$D_e = \frac{3\pi}{32 n_p} \left(\frac{8kT_e}{\pi\, m_e}\right)^{1/2} \frac{1}{\bar{Q}_e} \tag{C-49}$$

where T_e is the electron temperature at the sheath edge. Since

$$\bar{c}_e = \left(\frac{8kT_e}{\pi\, m_e}\right)^{1/2} , \tag{C-50}$$

Equation (49) becomes

$$D_e = \frac{3\pi\, \bar{c}_e}{32 n_p \bar{Q}_e} , \tag{C-51}$$

and hence

$$\frac{a}{D_e n_o} = \frac{32}{3\sqrt{2}\, \pi\, \bar{c}_e\, n_o} \frac{\bar{Q}_e}{\bar{Q}_i} . \tag{C-52}$$

The reduced mass for the negative ions is given by

$$\bar{m}_n = \frac{m_p m_n}{m_p + m_n} \tag{C-53}$$

thus Equation (40) becomes

$$D_n = \frac{3\pi}{32 n_p} \left[\frac{8kT_n}{\pi\, m_n} \left(\frac{m_p + m_n}{m_p}\right)^{1/2}\right] \frac{1}{\bar{Q}_n} \left(\frac{T_{na}}{T_n}\right)^{1/2} \tag{C-54}$$

where T_n is the negative ion temperature at the sheath edge. Since

$$\bar{c}_n = \left(\frac{8kT_n}{\pi m_n}\right)^{1/2} , \tag{C-55}$$

Equation (54) becomes

$$D_n = \frac{3\pi\bar{c}_n}{32n_p}\left(\frac{m_p + m_n}{m_p}\right)^{1/2}\frac{1}{\bar{Q}_n}\left(\frac{T_{na}}{T_N}\right)^{1/2} \tag{C-56}$$

and hence

$$\frac{a}{D_n n_o} = \frac{32\left(\frac{T_n}{T_{na}}\right)^{1/2}}{3\pi\sqrt{2}\,\bar{c}_n n_o}\left(\frac{m_p}{m_p + m_n}\right)^{1/2}\frac{\bar{Q}_n}{\bar{Q}_i} . \tag{C-57}$$

Combining Equations (34) and (46) yields

$$\frac{\Gamma_{io}a}{D_i n_o} = \frac{-\frac{1}{4}n_o\bar{c}_i\,16\left(\frac{T_i}{T_{ia}}\right)^{1/2}}{3\pi\,\bar{c}_i n_o} = -\frac{4}{3\pi}\left(\frac{T_i}{T_{ia}}\right)^{1/2} \tag{C-58}$$

when the probe potential is equal to the plasma potential. The positive ion flux varies with the probe potential and hence the parameter J_i given by

$$J_i = \frac{\Gamma_i}{\Gamma_{io}} \tag{C-59}$$

is introduced to give

$$\frac{\Gamma_i a}{D_i n_o} = -\frac{4}{3\pi}\left(\frac{T_i}{T_{ia}}\right)^{1/2} J_i \quad . \tag{C-60}$$

Combining Equations (35) and (52) yields

$$\frac{\Gamma_{eo} a}{D_e n_o} = \frac{-\frac{(1-\alpha)}{4} n_o \bar{c}_e \; 32}{3\sqrt{2}\,\pi\,\bar{c}_e n_o} \frac{\bar{Q}_e}{\bar{Q}_i} \tag{C-61}$$

and introducing the parameter J_e given by

$$J_e = \frac{\Gamma_e}{\Gamma_{eo}} \tag{C-62}$$

yields

$$\frac{\Gamma_e a}{D_e n_o} = -\frac{8(1-\alpha)}{3\sqrt{2}\,\pi} \frac{\bar{Q}_e}{\bar{Q}_i} J_e \quad . \tag{C-63}$$

Combining Equations (36) and (57) yields

$$\frac{\Gamma_{no} a}{D_n n_o} = \frac{-\frac{\alpha}{4} n_o \bar{c}_n \; 32}{3\pi\,\sqrt{2}\,\bar{c}_n n_o} \left(\frac{m_p}{m_p + m_n}\right)^{1/2} \frac{\bar{Q}_n}{\bar{Q}_i} \left(\frac{T_n}{T_{na}}\right)^{1/2} \tag{C-64}$$

and introducing the parameter J_n given by

$$J_n = \frac{\Gamma_n}{\Gamma_{no}} \tag{C-65}$$

yields

$$\frac{\Gamma_n a}{D_n n_o} = - \frac{8\alpha}{3\sqrt{2}\,\pi} \left(\frac{m_p}{m_p + m_n}\right)^{\frac{1}{2}} \frac{\overline{Q}_n}{\overline{Q}_i} \left(\frac{T_n}{T_{na}}\right)^{\frac{1}{2}} J_n \ . \qquad \text{(C-66)}$$

Substituting Equations (60), (63), and (66) into Equation (33) yields

$$n = \frac{\frac{4\zeta}{3\pi}}{\frac{1-\alpha}{\varepsilon} + \alpha + 1} \left[\left(\frac{1-\alpha}{\varepsilon} + \alpha\right) \left(\frac{T_i}{T_{ia}}\right)^{\frac{1}{2}} J_i + \frac{2(1-\alpha)}{\sqrt{2}} \frac{\overline{Q}_e}{\overline{Q}_i} J_e \right. \qquad \text{(C-67)}$$

$$\left. + \frac{2\alpha}{\sqrt{2}} \left(\frac{T_n}{T_{na}}\right)^{\frac{1}{2}} \left(\frac{m_p}{m_p + m_n}\right)^{\frac{1}{2}} \frac{\overline{Q}_n}{\overline{Q}_i} J_n \right] .$$

The sheath thickness, ζ_s, is found by setting n = 1 giving

$$1 = \frac{1}{\frac{1-\alpha}{\varepsilon} + \alpha + 1} \left[\left(\frac{1-\alpha}{\varepsilon} + \alpha\right) \left(\frac{T_i}{T_{ia}}\right)^{\frac{1}{2}} J_i + \frac{2(1-\alpha)}{\sqrt{2}} \frac{\overline{Q}_e}{\overline{Q}_i} J_e \right. \qquad \text{(C-68)}$$

$$\left. + \frac{2\alpha}{\sqrt{2}} \left(\frac{T_n}{T_{na}}\right) \left(\frac{m_p}{m_p + m_n}\right)^{\frac{1}{2}} \frac{\overline{Q}_n}{\overline{Q}_i} J_n \right] \frac{4\zeta_s}{3\pi}$$

and hence

$$\zeta_s = \frac{\left(\frac{1-\alpha}{\varepsilon} + \alpha + 1\right) \frac{3\pi}{4}}{\left(\frac{1-\alpha}{\varepsilon} + \alpha\right) \left(\frac{T_i}{T_{ia}}\right)^{\frac{1}{2}} J_i + \frac{2(1-\alpha)}{\sqrt{2}} \frac{\overline{Q}_e}{\overline{Q}_i} J_e + \frac{2\alpha}{\sqrt{2}} \left(\frac{m_p}{m_p + m_n}\right)^{\frac{1}{2}} \left(\frac{T_n}{T_{na}}\right)^{\frac{1}{2}} \frac{\overline{Q}_n}{\overline{Q}_i} J_n} \ . \qquad \text{(C-69)}$$

Equation (69) is a general equation for the sheath thickness

and can be used in any continuum plasma in which the molecular properties of the ions and neutral molecules are known. In the present work, the positive ions and the neutral particles were argon ions and molecules and the negative ions were either sulphur hexafluoride or uranium hexafluoride ions. By noting certain relationships between these species' properties, further simplification to Equation (69) can be made. The first term in the denominator of Equation (69), $(T_i/T_{ia})^{\frac{1}{2}}\,[(1-\alpha)/\varepsilon + \alpha]J_i$, can be simplified if the ratio between T_i and T_{ia} is known. In Appendix A, the plasma temperature near the probe surface is shown to be proportional to the square root of the distance from the probe surface. Since T_{ia} is the temperature found at one-half of the sheath thickness, it is given by

$$T_{ia} = \sqrt{\frac{1}{2}}\, T_i \tag{C-70}$$

and consequently

$$\left(\frac{T_i}{T_{ia}}\right)^{\frac{1}{2}} = \sqrt[4]{2} = 1.189 \tag{C-71}$$

which results in

$$\left(\frac{T_i}{T_{ia}}\right)^{\frac{1}{2}}\left(\frac{1-\alpha}{\varepsilon} + \alpha\right)J_i = 1.189\left(\frac{1-\alpha}{\varepsilon} + \alpha\right)J_i \tag{C-72}$$

for the first term in the denominator of Equation (69).

The third term in the denominator of Equation (69) is given by

$$\frac{2\alpha}{\sqrt{2}} \left(\frac{m_p}{m_p + m_n} \right)^{\frac{1}{2}} \frac{\bar{Q}_n}{\bar{Q}_i} \left(\frac{T_n}{T_{na}} \right)^{\frac{1}{2}} J_n$$

and it can also be simplified. The negative ion temperature ratio is the same as that of the positive ions thus

$$\left(\frac{T_n}{T_{na}} \right)^{\frac{1}{2}} = 1.189 \ . \qquad \text{(C-73)}$$

The ratio $[m_p/(m_p + m_n)]^{\frac{1}{2}}$ depends upon the molecular weights of the neutral particles and the negative ions. For the present experiments, the neutral particles were argon atoms with an atomic weight of 40 and the negative ions were either sulphur hexafluoride ions with a molecular weight of 146 or uranium hexafluoride ions with a molecular weight of 352. Hence for the plasmas with the sulphur hexafluoride additive

$$\left(\frac{m_p}{m_p + m_{SF_6}} \right)^{\frac{1}{2}} = \left(\frac{40}{40 + 146} \right)^{\frac{1}{2}} = 0.464 \qquad \text{(C-74)}$$

and for the plasmas with the uranium hexafluoride additive

$$\left(\frac{m_p}{m_p + m_{SF_6}} \right)^{\frac{1}{2}} = \left(\frac{40}{40 + 352} \right)^{\frac{1}{2}} = 0.320 \qquad \text{(C-75)}$$

where the subscripts SF_6 and UF_6 indicate that the negative ions are sulphur hexafluoride and uranium hexafluoride ions respectively.

The collision cross sections for sulphur hexafluoride and uranium hexafluoride are known for temperatures near 300°K but little information

is available for temperatures above 1000°K. Svehla[28] has determined the low-velocity collision diameters for argon, sulphur hexafluoride, and uranium hexafluoride and found them to be

$$\sigma_{Ar} = 3.542 \ \mathring{A} , \tag{C-76}$$

$$\sigma_{SF_6} = 5.128 \ \mathring{A} , \tag{C-77}$$

and

$$\sigma_{UF_6} = 5.967 \ \mathring{A} . \tag{C-78}$$

Using these values, the low-velocity collision cross sections for sulphur hexafluoride and uranium hexafluoride collisions with argon are given by

$$\overline{Q}_{SF_6} = \pi\left(\frac{\sigma_{SF_6} + \sigma_{Ar}}{2}\right)^2 = \pi\left(\frac{5.128 + 3.542}{2}\right)^2 \mathring{A}^2 = 59.0 \ \mathring{A}^2 \tag{C-79}$$

and

$$\overline{Q}_{UF_6} = \pi\left(\frac{\sigma_{UF_6} + \sigma_{Ar}}{2}\right)^2 = \pi\left(\frac{5.967 + 3.542}{2}\right)^2 \mathring{A}^2 = 71.1 \ \mathring{A}^2 \tag{C-80}$$

and the argon collision cross section is given by

$$\overline{Q}_i = \pi \sigma_{Ar}^2 = 39.5 \ \mathring{A}^2 . \tag{C-81}$$

The ratios of the low-velocity collision cross sections are thus given by

$$\frac{\overline{Q}_{SF_6}}{\overline{Q}_i} = 1.492 \tag{C-82}$$

and

$$\frac{\overline{Q}_{UF_6}}{\overline{Q}_i} = 1.80 \ . \qquad \text{(C-83)}$$

A comparison of the argon viscosities determined by Devoto[29] and Bromley and Wilke[30] with the sulphur hexafluoride viscosities determined by Frost and Liebermann[31] and Svehla[28] and also with the uranium hexafluoride viscosities determined by Svehla[28] indicates that for temperatures up to 6000°K the ratios in Equations (82) and (83) remain valid. Since, in the present experiments, the temperatures within the plasma sheath were always below 6000°K, the ratios in Equations (82) and (83) are considered sufficiently accurate to be used for all of the sheath thickness calculations.

Combining Equations (73), (74), and (82) yields for the third term in the denominator of Equation (69)

$$\frac{2\alpha}{\sqrt{2}} \left(\frac{m_p}{m_p + m_n} \right)^{\frac{1}{2}} \frac{\overline{Q}_n}{\overline{Q}_i} \left(\frac{T_n}{T_{na}} \right)^{\frac{1}{2}} J_n = 1.16 \ \alpha \ J_n \qquad \text{(C-84)}$$

when the electrophilic additive is sulphur hexafluoride. Combining Equations (73), (75), and (83) yields

$$\frac{2\alpha}{\sqrt{2}} \left(\frac{m_p}{m_p + m_n} \right)^{\frac{1}{2}} \frac{\overline{Q}_n}{\overline{Q}_i} \left(\frac{T_n}{T_{na}} \right)^{\frac{1}{2}} J_n = 0.97 \ \alpha \ J_n \qquad \text{(C-85)}$$

for the third term in the denominator of Equation (69) when the

electrophilic additive is uranium hexafluoride.

Substituting Equations (72) and (84) into Equation (69) yields

$$\zeta_s = \frac{\frac{1-\alpha}{\varepsilon} + \alpha + 1}{1.189\left(\frac{1-\alpha}{\varepsilon} + \alpha\right)J_i + \sqrt{2}(1-\alpha)\frac{\overline{Q}_e}{\overline{Q}_i}J_e + 1.16\,\alpha\,J_n}\,\frac{3\pi}{4} \qquad \text{(C-86)}$$

for the sheath thickness equation when the electrophilic additive is sulphur hexafluoride. Substituting Equations (72) and (85) into Equation (69) yields

$$\zeta_s = \frac{\frac{1-\alpha}{\varepsilon} + \alpha + 1}{1.189\left(\frac{1-\alpha}{\varepsilon} + \alpha\right)J_i + \sqrt{2}(1-\alpha)\frac{\overline{Q}_e}{\overline{Q}_i}J_e + 0.97\,\alpha\,J_n}\,\frac{3\pi}{4} \qquad \text{(C-87)}$$

for the sheath thickness equation when the electrophilic additive is uranium hexafluoride.

During the data reduction process, the ratio of the positive ion saturation current to the negative particle saturation current was used in the floating potential calculations to determine the positive ion temperature from the electron temperature. The saturation currents used in determining this ratio were those which existed when the probe potential equaled the plasma potential and, as a consequence, the resulting particle temperatures and concentrations were also those which existed at the sheath edge when the probe potential was equal to the plasma potential. This was done in order to avoid calculations to determine the values of J_i, J_e, and J_n which involved determining which part of

the negative particle current was due to the electrons and which part was due to the negative ions. Because the resulting temperatures and concentrations were equal to those at the sheath edge when the probe potential was equal to the plasma potential, the values of J_i, J_e, and J_n could each be taken to be unity and consequently the sheath thickness equations became

$$\zeta_s = \frac{\frac{1-\alpha}{\varepsilon} + \alpha + 1}{1.189\left(\frac{1-\alpha}{\varepsilon} + \alpha\right) + \sqrt{2}(1-\alpha)\frac{\overline{Q}_e}{\overline{Q}_i} + 1.16\ \alpha}\ \frac{3\pi}{4} \qquad \text{(C-88)}$$

when the electrophilic additive was sulphur hexafluoride and

$$\zeta_s = \frac{\frac{1-\alpha}{\varepsilon} + \alpha + 1}{1.189\left(\frac{1-\alpha}{\varepsilon} + \alpha\right) + \sqrt{2}(1-\alpha)\frac{\overline{Q}_e}{\overline{Q}_i} + 0.97\ \alpha}\ \frac{3\pi}{4} \qquad \text{(C-89)}$$

when the electrophilic additive was uranium hexafluoride.

Since ζ_s is the ratio of the sheath thickness to the positive ion mean free path, the sheath thickness can readily be determined from Equation (88) or (89) once the plasma temperature and particle number density is known at the sheath edge. These parameters can be determined by using the electrostatic probe equations derived in Appendix B. The cross sections for collisions between the electrons or the argon ions and the neutral argon atoms are also needed to employ either Equation (88) or Equation (89). The data of Devoto[29] were used in this work.

APPENDIX D

SAMPLE CALCULATIONS

The results of the experimental test program are presented in Chapter VI. The purpose of this appendix is to present the data reduction procedure in more detail. The method by which the data were reduced depended upon whether the accuracy of the electrostatic probe theory or the effectiveness of an electrophilic additive was being determined. When the accuracy of the probe theory was being checked, the plasma temperature at the sheath edge could be determined by use of the electrostatic probe theory presented in Appendix B. Since the boundary layer parameters depended upon the free stream temperature, an iterative process was needed to determine the free stream temperature from the sheath edge temperature. A free stream stagnation temperature was assumed and used to determine the boundary layer parameters. These parameters were then used to convert the sheath edge temperature into a free stream stagnation temperature. This new stagnation temperature was then compared with the assumed temperature; and, if the two values were not sufficiently close, a new free stream stagnation temperature was assumed and the process continued until sufficient convergence was achieved.

When the effectiveness of an electrophilic additive was being determined, the plasma temperature at the sheath edge could not be determined through use of the electrostatic probe theory because the negative ion concentration was unknown. To determine the negative ion

concentration, a heat balance was used to determine the free stream stagnation temperature. This temperature was then used to determine the actual boundary layer parameters. A ratio of electron to positive ion number densities was assumed and the electrostatic probe theory was used to determine a corresponding sheath edge temperature. The actual boundary layer parameters were then used to convert this sheath edge temperature into a free stream stagnation temperature and this temperature was compared to the actual free stream temperature. The assumed ratio of electron to positive ion number densities was then iterated until the calculated free stream stagnation temperature and the actual free stream temperature were sufficiently close. When convergence was achieved, the calculated sheath edge temperature could be used to determine the remaining sheath edge parameters such as electron and ion number densities. These methods of data reduction are illustrated in the sample calculations presented below.

Data Reduction with No Negative Ions

Figure 18 shows a typical current-voltage characteristic curve for the case in which the only charged particles within the plasma are positive ions and electrons. The absolute value of the current to the collecting electrode is shown so that the magnitudes of the saturation currents may be more easily compared. The positive ion and electron saturation currents are not constant with probe potential because of the growth of the plasma sheath thickness as the probe potential differs increasingly from the plasma potential.

The equation

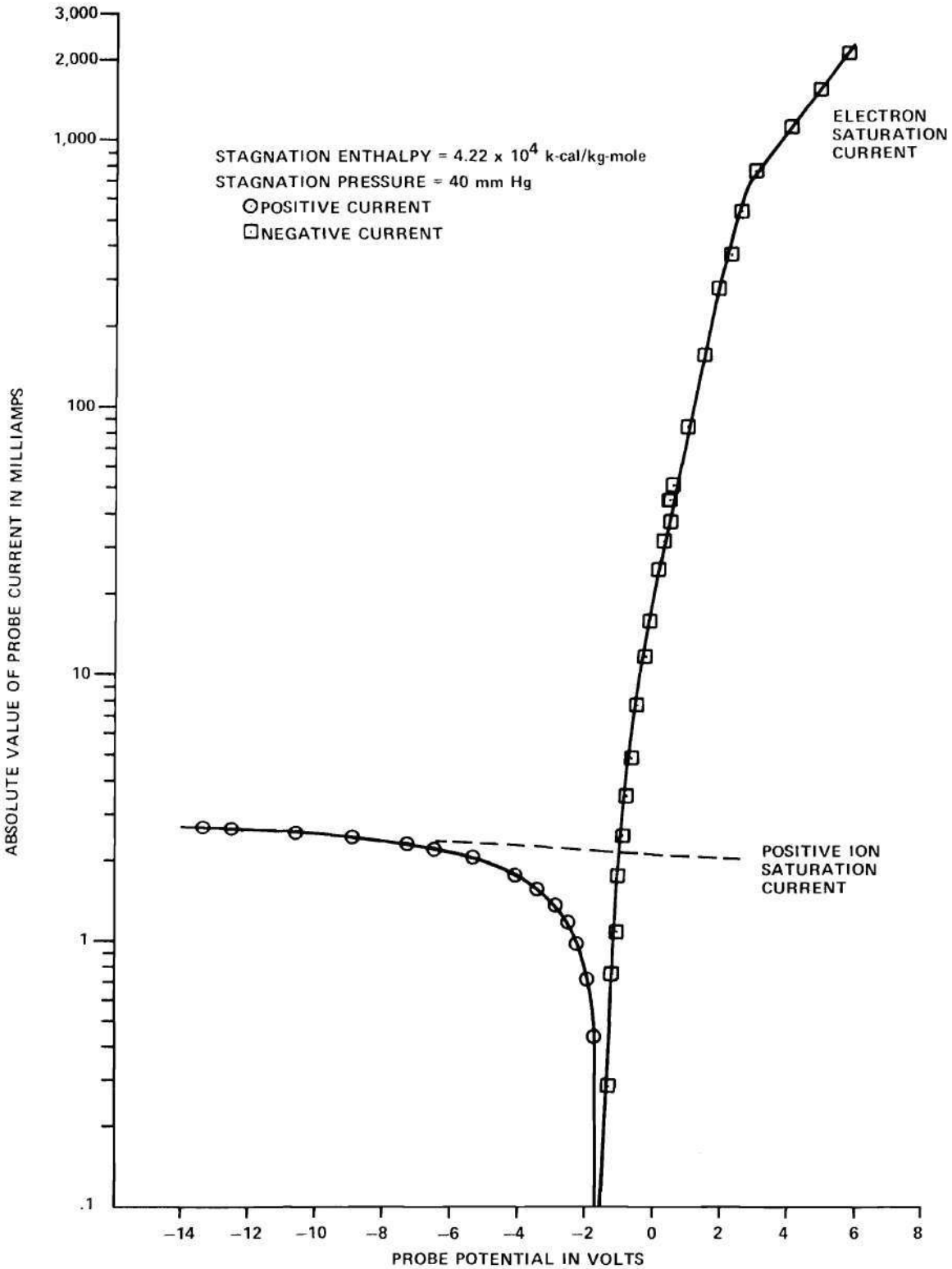

Figure 18. Current-Voltage Characteristic for No Electron Absorption

$$j_e = j - j_i \ , \qquad \text{(D-1)}$$

where j is the net current to the collecting electrode and j_e and j_i are the electron and positive ion currents to the electrode respectively, is used to determine the electron current as a function of probe potential. For probe potentials which are less than the plasma potential, the positive ion saturation current, j_{is}, is used in place of j_i in Equation (1). For probe potentials greater than the plasma potential, the positive ion current is sufficiently small compared to the electron current so that it may be neglected in Equation (1).

Figure 19 shows the electron current to the collecting electrode as a function of the probe potential. The plasma potential, ϕ_p, is indicated by the sharp change in the slope of the electron current. When the probe potential is less than the plasma potential, the slope of the electron current is given by

$$\frac{d \ \ell n|j_e|}{d\phi} = \frac{e}{kT_e} \qquad \text{(D-2)}$$

where ϕ is the probe potential, e is the electronic charge given by

$$e = 1.60 \times 10^{-19} \text{ coulomb} \ , \qquad \text{(D-3)}$$

k is the Boltzmann constant given by

$$k = 1.38 \times 10^{-16} \text{ erg/°K} \ , \qquad \text{(D-4)}$$

and T_e is the electron temperature. In the present example, the slope of the electron current is found to be

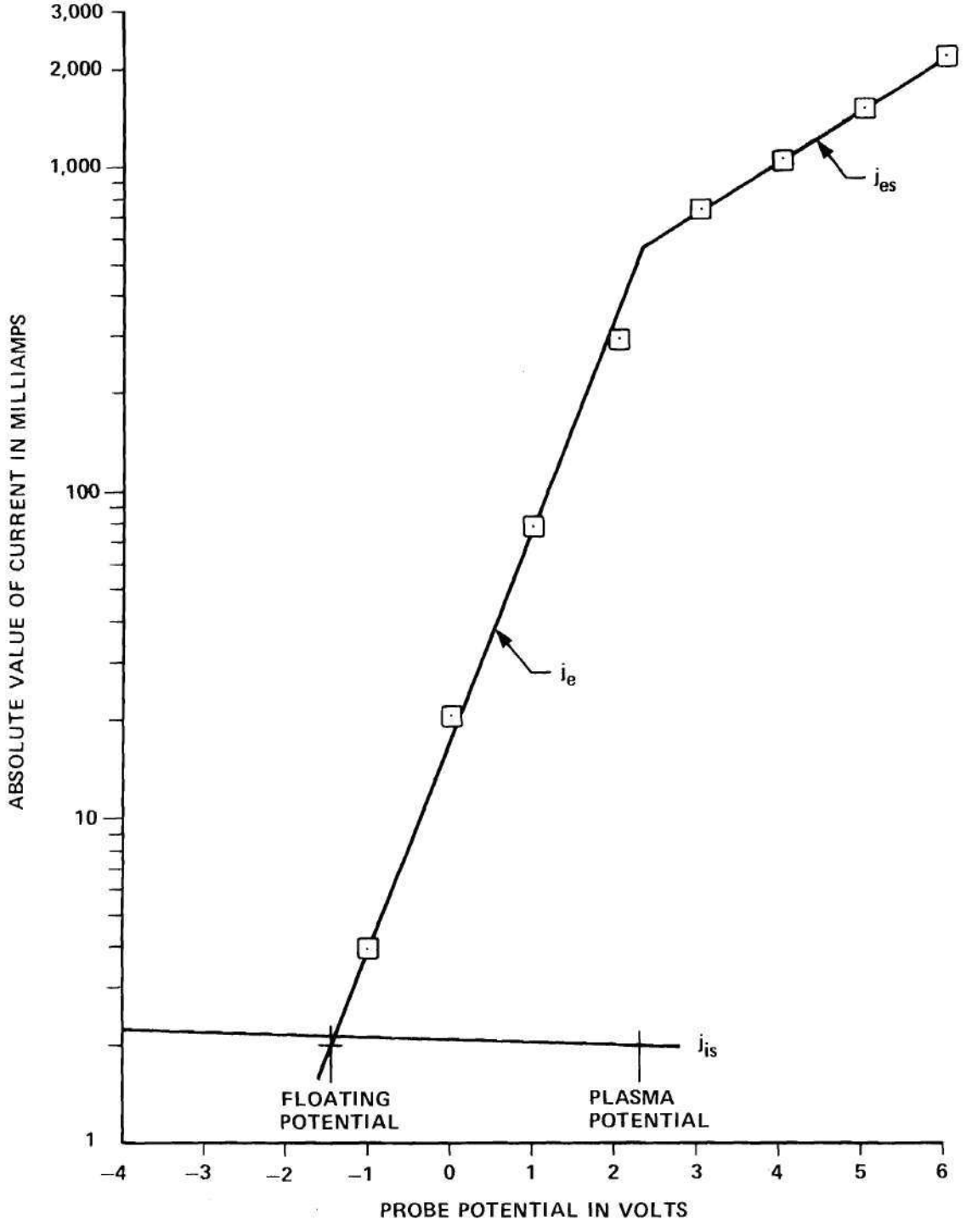

Figure 19. Electron Current for No Electron Absorption

$$\frac{d\ \ell n|j_e|}{d\phi} = \frac{e}{kT_e} = 1.527\ \text{volts}^{-1} \qquad \text{(D-5)}$$

and hence

$$T_e = 7600°K \qquad \text{(D-6)}$$

The floating potential, ϕ_f, is the potential, relative to the plasma potential, at which no net current flows to the collecting electrode and is given by

$$\phi_f = \phi_o - \phi_p \qquad \text{(D-7)}$$

where ϕ_o is the probe potential at which no net current flows to the collecting electrode. The condition of no net current to the probe implies that the positive ion current is equal to the electron current. The positive ion saturation current is also shown in Figure 19 and the value for ϕ_o would normally be the probe potential at which the curves for the positive ion saturation current and the electron current intersect on the figure. In order to simplify the calculations for the sheath thickness, however, a slightly different value for ϕ_o was used, as was noted in Appendix C. The value for ϕ_o was chosen to be the probe potential at which the electron current equalled the positive ion current which flowed when the probe was at the plasma potential. In the present example, the positive ion saturation current at the plasma potential is equal to 2.00 ma, and the probe potential at which the electron current is equal to -2.00 ma is -1.48 volts. Hence

$$\phi_o = -1.48\ \text{volts} . \qquad \text{(D-8)}$$

From Figure 19 the plasma potential is seen to be

$$\phi_p = 2.30 \text{ volts} , \tag{D-9}$$

and hence the floating potential given by Equation (7) is

$$\phi_f = -3.78 \text{ volts} . \tag{D-10}$$

The relationship between the floating potential and the positive ion temperature is given by

$$\phi_f = \frac{kT_e}{e} \ln\left(\frac{\bar{c}_i}{\bar{c}_e}\right) \tag{D-11}$$

where $\bar{c}_i$ and $\bar{c}_e$ are the average speeds of the positive ions and the electrons respectively at the plasma sheath edge and kT_e/e is given by Equation (5). The ratio of $\bar{c}_i$ to $\bar{c}_e$ is given by

$$\frac{\bar{c}_i}{\bar{c}_e} = \sqrt{\frac{T_i m_e}{T_e m_i}} \tag{D-12}$$

where T_i is the positive ion temperature at the plasma sheath edge and m_e and m_i are the masses of the electrons and the positive ions respectively. Solving Equations (11) and (12) for the positive ion temperature yields

$$T_i = T_e \frac{m_i}{m_e} \exp\left(\frac{2e\phi_f}{kT_e}\right) . \tag{D-13}$$

The mass of an argon ion is given by

$$m_i = 6.65 \times 10^{-23} \text{ gm} \tag{D-14}$$

and the mass of an electron is given by

$$m_e = 9.1 \times 10^{-28} \text{ gm} \tag{D-15}$$

hence Equation (13) yields

$$T_i = 5345^\circ K \tag{D-16}$$

for the sheath edge positive ion temperature.

At the plasma potential, the positive ion saturation current is given by

$$j_{is} = 2.00 \text{ ma} . \tag{D-17}$$

The positive ion number density is given by

$$n_i = \frac{4j_{is}}{eA_w}\sqrt{\frac{\pi m_i}{8kT_i}} \tag{D-18}$$

where A_w is the cross sectional area of the collecting electrode and is equal to 1.822×10^{-2} cm^2. The positive ion number density is thus

$$n_i = 1.66 \times 10^{13} \frac{\text{ions}}{cm^3} . \tag{D-19}$$

The stagnation pressure at the probe surface is given by

$$p_o = 40.0 \text{ mm Hg} \tag{D-20}$$

and the total particle number density at the sheath edge is given by

$$n = \frac{p_o}{kT_i} \tag{D-21}$$

and thus from Equation (21)

$$n = 7.20 \times 10^{16} \text{ cm}^{-3} . \tag{D-22}$$

At the sheath edge, the plasma particles are positive ions, electrons, and neutral gas particles and hence

$$n = n_i + n_e + n_p \tag{D-23}$$

where n_p is the neutral gas particle number density. For each neutral particle which is ionized, both a positive ion and an electron are produced and hence

$$n = n_p + 2n_i . \tag{D-24}$$

The number density which would exist if there were no ionization, n_{po}, is given by

$$n_{po} = n_p + n_i . \tag{D-25}$$

The sheath edge ionization percentage which is the ratio of n_i to n_{po} expressed as a percentage is thus given by

$$\frac{n_i}{n_{po}} \times 100\% = \frac{n_i}{n-n_i} \times 100\% = 2.31 \times 10^{-2}\% \text{ ionization} . \tag{D-26}$$

The ion mean free path, λ_i, is given by

$$\lambda_i = \frac{1}{\sqrt{2}\, n\, \overline{Q}_i} \qquad (D\text{-}27)$$

where $\overline{Q}_i$ is the average collision cross section between the positive ions and the neutral particles. Figure 20 shows the argon momentum transfer cross section as a function of temperature determined by Devoto.[29] For a temperature of 5345°K the collision cross section is 1.98×10^{-16} cm^2. This cross section, however, is for a single argon atom. For a collision between two argon atoms or an atom and a positive ion, the cross section is four times the value shown in Figure 20. The average collision cross section is thus

$$\overline{Q}_i = 7.92 \times 10^{-16} \text{ cm}^2 \qquad (D\text{-}28)$$

and from Equation (27) the ion mean free path is

$$\lambda_i = 1.24 \times 10^{-2} \text{ cm} . \qquad (D\text{-}29)$$

From Appendix C, the sheath thickness equation is

$$\lambda_d = \frac{\left(\frac{1-\alpha}{\varepsilon} + \alpha + 1\right) \frac{3\pi}{4} \lambda_i}{1.19\left(\frac{1-\alpha}{\varepsilon} + \alpha\right) + \sqrt{2}(1-\alpha)\, \frac{\overline{Q}_e}{\overline{Q}_i} + 1.16\alpha} \qquad (D\text{-}30)$$

where α is the ratio of negative ions to positive ions at the sheath edge, ε is the ratio of the electron temperature to the positive ion temperature at the sheath edge, $\overline{Q}_e$ is the average collision cross section of the electrons with the argon atoms, and $\overline{Q}_i$ is the average collision

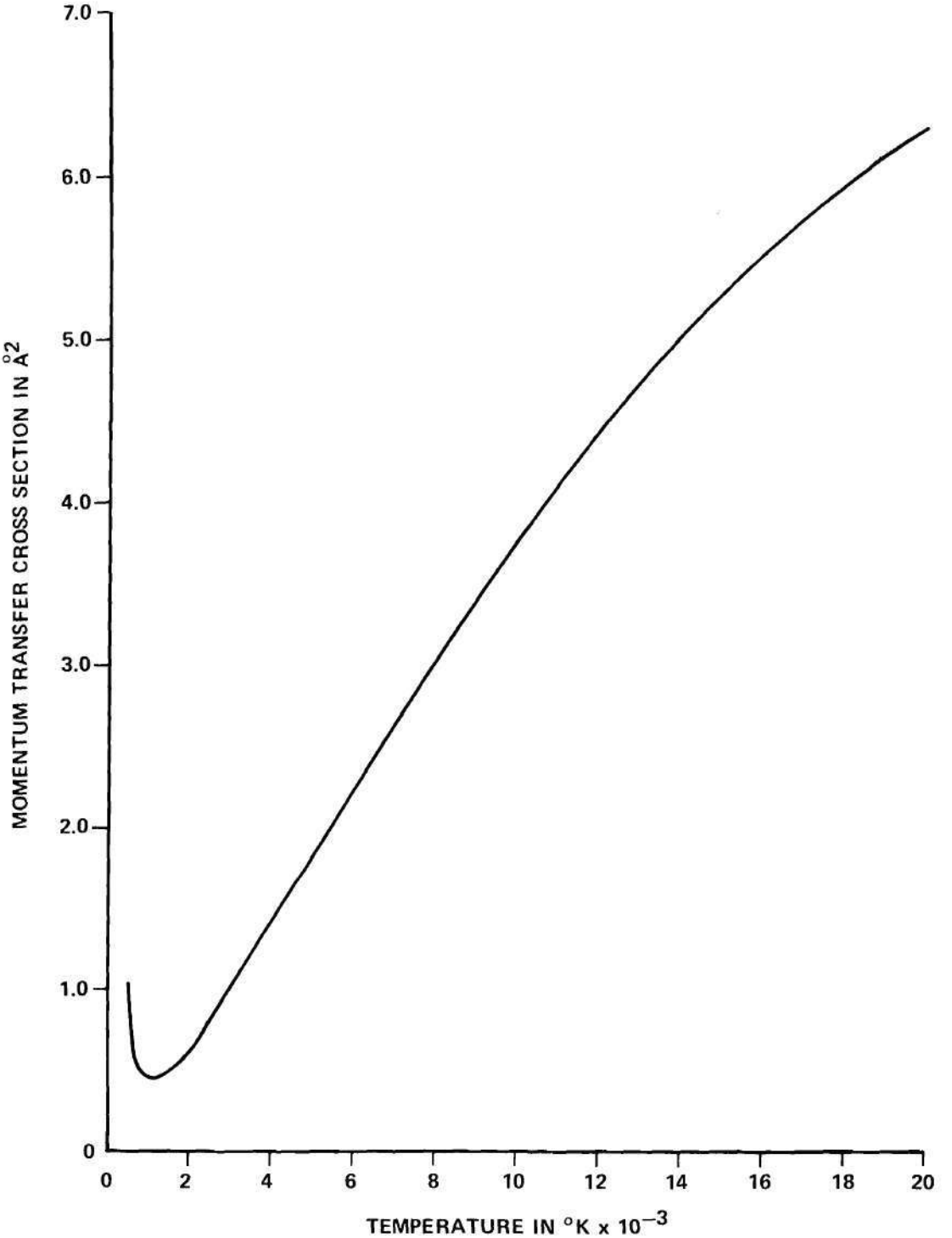

Figure 20. Argon Momentum Transfer Cross Section

cross section between the positive ions and the argon atoms within the sheath. In the present example, no negative ions are present in the plasma and hence

$$\alpha = 0 \ . \tag{D-31}$$

The value of ε is given by

$$\varepsilon = \frac{7600^\circ K}{5345^\circ K} = 1.422 \tag{D-32}$$

and since the electrons can be treated as particles with negligible cross section the value for $\overline{Q}_e$ can be read directly from Figure 20. For an electron temperature of 7600°K the value of $\overline{Q}_e$ is

$$\overline{Q}_e = 2.85 \times 10^{-16} \ cm^2 \ . \tag{D-33}$$

As noted in Appendix C, the value of $\overline{Q}_i$ to be used is the value which corresponds to the average ion temperature within the boundary layer. This average ion temperature, T_{ia}, is equal to

$$T_{ia} = \sqrt{\frac{1}{2}}\, T_i \tag{D-34}$$

and hence

$$T_{ia} = 3780^\circ K \ . \tag{D-35}$$

Since the collisions are between argon atoms and argon ions, the value for $\overline{Q}_i$ is equal to four times the value for the collision cross section given in Figure 20 for a temperature equal to T_{ia}. For an average temperature of 3780°K, the value of $\overline{Q}_i$ is

$$\overline{Q}_i = 5.24 \times 10^{-16} \text{ cm}^2 . \qquad \text{(D-36)}$$

From Equation (30), the sheath thickness is thus given by

$$\lambda_d = 3.10 \times 10^{-2} \text{ cm} . \qquad \text{(D-37)}$$

To continue the solution, a value for the free stream stagnation temperature, T_2, must be assumed. The value assumed is

$$T_2 = 9000°K . \qquad \text{(D-38)}$$

For this temperature, the stagnation values of the density, ρ_2; Prandtl number, $\overline{\sigma}$; and viscosity, μ_2, are needed. The values for argon density as a function of pressure and temperature are given in tabular form by Brahinsky and Neel.[32] For a stagnation temperature of 9000°K and a stagnation pressure of 40 mm. Hg., Brahinsky and Neel give a value of

$$\rho_2 = 2.77 \times 10^{-6} \text{ gm/cm}^3 \qquad \text{(D-39)}$$

for the sheath edge density. The value for the Prandtl number, given by Talbot,[12] is

$$\overline{\sigma} = \frac{2}{3} . \qquad \text{(D-40)}$$

The value for the argon viscosity as a function of temperature has been determined by Devoto[29] and Bromley and Wilke[30] and their results are shown in Figure 21. From Figure 21, the argon viscosity corresponding to a temperature of 9000°K is

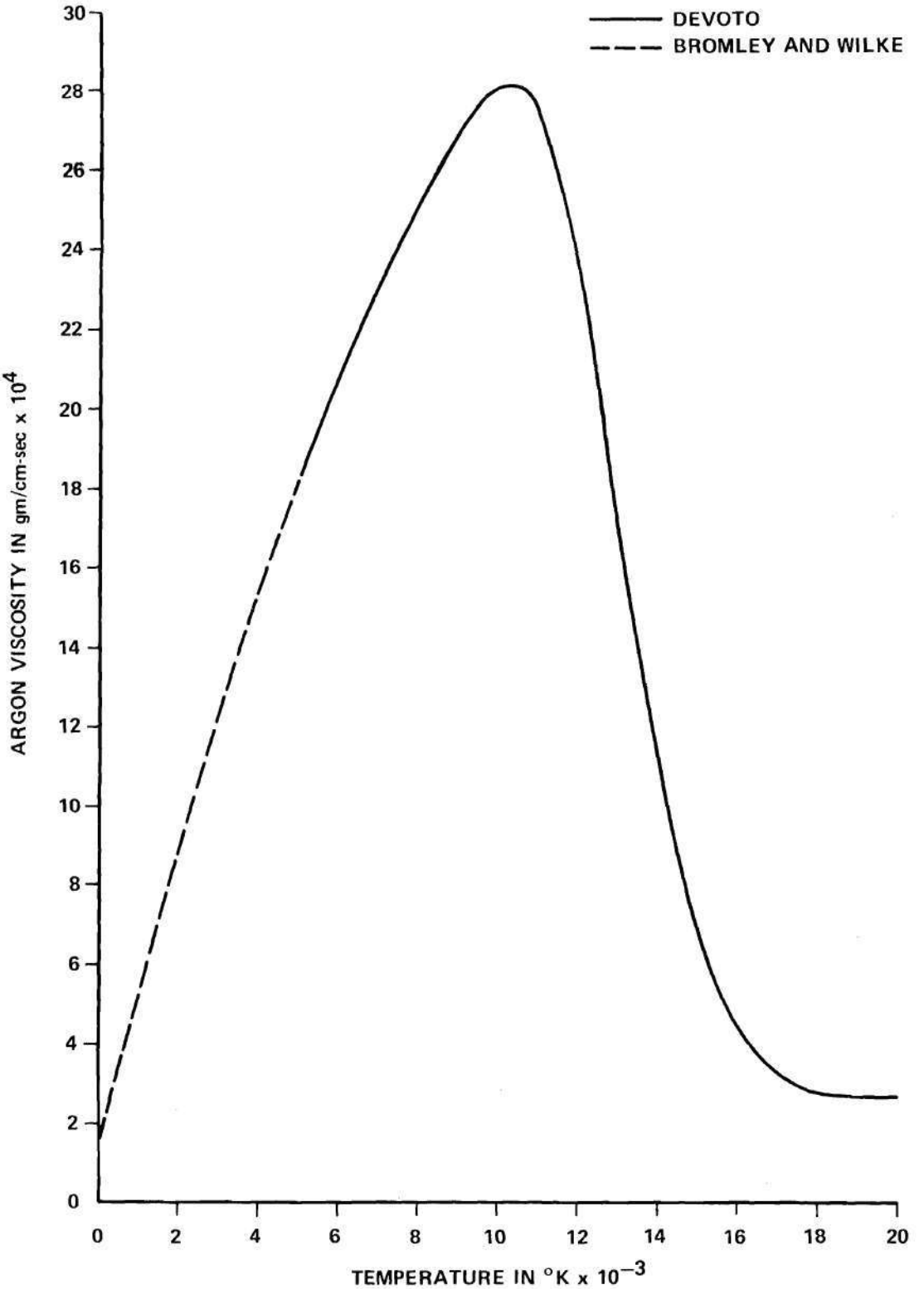

Figure 21. Argon Viscosity As a Function of Temperature

$$\mu_2 = 2.71 \times 10^{-3} \frac{gm}{cm\text{-}sec} . \qquad (D\text{-}41)$$

The pressure gradient parameter, $\overline{\beta}$, is given by

$$\overline{\beta} = \frac{2}{D_o} \sqrt{\frac{p_o - p_s}{\rho_2}} \qquad (D\text{-}42)$$

where D_o is the electrostatic probe diameter given by

$$D_o = 1.905 \text{ cm} \qquad (D\text{-}43)$$

and p_s is the free stream static pressure which, for the present example, is given by

$$p_s = 31 \text{ mm. Hg.} \qquad (D\text{-}44)$$

The pressure gradient parameter is thus

$$\overline{\beta} = 1.01 \times 10^5 \text{ sec}^{-1} . \qquad (D\text{-}45)$$

The sheath edge value for the nondimensional boundary layer parameter, η, is given by

$$\eta_d = \frac{\lambda_d^{1/2}}{\left[0.18(\overline{\sigma})^{1/3}\left(\frac{\mu_2}{\overline{\beta}\rho_2}\right)^{1/2}\right]^{1/2}} , \qquad (D\text{-}46)$$

or for the present example

$$\eta_d = 1.413 . \qquad (D\text{-}47)$$

The ratio of the sheath edge ion temperature to the free stream stagnation temperature, $\bar{g}(\eta_d)$, is given by

$$\bar{g}(\eta_d) = 0.50\ \bar{\sigma}^{1/3}\ \eta_d \qquad \text{(D-48)}$$

and, for the present example,

$$\bar{g}(\eta_d) = 0.63\ . \qquad \text{(D-49)}$$

The free stream stagnation temperature, T_2, is thus given by

$$T_2 = \frac{T_i}{\bar{g}(\eta_d)} = 8480°K\ . \qquad \text{(D-50)}$$

This value for T_2 is less than the assumed value for T_2 thus indicating that the initial guess was too high. A lower free stream stagnation temperature is chosen and the above calculations are repeated. This process continues until the assumed free stream stagnation temperature and the calculated temperature agree. For the present example, this iterative process converged on a value for T_2 of

$$T_2 = 8260°K\ . \qquad \text{(D-51)}$$

Since the sheath edge ionization percentage is assumed to be equal to the free stream ionization percentage, the predicted free stream ionization percentage, given by Equation (26), is equal to 2.31×10^{-2} percent.

For this example, the power input to the plasma torch was 88.4 kilowatts or 5020 BTU/min and the rate of heat removal by the cooling water was 3281 BTU/min for a net power addition to the argon of 1739

BTU/min. The argon flow rate through the plasma torch was 0.625 kg.-mole/hr and hence the argon stagnation enthalpy, h_o, was

$$h_o = 4.22 \times 10^4 \frac{\text{k-cal.}}{\text{kg.-mole}} . \qquad \text{(D-52)}$$

For this enthalpy and a stagnation pressure of 40 mm. Hg., Brahinsky and Neel[32] give a free stream stagnation temperature of

$$T_o = 7970°K \qquad \text{(D-53)}$$

where the subscript o is used to differentiate the stagnation temperature determined by Brahinsky and Neel from the stagnation temperature, T_2, determined by the electrostatic probe theory.

The free stream static temperature, T_{FS}, is determined from the stagnation temperature by

$$T_{FS} = T_o \left(\frac{p_s}{p_o}\right)^{\frac{\gamma-1}{\gamma}} \qquad \text{(D-54)}$$

where γ is the ratio of specific heats for argon. With the value of γ equal to 1.67 and p_s and p_o given by Equations (44) and (20), Equation (54) yields

$$T_{FS} = 7200°K . \qquad \text{(D-55)}$$

For this free stream temperature and a static pressure of 31 mm. Hg., Brahinsky and Neel give a free stream ionization of 0.192 percent. Since the argon plasma is assumed to be in equilibrium in the free stream and chemically frozen within the probe boundary layer, the

ionization level measured by the electrostatic probe would be expected to be equal to this value.

The heat balance technique thus predicts a free stream stagnation temperature of 7970°K and a free stream ionization of 0.192 percent while the electrostatic probe theory gives a free stream stagnation temperature of 8260°K and, from Equation (26), a free stream ionization of 2.31×10^{-2} percent. The free stream stagnation temperature predicted by the electrostatic probe theory differs from the free stream stagnation temperature predicted by the heat balance by only 3.6 percent thus indicating the good agreement between the two methods for determining the free stream stagnation temperature. The value for the free stream ionization predicted by the probe theory differs from that predicted by the heat balance by -88 percent. As noted in Chapter VI this large error is due to recombination within the boundary layer of the electrostatic probe.

In these calculations, an adjusted value of the floating potential was used to determine the sheath edge temperature so that the sheath thickness which existed when the collecting electrode was at the plasma potential could be used in the calculations. To determine if any significant error was introduced by this method of calculation, the above calculations were repeated using the actual floating potential and the sheath thickness which existed at that potential. The results showed a predicted free stream stagnation temperature of 8200°K and a predicted ionization of 2.74×10^{-2} percent. These results are in good agreement with the previous results.

Data Reduction with Nearly Complete Electron Quenching

Figure 22 shows a typical current-voltage characteristic curve for the case in which the electrons have been almost completely absorbed by the sulphur hexafluoride additive. The absolute value of the current to the collecting electrode is shown so that the magnitudes of the saturation currents may be more easily compared. The negative particle saturation current, which is the sum of the electron and negative ion saturation currents, shows much less variation in magnitude with probe potential than did the electron saturation current in the previous example. This shows the decrease in the rate of growth of the sheath thickness with probe potential which occurs as free electrons are removed from the plasma. The equation

$$j = j_e + j_n + j_i , \tag{D-56}$$

where j_n is the negative ion current to the collecting electrode, is used to determine the positive ion and the negative particle currents as a function of probe potential. These currents are shown in Figure 23. The plasma potential is indicated by the sharp changes in slopes of both the positive ion current and the negative particle current, $j_{e,n}$. With the electrostatic probe potential greater than the plasma potential, the slope of the positive ion current is given by

$$\frac{d \ln j_i}{d\phi} = - \frac{e}{kT_i} . \tag{D-57}$$

In the present example, the slope of the positive ion current is found to be

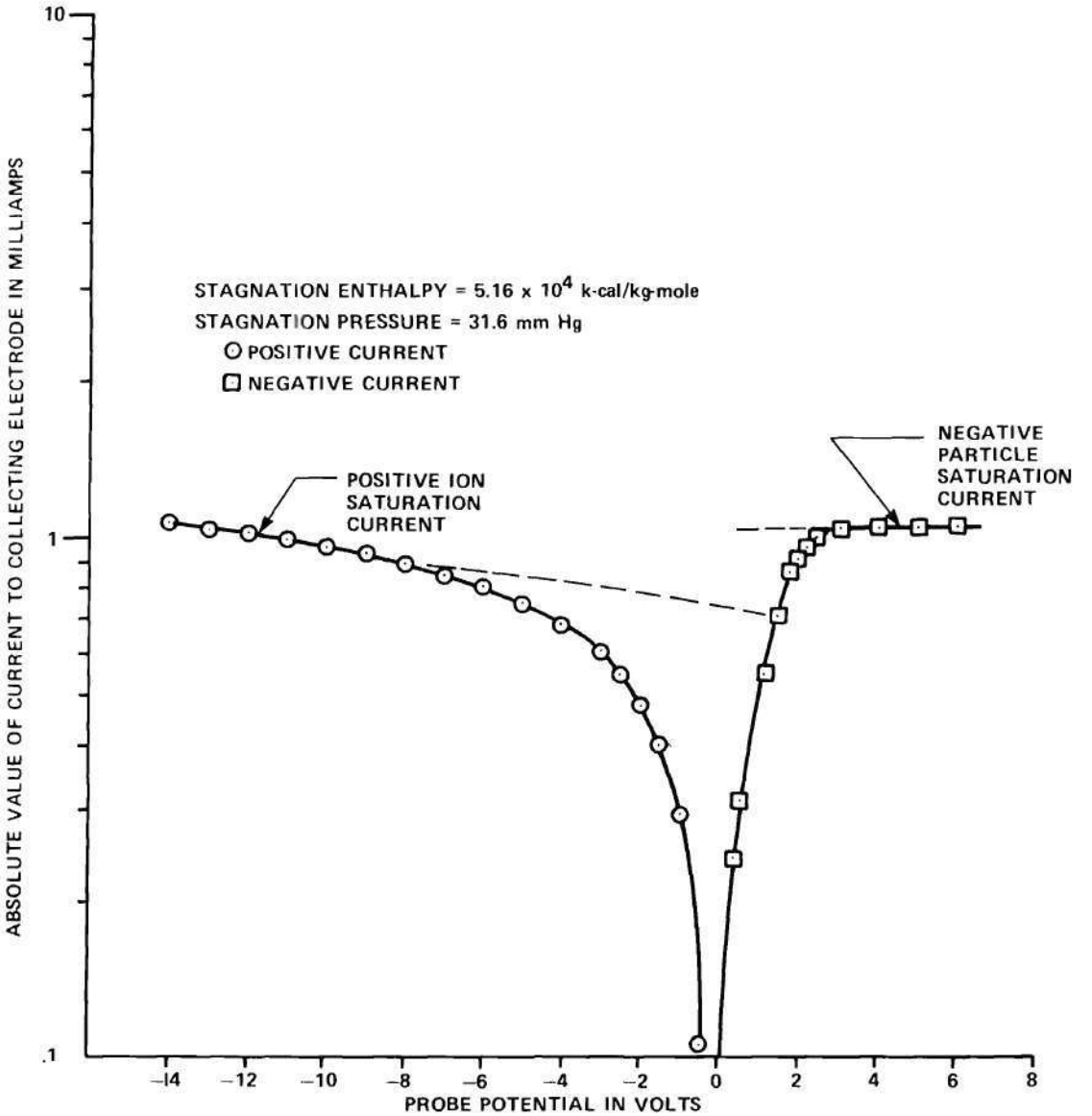

Figure 22. Current-Voltage Characteristic for Nearly Complete Electron Absorption

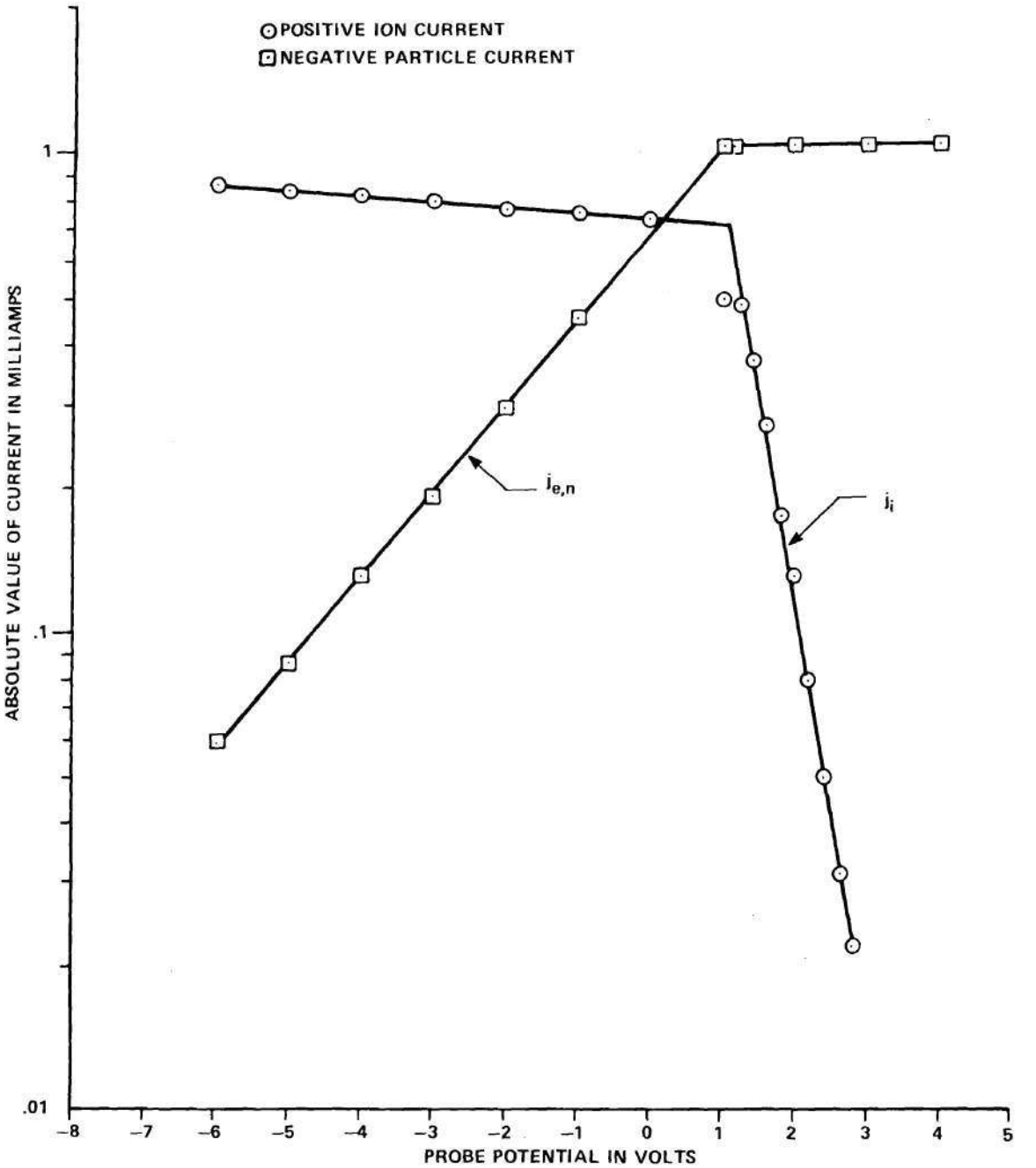

Figure 23. Particle Currents for Nearly Complete Electron Absorption

$$\frac{d\ \ell n\ j_i}{d\phi} = -2.006\ \text{volts}^{-1} \tag{D-58}$$

and hence

$$T_i = 5780°K\ . \tag{D-59}$$

With the electrostatic probe potential less than the plasma potential, the slope of the negative particle current is given in Appendix B as

$$\frac{d\ \ell n|j_{e,n}|}{d\phi} = \frac{d}{d\phi}\ \ell n\left[e^{\frac{e(\phi-\phi_p)}{kT_e}} + \frac{n_n\bar{c}_n}{n_e\bar{c}_e}\, e^{\frac{e(\phi-\phi_p)}{kT_n}}\right] \tag{D-60}$$

where n_n is the negative ion number density at the sheath edge, $\bar{c}_n$ and $\bar{c}_e$ are the average velocities of the negative ions and electrons respectively at the sheath edge, and T_n is the negative ion temperature at the sheath edge. In general, the momentum transfer rate in collisions between the negative ions, the positive ions, and neutral particles is high enough so that it may be assumed that

$$T_n = T_i\ . \tag{D-61}$$

In addition, in each of the present experiments, the electron velocity was sufficiently high compared to the negative ion velocity to that

$$\frac{n_n\bar{c}_n}{n_e\bar{c}_e} < 1 \tag{D-62}$$

and the electron temperature was sufficiently high compared to the negative ion temperature so that

$$e^{\frac{e(\phi-\phi_p)}{kT_n}} < e^{\frac{e(\phi-\phi_p)}{kT_e}} \tag{D-63}$$

and hence, for probe potentials such that

$$\phi - \phi_p < -2 \text{ volts} , \tag{D-64}$$

a very good approximation to Equation (60) is given by

$$\frac{d \ln|j_{e,n}|}{d\phi} = \frac{e}{kT_e} . \tag{D-65}$$

In the present example, the slope of the negative particle current is given by

$$\frac{d \ln|j_{e,n}|}{d\phi} = 0.41 \text{ volts}^{-1} \tag{D-66}$$

and hence

$$T_e = 28,300°K . \tag{D-67}$$

The validity of Equation (65) can be demonstrated by noting that, for a value of

$$\phi - \phi_p = -2 \text{ volts} , \tag{D-68}$$

the ratio of the two exponential terms in Equation (60) is

$$\frac{e^{\frac{e(\phi-\phi_p)}{kT_e}}}{e^{\frac{e(\phi-\phi_p)}{kT_i}}} = 24 \qquad \text{(D-69)}$$

and hence the term involving the negative ion temperature can be dropped from Equation (60) with little loss in accuracy.

At the plasma potential, the positive ion saturation current is given by

$$j_{is} = 0.72 \text{ ma.} \qquad \text{(D-70)}$$

and hence, from Equation (18), the positive ion number density is

$$n_i = 5.67 \times 10^{12} \frac{\text{ions}}{\text{cm}^3} . \qquad \text{(D-71)}$$

The stagnation pressure at the probe surface is given by

$$p_o = 31.6 \text{ mm. Hg.} \qquad \text{(D-72)}$$

and from Equation (21) the total particle number density at the sheath edge is

$$n = 5.28 \times 10^{16} \text{ cm}^{-3} . \qquad \text{(D-73)}$$

From Equation (26), the ionization percentage is given by

$$\frac{n_i}{n-n_i} \times 100\% = 1.07 \times 10^{-2}\% \text{ ionization} . \qquad \text{(D-74)}$$

The positive ion mean free path, determined from Equation (27) with

$$\overline{Q}_i = 8.60 \times 10^{-16} \text{ cm}^2 , \tag{D-75}$$

is equal to

$$\lambda_i = 1.56 \times 10^{-2} \text{ cm} . \tag{D-76}$$

The sheath thickness is given by Equation (30). For this example, the value of α in Equation (30) is so close to one that the equation can be simplified to

$$\lambda_d = \frac{2}{2.35} \frac{3\pi}{4} \lambda_i \tag{D-77}$$

and hence

$$\lambda_d = 3.13 \times 10^{-2} \text{ cm} . \tag{D-78}$$

As in the previous example, a value for the free stream stagnation temperature is assumed. The value assumed is

$$T_2 = 8600°\text{K} . \tag{D-79}$$

From Brahinsky and Neel, the density at the sheath edge is

$$\rho_2 = 2.31 \times 10^{-6} \frac{\text{gm}}{\text{cm}^3} \tag{D-80}$$

and from Figure (21) the viscosity is found to be

$$\mu_2 = 2.64 \times 10^{-3} \frac{gm}{cm\text{-}sec} . \tag{D-81}$$

The free stream static pressure in this example is

$$p_s = 19.8 \text{ mm. Hg.} \tag{D-82}$$

and hence from Equation (42) the pressure gradient parameter is

$$\overline{\beta} = 1.223 \times 10^5 \text{ sec}^{-1} . \tag{D-83}$$

From Equation (46), the nondimensional boundary layer parameter is

$$\eta_d = 1.431 \tag{D-84}$$

and from Equation (48)

$$\overline{g}(\eta_d) = 0.638 . \tag{D-85}$$

The free stream stagnation temperature is thus

$$T_2 = \frac{T_i}{\overline{g}(\eta_d)} = 9070°K . \tag{D-86}$$

This value of T_2 is higher than the assumed value for T_2 indicating that the initial guess was too low. A higher value for the free stream stagnation temperature is chosen and the above calculations are repeated. For this example, the iteration process converged on a value of

$$T_2 = 9250°K . \tag{D-87}$$

The stagnation enthalpy for this example was

$$h_o = 5.16 \times 10^4 \frac{\text{k-cal.}}{\text{kg.-mole}} \tag{D-88}$$

and from Brahinsky and Neel this yields a value of

$$T_o = 8650°K \tag{D-89}$$

for the free stream stagnation temperature and a value of 0.24 percent for the free stream ionization. The free stream stagnation temperature predicted by the electrostatic probe theory thus differs from that which was predicted by the heat balance technique by 6.9 percent while the free stream ionization predicted by the electrostatic probe theory differs from the free stream ionization predicted by the heat balance technique by -96 percent. Again, this large error is due to recombination within the electrostatic probe boundary layer.

Data Reduction with Partial Electron Quenching

Figure 24 shows a typical current-voltage characteristic curve for the case in which a fraction of the electrons have been absorbed by the sulphur hexafluoride additive. As in the previous examples, the absolute value of the current to the collecting electrode is shown in the figure. Equation (56) is used to determine the positive ion and negative particle currents. These currents are shown in Figure 25. The plasma potential is indicated by the sharp change in the slope of the negative particle current as it was in the first example. The electron temperature is determined from Equation (65) where for this example

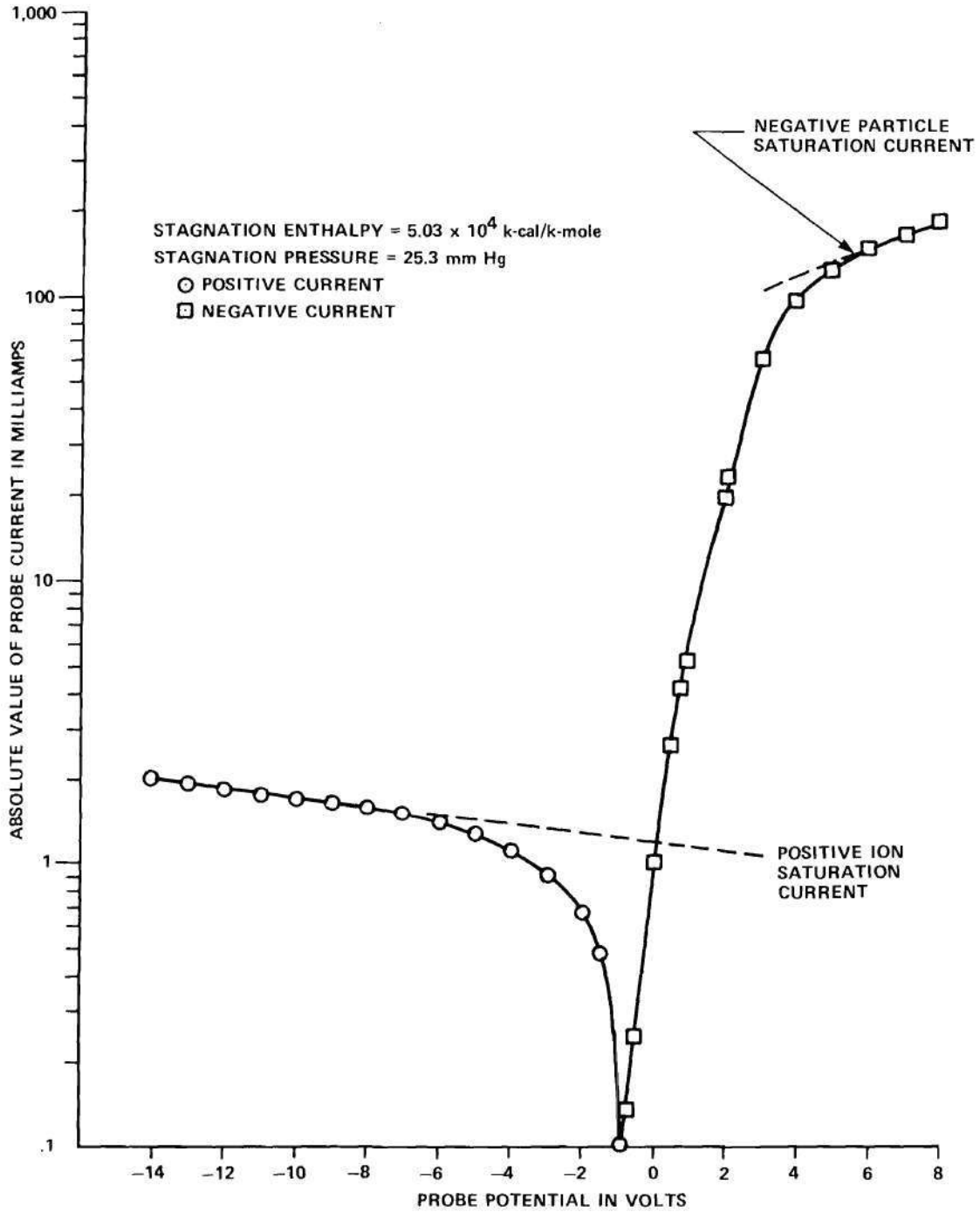

Figure 24. Current-Voltage Characteristic for Partial Electron Absorption

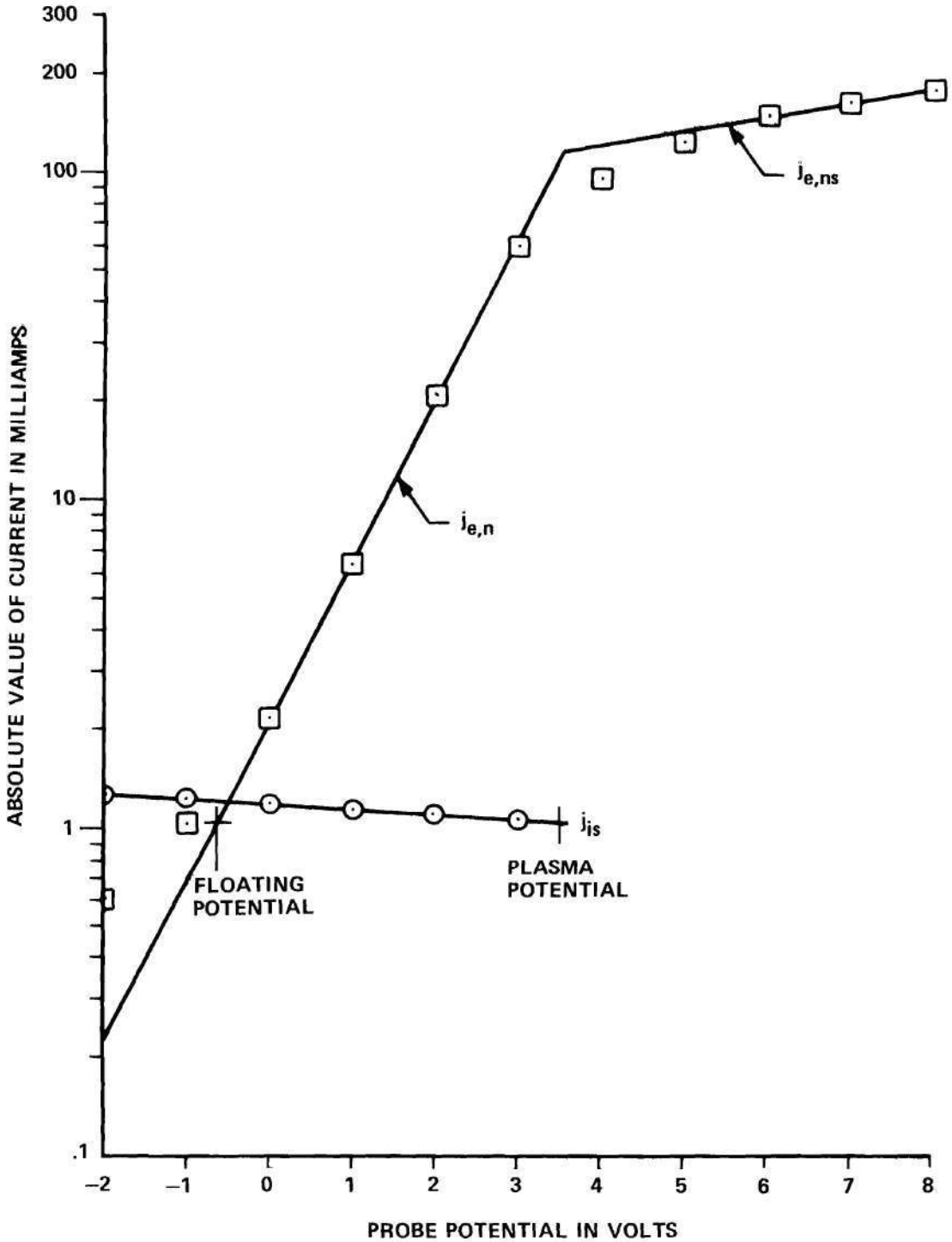

Figure 25. Particle Currents for Partial Electron Absorption

$$\frac{e}{kT_e} = 1.13 \text{ volts} \tag{D-90}$$

and hence

$$T_e = 10{,}280°K \ . \tag{D-91}$$

From Figure 25, it can be seen that the plasma potential is

$$\phi_p = 3.52 \text{ volts} \ . \tag{D-92}$$

The value for ϕ_o is chosen in the same manner as it was in the first example and from Figure 25 is found to be

$$\phi_o = -0.63 \text{ volts} \tag{D-93}$$

and hence the floating potential is

$$\phi_f = -4.15 \text{ volts} \ . \tag{D-94}$$

From Appendix B, the relationship between the floating potential, the charged particle number densities, and the charged particle temperatures of the sheath edge is given by

$$\phi_f = \frac{kT_e}{e} \ln\left(\frac{n_i \bar{c}_i}{n_e \bar{c}_e} - \frac{n_n \bar{c}_n}{n_e \bar{c}_e} e^{\frac{e\phi_f}{kT_n}}\right) \ . \tag{D-95}$$

In general, the second term in the brackets is small compared to the first term and can be neglected. Equation (95) thus becomes

$$\phi_f = \frac{kT_e}{e} \ln\left(\frac{n_i \bar{c}_i}{n_e \bar{c}_e}\right) \tag{D-96}$$

and hence

$$\frac{n_i \bar{c}_i}{n_e \bar{c}_e} = 0.0092 \ . \tag{D-97}$$

Since the object of the partial electron quenching experiments was to determine the effectiveness of sulphur hexafluoride as an electrophilic compound, the ratio of n_i to n_e in Equation (97) is an unknown and thus the sheath edge positive ion temperature cannot be determined directly from the current-voltage characteristic as was the case in the previous two examples. The iterative technique which follows is used to solve for the ratio of n_e to n_i.

For this example, the heat balance gives a stagnation enthalpy of

$$h_o = 5.03 \times 10^4 \ \frac{\text{k-cal.}}{\text{kg.-mole}} \tag{D-98}$$

and the stagnation and free stream static pressures are 25.3 mm. Hg. and 19.8 mm. Hg. respectively. From Brahinsky and Neel, these parameters yield a free stream stagnation temperature and density of

$$T_o = 8540°K \tag{D-99}$$

and

$$\rho_2 = 1.86 \times 10^{-6} \text{ gm/cm}^3 \tag{D-100}$$

respectively. The value of the Prandtl number is

$$\overline{\sigma} = \frac{2}{3} \tag{D-101}$$

and from Figure 21 the argon viscosity is

$$\mu_2 = 2.63 \times 10^{-3} \frac{\text{gm}}{\text{cm-sec}} . \tag{D-102}$$

The pressure gradient parameter, given by Equation (42), is thus

$$\overline{\beta} = 9.33 \times 10^{4} \text{ sec}^{-1} \tag{D-103}$$

and the nondimensional boundary layer parameter, given by Equation (46), is

$$\eta_d = \frac{(\lambda_d)^{\frac{1}{2}}}{0.140 \text{ cm}^{\frac{1}{2}}} \tag{D-104}$$

where the positive ion mean free path at the plasma sheath edge, λ_d, has to be determined.

The ratio of the plasma sheath edge number densities of the electrons to the positive ions is assumed to be

$$\frac{n_e}{n_i} = 0.233 \tag{D-105}$$

and hence from Equation (97)

$$\frac{\overline{c}_i}{\overline{c}_e} = 2.14 \times 10^{-3} \tag{D-106}$$

and from Equation (12)

$$T_i = 3440°K \ . \tag{D-107}$$

From Equation (21), the sheath edge total particle number density becomes

$$n = 7.12 \times 10^{16} \ cm^{-3} \tag{D-108}$$

and from Equation (27) the positive ion mean free path becomes

$$\lambda_i = 2.12 \times 10^{-2} \ cm \tag{D-109}$$

where the value of $\overline{Q}_i$, determined from Figure 20, is

$$\overline{Q}_i = 4.68 \times 10^{-16} \ cm^2 \ . \tag{D-110}$$

The plasma sheath thickness, given by Equation (30), where for the present iteration

$$\alpha = 1 - \frac{n_e}{n_i} = 0.767 \ , \tag{D-111}$$

$$\varepsilon = \frac{T_e}{T_i} = 2.99 \ , \tag{D-112}$$

$$\overline{Q}_e = 3.89 \times 10^{-16} \ cm^2 \ , \tag{D-113}$$

and

$$\overline{Q}_i = 3.16 \times 10^{-16} \ cm^2 \ , \tag{D-114}$$

is found to be

$$\lambda_d = 4.006 \times 10^{-2} \text{ cm} . \tag{D-115}$$

Equation (104) thus yields

$$\eta_d = 1.433 , \tag{D-116}$$

Equation (48) yields

$$\bar{g}(\eta_d) = 0.639 \tag{D-117}$$

and Equation (50) gives

$$T_2 = 5380°K . \tag{D-118}$$

This value for T_2 is lower than the value given by the heat balance and thus the assumed value of n_e/n_i is also too low. A higher value for n_e/n_i is assumed and the above calculations are repeated. The process is continued until the calculated free stream stagnation temperature and the temperature predicted by the heat balance agree. For the present example, this iterative process converged on a value of

$$\frac{n_e}{n_i} = 0.291 \tag{D-119}$$

for which

$$T_i = 5400°K \tag{D-120}$$

and

$$n = 4.54 \times 10^{16} \text{ cm}^{-3} . \tag{D-121}$$

At the plasma potential, the positive ion saturation current is

$$j_{is} = 1.03 \text{ ma.} \tag{D-122}$$

and thus from Equation (18)

$$n_i = 8.37 \times 10^{12} \text{ cm}^{-3} \tag{D-123}$$

and the ionization percentage at the sheath edge is given by

$$\frac{n_i}{n-n_i} \times 100\% = 0.019\% \text{ ionization} . \tag{D-124}$$

The number density of the sulphur hexafluoride molecules at the sheath edge, n_{SF_6}, is given by

$$n_{SF_6} = n \frac{SF_6 \text{ flow rate}}{\text{argon flow rate}} \tag{D-125}$$

where the argon flow rate is the rate at which argon is supplied to the plasma torch and the sulphur hexafluoride flow rate is the rate at which sulphur hexafluoride is added to the argon plasma. For the present example, the sulphur hexafluoride flow rate was 0.134 standard cubic feet per hour (scfh) and the argon flow rate was 222 scfh, hence

$$n_{SF_6} = 2.73 \times 10^{13} \text{ cm}^{-3} \tag{D-126}$$

and the ratio at the plasma sheath edge of the sulphur hexafluoride number density to the positive ion number density is

$$\frac{n_{SF_6}}{n_i} = 3.26 . \tag{D-127}$$

The sulphur hexafluoride electron capture cross section, σ, is given by

$$\sigma = \frac{1}{\bar{c}_e \frac{n_{SF_6}}{n_i} n_i t} \ln \left(\frac{\frac{n_e}{n_i} + \frac{n_{SF_6}}{n_i}}{\frac{n_e}{n_i} \frac{n_{io}}{n_{eo}}} \right) \qquad \text{(D-128)}$$

where $\bar{c}_e$ is the average speed of the electrons and t is the absorption time. The average speed of the electrons is given by

$$\bar{c}_e = 5.93 \times 10^7 \sqrt{\frac{T_e}{11{,}600^\circ K}} \ \frac{cm}{sec} \ . \qquad \text{(D-129)}$$

An assumption in the derivation of Equation (128) is that most of the electron absorption occurs within the electrostatic probe boundary layer. The appropriate value for t, then, is the time of passage from the edge of the boundary layer to the probe surface. In Chapter II this time of passage is given by

$$t = \frac{1.05}{\bar{\beta}} \qquad \text{(D-130)}$$

and since, in this example, $\bar{\beta}$ is equal to 9.33×10^4 sec^{-1} the value of t is

$$t = 1.13 \times 10^{-5} \text{ sec} \ . \qquad \text{(D-131)}$$

For reasons presented in Chapter VI, the free stream static temperature rather than the electron temperature measured by the electrostatic probe is used in Equation (129). In this example, the heat balance technique

gave a free stream static temperature of 7740°K and hence

$$\bar{c}_e = 4.85 \times 10^7 \text{ cm/sec} . \qquad \text{(D-132)}$$

Brahinsky and Neel give an equilibrium free stream ionization percentage of 0.60 percent. Thus, if no recombination occurred within the probe boundary layer, the positive ion number density at the sheath edge would be

$$n_{io} = 2.72 \times 10^{14} \text{ cm}^{-3} . \qquad \text{(D-133)}$$

The initial electron number density is given by

$$n_{eo} = n_{io} - n_{SF_6} = 2.45 \times 10^{14} \text{ cm}^{-3} \qquad \text{(D-134)}$$

since, as noted in Chapter VI, the sulphur hexafluoride is assumed to have become very nearly completely ionized by the time it reaches the location of the electrostatic probe. Equation (128) thus gives a value of

$$\sigma = 1.602 \times 10^{-16} \text{ cm}^2 \qquad \text{(D-135)}$$

for the electron attachment coefficient of sulphur hexafluoride at the test conditions of this example.

APPENDIX E

COMPILATION OF DATA

The results of the experimental investigation were presented in Chapter VI. These results are presented in more detail in this appendix. The results of the experimental evaluation of the electrostatic probe theory for the case in which no negative ions are present in the plasma are presented in Table 2. Similarly, the results of the experimental evaluation for the case in which nearly complete electron quenching occurs are presented in Table 3.

The results of the experimental evaluation of sulphur hexafluoride as an electrophilic additive are shown in Table 4. In Table 4, n_i is the positive ion number density at the plasma sheath edge, n_e/n_i is the ratio, at the sheath edge, of the electron to the positive ion number density, and n_{SF_6}/n_i is the ratio, at the plasma sheath edge, of the sulphur hexafluoride number density to the positive ion number density.

The data for the calculations of the argon recombination coefficient are presented in Table 5. As noted in Chapter VI, the recombination coefficient, α_r, is given by

$$\alpha_r = \frac{n_{i2} - n_i}{n_i n_{i2} t} \qquad \text{(E-1)}$$

where n_{i2} is the initial number density of the argon ions, and t is the recombination time. The values for n_{i2} and n_i are determined from the total particle number density, found in Table 5, by converting the free

Table 2. Experimental Results for No Electron Quenching

	Heat Balance Results					Electrostatic Probe Measurements		
	Stagnation Conditions		Free Stream Static Conditions					
Enthalpy	Pressure	Temperature	Pressure	Temperature	Ionization	Stagnation Temperature	Ionization	Electron Temperature
$\frac{\text{k-cal.}}{\text{kg.-mole}}$	mm. Hg.	°K	mm. Hg.	°K	Percent	°K	Percent	°K
3.86×10^4	25.7	7480	19.8	6740	0.093	6700	0.031	6900
4.22×10^4	40.0	7970	31.0	7200	0.192	8260	0.023	7600
4.46×10^4	29.2	8015	14.9	6120	0.024	6800	0.046	12300
4.95×10^4	47.7	8630	40.7	8100	0.81	8600	0.018	7800
5.21×10^4	32.1	8740	14.9	6440	0.054	7200	0.121	10580
6.03×10^4	42.4	9200	27.7	7760	0.492	8970	0.055	8050
9.04×10^4	55.3	10100	44.4	9250	3.26	11650	0.061	10710

Table 3. Experimental Results for Nearly Complete Electron Quenching

	Heat Balance Results					Electrostatic Probe Measurements		
	Stagnation Conditions		Free Stream Static Conditions			Stagnation		Electron
Enthalpy	Pressure	Temperature	Pressure	Temperature	Ionization	Temperature	Ionization	Temperature
k-cal./kg.-mole	mm. Hg.	°K	mm. Hg.	°K	Percent	°K	Percent	°K
3.99×10^4	28.6	7650	20.0	6630	0.073	7200	0.013	18,620
4.31×10^4	40.0	8060	32.0	7370	0.263	9400	0.014	10,590
5.16×10^4	31.6	8650	19.8	7200	0.24	9250	0.011	28,300
5.33×10^4	47.7	8860	40.9	8330	1.14	9060	0.0038	40,850
5.51×10^4	53.0	9010	41.3	8154	0.868	8800	0.0017	23,290
5.65×10^4	40.2	9010	29.6	7980	0.795	11150	0.0048	15,200
5.74×10^4	45.6	9090	30.3	7720	0.504	9250	0.0082	40,000
6.02×10^4	42.0	9195	32.3	8350	1.32	9180	0.0031	20,900
6.54×10^4	43.7	9400	28.4	7910	0.714	8200	0.021	26,700
6.60×10^4	42.7	9433	29.2	8100	0.951	9050	0.058	33,600
7.56×10^4	46.6	9771	29.9	8190	1.08	12100	0.107	21,500
8.76×10^4	55.3	10150	44.6	9320	3.63	11200	0.035	28,200

Table 4. Experimental Results for the Sulphur Hexafluoride Additive

	Heat Balance Results					Electrostatic Probe Measurements				
	Stagnation Conditions		Free Stream Static Conditions							
Enthalpy	Pressure	Temperature	Pressure	Temperature	Ionization	Ionization	Electron Temperature	n_i	$\frac{n_e}{n_1}$	$\frac{n_{SF_6}}{n_i}$
k-cal./kg.-mole	mm. Hg.	°K	mm. Hg.	°K	Percent	Percent	°K	ions/cm^3		
3.98×10^4	24.8	7600	19.6	6950	0.14	0.017	12,180	8.23×10^{12}	0.265	3.10
3.99×10^4*	28.6	7650	20.0	6630	0.07	0.013	18,620	7.47×10^{12}	0.011	8.34
4.13×10^4	24.6	7800	19.8	7300	0.30	0.021	16,500	1.00×10^{13}	0.052	3.91
4.20×10^4	24.6	7860	19.8	7350	0.33	0.021	12,340	1.00×10^{13}	0.135	3.27
4.40×10^4	24.8	7950	19.6	7250	0.27	0.011	17,450	5.40×10^{12}	0.030	9.11
4.79×10^4	25.1	8400	19.8	7650	0.54	0.036	18,100	1.63×10^{13}	0.074	2.07
4.84×10^4	28.6	8440	20.2	7340	0.31	0.067	8,080	3.18×10^{13}	0.625	1.08
5.03×10^4	25.3	8540	19.8	7740	0.60	0.019	10,280	8.37×10^{12}	0.291	3.26
5.10×10^4	25.1	8540	19.5	7740	0.60	0.023	19,550	1.03×10^{13}	0.023	4.84
5.16×10^4*	31.6	8650	19.8	7200	0.24	0.011	28,300	5.67×10^{12}	0.0015	12.02
5.38×10^4	30.8	8790	20.2	7420	0.36	0.042	11,430	2.21×10^{13}	0.409	3.62
5.54×10^4	25.7	8850	19.6	7800	0.70	0.070	12,920	3.16×10^{13}	0.083	0.961
5.55×10^4	52.7	9030	44.8	8460	1.28	0.0028	8,150	3.10×10^{12}	0.316	15.3
5.60×10^4	52.7	9030	44.8	8460	1.28	0.0029	8,030	3.30×10^{12}	0.110	19.7
5.73×10^4	26.2	8950	19.8	8000	0.98	0.039	11,050	1.74×10^{13}	0.302	1.89
5.81×10^4	24.6	8950	19.5	8150	1.00	0.096	19,240	4.07×10^{13}	0.054	1.09
5.88×10^4	53.0	9200	41.5	8360	1.04	0.023	6,680	2.22×10^{13}	0.825	1.77
5.92×10^4	40.5	9133	29.9	8100	0.93	0.011	9,570	7.87×10^{12}	0.270	7.93
6.12×10^4	52.0	9300	44.6	8750	1.97	0.018	12,050	1.37×10^{13}	0.661	1.99
6.14×10^4	30.5	9140	20.0	7720	0.62	0.052	7,600	2.56×10^{13}	0.350	1.70

*Taken from nearly complete electron quenching results

Table 5. Argon Recombination Coefficient

Free Stream Static Conditions		Sheath Edge Conditions					
Temperature	Ionization	Ionization	Total Particle Number Density	Pressure Gradient Parameter	Electron Temperature	$\frac{n_{SF_6}}{n_i}$	Recombination Coefficient
°K	Percent	Percent	cm^{-3}	sec^{-1}	°K		cm^3/sec
6740	0.093	0.031	4.75×10^{16}	8.36×10^{4}	6,900	0.0	3.60×10^{-9}
7200	0.192	0.023	7.20×10^{16}	9.54×10^{4}	7,600	0.0	4.84×10^{-9}
8100	0.81	0.018	9.61×10^{16}	7.69×10^{4}	7,800	0.0	4.12×10^{-9}
7760	0.492	0.055	7.01×10^{16}	1.22×10^{5}	8,050	0.0	2.72×10^{-9}
9250	3.26	0.061	8.82×10^{16}	1.24×10^{5}	10,710	0.0	2.14×10^{-9}
6950	0.14	0.017	4.94×10^{16}	8.51×10^{4}	12,180	3.10	8.49×10^{-9}
6630	0.073	0.013	5.67×10^{16}	9.49×10^{4}	18,620	8.34	10.05×10^{-9}
7300	0.30	0.021	4.79×10^{16}	8.46×10^{4}	16,500	3.91	7.46×10^{-9}
7350	0.33	0.021	4.76×10^{16}	8.46×10^{4}	12,340	3.27	7.48×10^{-9}
7250	0.27	0.011	4.77×10^{16}	8.74×10^{4}	17,450	9.11	15.22×10^{-9}
7650	0.54	0.036	4.57×10^{16}	9.11×10^{4}	18,100	2.07	4.92×10^{-9}
7340	0.31	0.067	4.77×10^{16}	1.07×10^{5}	8,080	1.08	2.50×10^{-9}
7740	0.60	0.019	4.54×10^{16}	9.33×10^{4}	10,280	3.26	9.98×10^{-9}
7740	0.60	0.023	4.55×10^{16}	9.50×10^{4}	19,550	4.84	8.30×10^{-9}
7200	0.24	0.011	5.28×10^{16}	1.28×10^{5}	21,324	12.02	24.6×10^{-9}
7420	0.36	0.042	5.32×10^{16}	1.20×10^{5}	11,430	3.62	4.51×10^{-9}
7800	0.70	0.070	4.53×10^{16}	9.96×10^{4}	12,920	0.96	2.70×10^{-9}
8460	1.28	0.0028	11.08×10^{16}	8.00×10^{4}	8,150	15.3	22.87×10^{-9}
8460	1.28	0.0029	11.40×10^{16}	8.00×10^{4}	8,030	19.7	22.19×10^{-9}
8000	0.98	0.039	4.51×10^{16}	1.02×10^{5}	11,050	1.89	5.33×10^{-9}
8150	1.00	0.096	4.26×10^{16}	9.15×10^{4}	19,240	1.09	1.93×10^{-9}
8360	1.04	0.023	9.71×10^{16}	9.75×10^{4}	6,680	1.77	4.06×10^{-9}
8100	0.93	0.011	7.34×10^{16}	9.80×10^{4}	9,570	7.93	11.46×10^{-9}
8750	1.97	0.018	11.60×10^{16}	7.95×10^{4}	12,050	1.99	3.59×10^{-9}
7720	0.62	0.052	4.95×10^{16}	1.23×10^{5}	7,600	1.70	4.09×10^{-9}
7370	0.263	0.014	7.45×10^{16}	9.79×10^{4}	10,590	--	5.22×10^{-9}
8330	1.14	0.0038	9.98×10^{16}	7.76×10^{4}	40,850	82.3	19.38×10^{-9}
8154	0.87	0.0017	11.05×10^{16}	9.67×10^{4}	23,290	269.0	48.66×10^{-9}
7980	0.80	0.0048	6.42×10^{16}	1.28×10^{5}	15,200	30.5	37.68×10^{-9}
7720	0.50	0.0082	8.45×10^{16}	1.21×10^{5}	40,000	--	16.82×10^{-9}
8350	1.32	0.0031	8.00×10^{16}	1.01×10^{5}	20,900	--	40.04×10^{-9}
7910	0.71	0.021	8.65×10^{16}	1.15×10^{5}	26,700	4.63	5.88×10^{-9}
8100	0.95	0.058	8.12×10^{16}	1.16×10^{5}	33,600	2.27	2.20×10^{-9}
8190	1.08	0.11	6.90×10^{16}	1.55×10^{5}	21,500	3.24	1.78×10^{-9}
9320	3.63	0.035	9.86×10^{16}	1.15×10^{5}	28,200	7.41	31.30×10^{-9}

stream static and the sheath edge ionizations respectively into particle number densities. The recombination time is given by

$$t = \frac{1.05}{\overline{\beta}} \tag{E-2}$$

where $\overline{\beta}$ is the pressure gradient parameter in Table 5. The ratio, at the plasma sheath edge, of the sulphur hexafluoride number density to the positive ion number density is included in Table 5 to illustrate the effect of sulphur hexafluoride on the recombination coefficient. This ratio could not be calculated for three data points due to an error in determining the sulphur hexafluoride flow rates at these points.

The data for the calculations of the sulphur hexafluoride electron capture cross section, σ_{SF_6}, are presented in Table 6. The equation used to calculate the electron capture cross section is given in Chapter VI as

$$\sigma_{SF_6} = \frac{1}{\overline{c}_e \frac{n_{SF_6}}{n_i} n_i t} \ln \frac{\frac{n_e}{n_i} + \frac{n_{SF_6}}{n_i}}{\frac{n_e}{n_i} \frac{n_{io}}{n_{eo}}} \tag{E-3}$$

where $\overline{c}_e$ is the average speed of the electrons given by

$$\overline{c}_e = 5.93 \times 10^7 \sqrt{\frac{T_e}{11{,}600^\circ K}} \quad \frac{cm}{sec} \tag{E-4}$$

and t is the electron capture time which is given by Equation (2). In Equation (4), T_e is the average electron temperature; however, for reasons presented in Chapter VI, the free stream static temperature, T_s,

Table 6. Sulphur Hexafluoride Electron Capture Cross Section

Free Stream Static Temperature	Sheath Edge Electron Temperature	Pressure Gradient Parameter	Sheath Edge Positive Ion Number Density	$\frac{n_e}{n_i}$	$\frac{n_{SF_6}}{n_i}$	$\frac{n_{io}}{n_{eo}}$	Electron Capture Cross Section
°K	°K	sec^{-1}	cm^{-3}				cm^2
6950	12,180	8.51×10^4	8.23×10^{12}	0.265	3.10	1.604	1.437×10^{-16}
7300	16,500	8.46×10^4	1.00×10^{13}	0.052	3.91	1.377	1.746×10^{-16}
7350	12,340	8.46×10^4	1.00×10^{13}	0.135	3.27	1.263	1.560×10^{-16}
7250	17,450	8.74×10^4	5.40×10^{12}	0.030	9.11	1.590	1.899×10^{-16}
7650	18,100	9.11×10^4	1.63×10^{13}	0.074	2.07	1.160	1.722×10^{-16}
7340	8,080	1.07×10^5	3.18×10^{13}	0.625	1.08	1.239	0.497×10^{-16}
7740	10,280	9.33×10^4	8.37×10^{12}	0.291	3.26	1.115	1.602×10^{-16}
7740	19,550	9.50×10^4	1.03×10^{13}	0.023	4.84	1.227	1.932×10^{-16}
7420	11,430	1.20×10^5	2.21×10^{13}	0.409	3.62	1.731	0.521×10^{-16}
7800	12,920	9.96×10^4	3.16×10^{13}	0.083	0.96	1.106	1.568×10^{-16}
8460	8,150	8.00×10^4	3.10×10^{12}	0.316	15.3	1.037	1.228×10^{-16}
8460	8,030	8.00×10^4	3.30×10^{12}	0.110	19.7	1.048	1.193×10^{-16}
8000	11,050	1.02×10^5	1.74×10^{13}	0.302	1.89	1.081	1.143×10^{-16}
8150	19,240	9.15×10^4	4.07×10^{13}	0.054	1.09	1.117	1.161×10^{-16}
8360	6,680	9.75×10^4	2.22×10^{13}	0.825	1.77	1.041	0.513×10^{-16}
8100	9,570	9.80×10^4	7.87×10^{12}	0.270	7.93	1.103	1.002×10^{-16}
8750	12,050	7.95×10^4	1.37×10^{13}	0.661	1.99	1.019	0.733×10^{-16}
7720	7,600	1.23×10^5	2.56×10^{13}	0.350	1.70	1.166	0.902×10^{-16}

is used in Equation (4) rather than T_e. Thus in Equation (3) the value for $\bar{c}_e$ is given by

$$\bar{c}_e = 5.93 \times 10^7 \sqrt{\frac{T_s}{11,600^\circ K}} \ \frac{cm}{sec} . \qquad (E-5)$$

The results of the experimental evaluation of uranium hexafluoride as an electrophilic additive are presented in Table 7. In order to make the calculations for the electrostatic probe measurements it was necessary to assume the positive ion temperature at the plasma sheath edge for some of the data points. These data points are those for which the ratio, at the sheath edge, of the uranium hexafluoride number density to the positive ion number density vary between 3.4×10^{-2} and 0.522. The argon ionization data tabulated by Brahinsky and Neel do not give ionization levels which are less than 10^{-3} percent, and hence the ionization percentages for the data in which the free stream static temperature was less than 5,000°K were not determined.

Table 7. Experimental Results for the Uranium Hexafluoride Additive

	Heat Balance Results					Electrostatic Probe Measurements				
	Stagnation Conditions		Free Stream Static Conditions							
Enthalpy	Pressure	Temperature	Pressure	Temperature	Ionization	Ionization	Election Temperature	n_i	$\frac{n_e}{n_i}$	$\frac{n_{UF_6}}{n_i}$
$\frac{\text{k-cal.}}{\text{kg.-mole}}$	mm. Hg.	°K	mm. Hg.	°K	Percent	Percent	°K	ions/cm^3		
2.73×10^4	18.0	5500	14.3	5020	0.001	5.52×10^{-3}	8,170	9.27×10^{12}	1.00	0.00
2.28×10^4	18.0	4590	14.3	4180	$<10^{-3}$	6.30×10^{-3}	6,700	10.97×10^{12}	0.90	3.4×10^{-2}
1.63×10^4	18.0	3280	14.3	2950	$<10^{-3}$	4.34×10^{-3}	6,200	7.55×10^{12}	0.49	0.111
2.19×10^4	18.0	4410	14.3	4025	$<10^{-3}$	3.58×10^{-3}	13,900	3.04×10^{12}	0.037	0.522
2.19×10^4	18.0	4410	14.1	4000	$<10^{-3}$	4.96×10^{-3}	13,650	2.32×10^{12}	0.019	1.025
2.74×10^4	18.9	5510	15.1	5040	0.001	3.65×10^{-3}	13,400	1.66×10^{12}	0.016	6.84

LITERATURE CITED

1. Langmuir, I. and Mott-Smith, H. M., General Electric Review, Vol. 26 (1923), p. 731; Vol. 27 (1924), p. 449, 583, 616, 726, 810; Physics Review, Vol. 28 (1926), p. 727.
Langmuir, I., The Collected Works of Irving Langmuir, ed. G. Suits (Pergamon Press, Inc., New York, 1961).

2. Guthrie, A. and Wakerling, R. K., The Characteristics of Electrical Discharges in Magnetic Fields, articles of D. Bohm (McGraw-Hill, New York, 1949).

3. Cohen, I. M., Physics of Fluids., Vol. 6 (1963), p. 1492.

4. Su, C. H. and Lam, S. H., Phys. Fluids, Vol. 6 (1963), p. 1479.

5. Bernstein, I. B. and Rabinowitz, I. N., Phys. Fluids., Vol. 2 (1959), p. 112.

6. Lam, S. H., Phys. Fluids., Vol. 8 (1965), p. 73.

7. Allen, J. E., Boyd, R. L. F., and Reynolds, P., Physical Society of London Proceedings, Vol. B70 (1957), p. 297.

8. Wasserstrom, E., Su, C. H., and Probstein, R. F., Phys. Fluids, Vol. 8 (1965), p. 56.

9. Chen, F. F., Journal of Applied Physics, Vol. 36 (1965), p. 675.

10. Chou, Y. S., Talbot, L., and Willis, D. R., Phys. Fluids, Vol. 9 (1966), p. 2150.

11. French, J. B., UTIA Report No. 79 AFOSR2159.

12. Talbot, L., Phys. Fluids, Vol. 3 (1960), p. 289.

13. Lees, L., Jet Propulsion, Vol. 26 (1956), p. 359.

14. Grey, J. and Jacobs, P. F., AIAA Journal, Vol. 5 (1967), p. 84.

15. Jacobs, P. F., "Electron-Heavy Particle Nonequilibrium in a Dense Argon Plasma," Ph.D. Thesis, Princeton University (1966).

16. Loeb, L. B., Basic Processes in Gaseous Electronics (University of California Press, Berkeley, California, 1955).

17. Maxwell, B. R. and Wessling, F. C., "Approximation to the Collisional-Radiative Recombination Coefficient in a Partially Ionized Gas," AIAA Journal, Vol. 11, No. 7 (1973), p. 1048.

18. Asundi, R. K. and Craggs, J. D., "Electron Capture and Ionization Phenomena in SF_6 and C_7F_{14}," Proc. Phys. Soc., Vol. 83 (1964), p. 611.

19. Hung, N. T. and Paquette, G., "Theory of Langmuir Probes in Plasmas Containing Negative Ions. Properties of the Sheath," Proceedings of the Seventh International Conferences on Phenomena in Ionized Gases. Edited by B. Perović and D. Tošić (Gradevinska Knjiga Publishing House, Beograd Yugoslavia, 1966).

20. Toba, K. and Sayano, S., "A Continuum Theory of Electrostatic Probes in a Slightly Ionized Gas," Journal of Plasma Physics, Vol. 1, part 4, p. 407.

21. Audeh, B. J., "Review of Eddy Viscosity Models for Jet Engine Exhaust/Air Mixing," Lockheed Missiles and Space Company Huntsville Research and Engineering Center Report LMSC-HRED D225588, June, 1972.

22. Menard, W. A., Thomas, G. M., and Helliwell, T. M., "Experimental and Theoretical Study of Molecular, Continuum, and Line Radiation from Planetary Atmospheres," AIAA Journal, Vol. 6, No. 4 (1968), p. 655.

23. Swift, J. D. and Schwar, M. J. R., Electrical Probes for Plasma Diagnostics (London Iliffe Books, American Elsevier Publishing Company, Inc., New York).

24. Huddlestone, R. H., and Leonard, S. L., Plasma Diagnostic Techniques (Academic Press, New York, 1965).

25. Cohen, C. B. and Reshotko, E., "Similar Solutions for the Compressible Laminar Boundary Layer with Heat Transfer and Pressure Gradient," NACA TN3325, 1955.

26. Probstein, R. F., "Inviscid Flow in the Stagnation Point Region of Very Blunt-Nosed Bodies at Hypersonic Flight Speeds," WADC TN 56-395, Brown University, Division of Engineering (1956).

27. Devoto, R. S., "Transport Properties of Ionized Monatomic Gases," Physics of Fluids, Vol. 9, No. 6 (1966), p. 1230.

28. Svehla, R. A., Estimated Viscosities and Thermal Conductivities of Gases at High Temperatures, National Aeronautics and Space Administration Technical Report R-132 (1962).

29. Devoto, R. S., "Transport Coefficients of Partially Ionized Argon," Physics of Fluids, Vol. 10, No. 2 (1967), p. 354.

30. Bromley, L. A. and Wilke, C. R., "Viscosity Behavior of Gases," Industrial and Engineering Chemistry, Vol. 43, No. 7 (1951), p. 1641.

31. Frost, L. S. and Liebermann, R. W., "Composition and Transport Properties of SF_6 and Their Use in a Simplified Enthalpy Flow Arc Model," Proceedings of the IEEE, Vol. 59, No. 4 (1971), p. 474.

32. Brahinsky, H. S. and Neel, C. A., Tables of Equilibrium Thermodynamic Properties of Argon, Arnold Engineering Development Center TR-69-19, March, 1969.

VITA

Basil Pearson Cooper, Jr. was born in Lexington, Virginia on May 17, 1942. He attended public schools in Arlington, Virginia and graduated from Washington-Lee High School in 1960.

In June, 1960, Mr. Cooper entered the Georgia Institute of Technology and he received the degree of Bachelor of Aerospace Engineering in June, 1965.

During his undergraduate studies, Mr. Cooper completed a cooperative program with the Naval Air Test Center, Patuxent River, Maryland. He was also a member of the Varsity Rifle Team and, during his senior year, was captain of the team. He returned to the Naval Air Test Center for employment as a Flight Test Engineer during the summer of 1965.

In September, 1965, Mr. Cooper returned to the Georgia Institute of Technology to study under the doctoral program in Aerospace Engineering. He received NSF and NDEA traineeships and a graduate assistantship from the Georgia Institute of Technology to study under this program. He received the degree of Master of Science in Aerospace Engineering in June, 1967.

On September 7, 1968, Mr. Cooper was married to the former Virginia Drewry Craighill of Arlington, Virginia.

Mr. Cooper has been employed by Northrop Services, Incorporated in Huntsville, Alabama since October, 1971. He is presently a member of the Research Staff of Northrop Services.

He is a member of the Phi Kappa Phi, Tau Beta Pi, and Sigma Gamma Tau honorary societies.